Homogenization and Localization for Composite Structures with Relieved Periodicity in the Thickness Direction

厚さ方向の周期性を緩和した複合構造のための均質化と局所化

MUHAMMAD RIDLO ERDATA NASUTION

DEPARTMENT OF AEROSPACE ENGINEERING

GRADUATE SCHOOL OF SYSTEM DESIGN

TOKYO METROPOLITAN UNIVERSITY

MARCH 2015

Homogenization and Localization for Composite Structures with Relieved Periodicity in the Thickness Direction

厚さ方向の周期性を緩和した複合構造のための均質化と局所化

by

Muhammad Ridlo Erdata Nasution
Student ID 11991572

Submitted to the Department of Aerospace Engineering,
Graduate School of System Design,
in partial fulfillment of the requirements for the degree of
Doctor of Philosophy in Aerospace Engineering
at the
TOKYO METROPOLITAN UNIVERSITY
March 2015

Certified by advisor

Professor Naoyuki Watanabe
Department of Aerospace Engineering
Graduate School of System Design
Tokyo Metropolitan University

Doctoral thesis committee:

Professor Naoyuki Watanabe	Tokyo Metropolitan University (Chairman)
Professor Hiroshi Suemasu	Sophia University
Associate Professor Koichi Kitazono	Tokyo Metropolitan University
Associate Professor Satoshi Kobayashi	Tokyo Metropolitan University

Abstract

This thesis aims to develop a novel asymptotic expansion (AE) homogenization and localization analysis for advanced composite structures by relieving periodicity in the thickness direction. Introduction of relieved periodicity is an enhanced approach in homogenization and localization method whereby the years developed method usually implements the periodicity in three directions, i.e. in-plane and out-of-plane directions of the unit-cell. In this regard, a modified periodic function is introduced in the numerical formulation. The present formulation and finite element implementation of AE homogenization and localization method are given, and utilized to investigate several types of composites, namely 2-D laminated composites, brick composites, 3-D orthogonal interlock composites and sandwich composites. Homogenized thermomechanical properties and stress responses within the unit-cell due to application of thermal and mechanical loads are of the main interests. It is found that relieving periodicity in the thickness direction has larger influence on the analyses of composites having geometrical and/or material non-uniformity in the in-plane direction. Some certain results of homogenization and localization analysis are compared with analytical and finite element analysis results. Based on the obtained outcomes, it can be emphasized that the application of free-traction boundary condition only on the top and bottom surfaces of the macroscopic model cannot accurately simulate the real condition. The relieving periodicity throughout the thickness direction of unit-cell is necessary in order to be able to obtain the accurate results.

Keywords: Homogenization, localization, asymptotic expansion, relieved periodicity, unit-cell

Contents

List of Figures

List of Tables

Nomenclature

Symbols	Definition
C	Elastic constants
C^0	Homogenized elastic constants
E	Young's modulus
e	Strain
f	Body force
$g(\mathbf{x},\mathbf{y})$	Periodic vector function
G	Shear modulus
p	Traction acting on internal boundary S
S	Internal boundary of unit-cell
S^0	Homogenized compliance constants
t	Traction
u	Displacement
v	Virtual displacement
V_f	Fiber volume fraction of composites
V_{ft}	Fiber volume fraction of tow
$\mathbf{x}$	Macroscopic coordinate system
$\mathbf{y}$	Microscopic coordinate system
$\mathbf{Y}$	Unit-cell dimension
$\|Y\|$	Unit-cell volume
¥	Solid part of unit-cell

$[B]$	Strain shape function matrix
$[C]$	Elastic constants matrix
$[C^0]$	Homogenized elastic constants matrix
$\{C\}_{kl}$	Column 'kl' of matrix $[C]$
$[N]$	Shape function matrix
$[S^0]$	Homogenized compliance matrix
$\{v\}$	Virtual displacement vector
α	Coefficients of thermal expansion
ΔT	Temperature difference
ε	Ratio between macroscopic and microscopic coordinate
Γ_d	Prescribed displacement
Γ_t	Prescribed traction
ν	Poisson's ratio
Φ	Y-periodic function
σ	Stress
τ	Shear stress
χ	Elastic corrector
ψ	Thermal corrector
Ω	Elastic body
$\{\alpha\}$	Coefficients of thermal expansion vector
$\{\chi\}^{kl}$	Elastic corrector vector of mode 'kl'
$\{\psi\}$	Thermal corrector vector

Chapter 1

Introduction

1.1 Background

1.1.1 Composites in Aircraft Structures

Application of composite materials in aircraft structures have been intensely increasing in the late decades. Starting in 1960s, commercial airplane manufacturers have shown a great interest in composites use due to its beneficial properties as compared to metallic materials. The excellent strength-to-weight ratio of composites is the main contributing factor to the rapid growth of composite materials in aircraft structures application whereby significant weight reduction is expected. The reduced aircraft weight directly leads to the reduction of fuel cost and, on the other hand, creates possibility to increase aircraft payload, which means escalating airline revenue. Moreover, the other benefits of composites, such as good corrosion resistance and durability, can reduce airline operating cost due to maintenance circumstances. These facts are great selling points for a commercial aircraft.

Fig. 1.1 [1] shows that the increase of composites use in commercial aircraft structures over time is non-linear as can be approximated by an exponential graph. Due

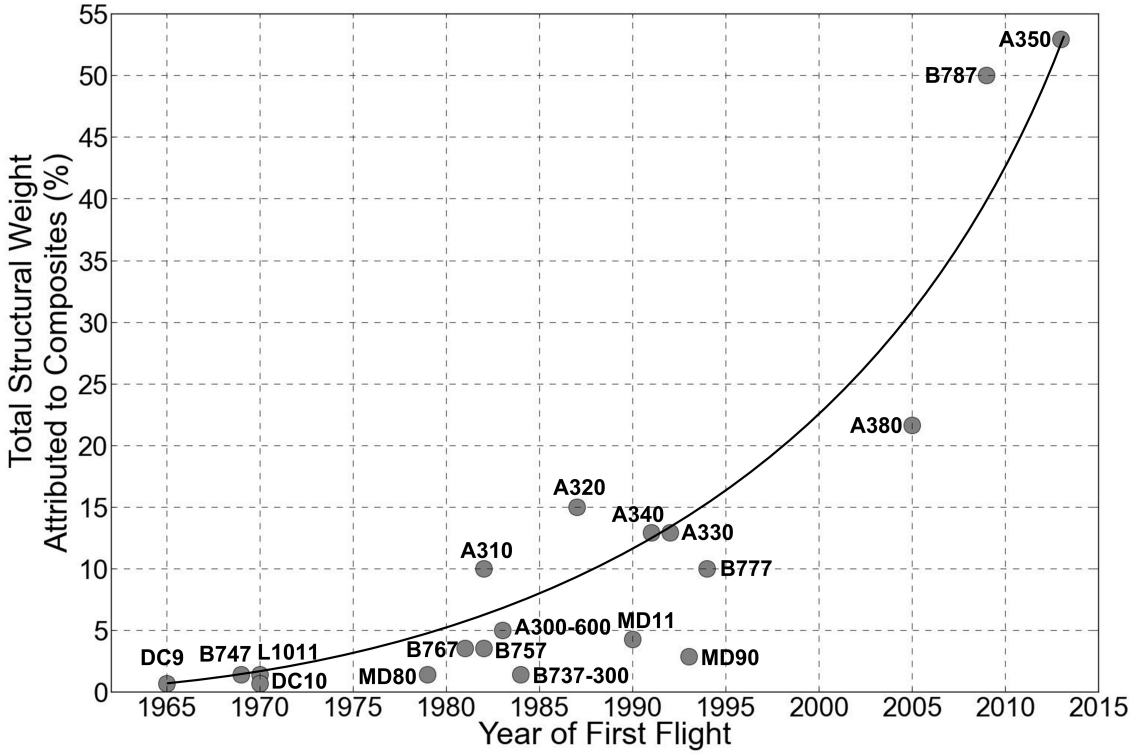

FIGURE 1.1: The use of composite materials in commercial aircraft [1]

to the very strict safety requirements particularly for commercial aircraft, composite materials were gradually used in three stages [2]. The early use of composite materials was limited on tertiary structures, for instance cabin interior and galleys. The next stage is application on secondary structure in the 1970s, and then development for primary structures, such as stabilizers, wings and fuselage, over the last three decades. The recent use of composite materials in aircraft structures has exceeded 50% of total airframe weight.

The increase of composite application consequently advances composite technology in many aspects, such as design process, manufacturing, maintenance, as well as the analysis of composite properties and behavior [3]. In regard to the properties and behavior of composites, experimental and numerical analyses are commonly performed. Recently, numerical analysis plays an important role in the investigation of composite materials and structures. Particularly for advanced composite structures, e.g. 3-D composites and sandwich honeycomb composites, numerical analysis

usually considers the composites from the viewpoint of several hierarchical scales, which is called multi-scale analysis.

1.1.2 Multi-scale Modeling Approach

Advanced composite structures often come with heterogeneous constituents with a very complex architecture. The complexity of composite structures causes their detail properties are very difficult to be experimentally investigated [4]. With the aim of reducing experimental efforts, numerical analysis can be a suitable method. However, an explicit modeling of the complex composite structures leads to a cumbersome and costly computational analysis. An excellent technique to deal with this problem is by performing multi-scale analysis. This analysis enables heterogeneous and complex structures to be observed from several hierarchical spatial scales. Consequently, such kind of approach creates a possibility to separately investigate the behavior and properties of the complex structure in each spatial scale with some appropriate idealization.

Multi-scale analysis in advanced composite structure is commonly performed in three hierarchical scales, namely micro-scale, meso-scale and macro-scale [5]. Micro-scale is the scale in which fiber and matrix are incorporated as a representative volume element (RVE) of a fiber tow or yarn with certain volume fraction. The equivalent properties of the tows (or simply laminates in 2-D composites) are then used in the analysis in meso-scale. In meso-scale, fiber tows architecture representing the whole composite structures is explicitly built. Subsequently, the obtained equivalent properties are employed for the analysis in macro-scale representation. In macro-scale, composite is considered to be a homogeneous structure having equivalent properties and behavior of the tows architecture. External loading conditions are applied on the homogeneous-considered structure.

Recently, multi-scale analysis is developing rapidly and commonly performed by

employing methods with averaging scheme to bridge between scales. A study of periodic boundary condition for multi-scale analysis in the prediction of equivalent stiffness of 3-D woven composites was performed by Wang et al. [6]. The calculation of equivalent stiffness was based on volume averaging technique. In the framework of asymptotic expansion analysis, multi-scale homogenization method had been employed for the thermomechanical analyses, e.g. for the prediction of the properties of random heterogeneous materials [7] and 3-D orthogonal interlock composites [8]. Xing et al. [9] developed a multi-scale eigenelement method for periodical composite structures.

In certain extent, multi-scale analysis was employed in damage analyses of composites under fatigue load [10] and impact load [11, 12]. Multi-scale analysis of fiber-reinforced composites was done by Wu et al. [13] by employing mean-field homogenization method. The matrix phase is considered as a non-linear isotropic material embedding damage. Multi-scale damage analysis was also performed by Visrolia and Meo [14] for the analysis of 3-D weave composites. The analysis was based on asymptotic homogenization utilizing meso-scale unit-cell model.

1.1.3 Overview of Homogenization and Localization Analysis

The early development of homogenization technique was mainly to analyze composites properties which gained a wider interest since the emergence of modern fiber composites in 1960s [15]. Some early analyses focused on the prediction of composite properties and behavior in microstructural level. Hashin and Shtrikman established variational formulations to analyze the elastic behavior of anisotropic and nonhomogeneous body [16] as well as multiphase materials [17]. An analysis for calculating the average stress of matrix in a system containing inclusions was done by Mori and Tanaka [18]. Some other early studies on the analysis of composite microstructure

(i.e. micro-scale level) can be found in the review paper of Kanoute et al. [19]. In textile composites, meso-scale RVE models were employed to investigate the stiffness and strength of woven fabric composites [20].

Homogenization regards heterogeneous structure as a homogeneous body possessing equivalent properties and behavior of its heterogeneous form. By performing homogenization analysis, the heterogeneous structure can be evaluated by focusing on its representative volume element. Such kind of analysis is worth to be done mainly due to the excellent computational cost. Moreover, the use of RVE consequently simplifies modeling efforts since all constituents of composite structures are not explicitly built. The aforementioned facts yield homogenization to be a preferable method in the determination of the equivalent properties of composite structures. After obtaining the equivalent properties, structural responses within the heterogeneous RVE due to application of external load on homogeneous structure can be evaluated by means of localization analysis, which can be seen as a reverse of homogenization analysis [21].

Homogenization is commonly employed by means of standard volume averaging technique or else asymptotic expansion technique. In hierarchical spatial representation, both techniques implement different volume averaging schemes. Standard averaging technique employs the averaging operator to the representative volume element as well as global structure of interest, whereas asymptotic expansion technique focuses on the averaging scheme of RVE or unit-cell [22]. This fact yields that the asymptotic technique can be powerful when dealing with composites structure consisting periodic microstructure [23], whereby the periodicity is considered in the modeling and analysis of unit-cell.

The asymptotic expansion (AE) homogenization method has been widely employed in the analysis of composite materials and structures since the publishing of the research of Guedes and Kikuchi [24]. The research presented a rigorous strong form formulation of AE homogenization method. The formulation is applicable for general composite structures. AE homogenization method has also been used to analyze several types of composites, for instance textile composites [25–27] and metal-matrix

composites [28]. In the case of linear thermoelasticity, asymptotic expansion technique was developed in the framework of homogenization by Francfort [29]. Several researchers also employed AE homogenization method by incorporating thermal effects in order to obtain mechanical properties as well as the coefficients of thermal expansions (CTE) [7, 30, 31].

With the aim of investigating structural response within a unit-cell, localization analysis can also be performed in the framework of asymptotic analysis. This analysis aims to obtain local stresses within a unit-cell in a microscopic representation due to the application of external loading on the homogeneous macrostructure. Several studies, e.g. in Refs. [24, 25, 32], performed asymptotic expansion homogenization and localization analyses by excluding thermal effects. In fact, the thermal effects, in terms of thermal residual stresses, may affect the damage behavior of composites [33, 34].

In homogenization and localization analysis, periodicity plays an important role in determining both homogenized equivalent properties as well as local structural response within the unit-cell. The years developed method usually implements the periodicity in three directions (i.e. x-, y- and z- directions). This means that the unit-cell is assumed to be infinitely repeated in those three directions. In Ref. [35], such kind of periodicity was deemed able to meet a good numerical accuracy in the analysis of particle-reinforced and fiber-reinforced composites. Nevertheless, composite laminates, especially in aircraft structures, are very thin. In addition, several types of composites, e.g. 3-D composites and sandwich honeycomb composites, do not possess repeating pattern in the thickness direction. Analysis of such kind of composites necessitates a model which represents the whole thickness of unit-cell (i.e. finite-thickness unit-cell model). Woo and Whitcomb [36] suggested to consider the influence of finite thickness effect in the analysis of textile composites as a future study. In this regard, the unit-cell should not be assumed to be repeated infinitely in the thickness direction. In other words, the unit-cell possesses only in-plane periodicity.

The existence of only in-plane periodicity was considered in several studies by employing plate theory. Rostam-Abadi et al. [37] performed a design analysis of composite laminates by AE homogenization method. The analysis utilized Kirchhoff-Love plate theory for the assumption of the displacement field. The Kirchhoff-Love theory in AE homogenization method was also employed by Buannic et al. [38] in the analysis of corrugated core sandwich panels. The aforementioned researches utilized asymptotic analysis on the evaluation of equivalent plate properties (i.e. by means of homogenization scheme) while the assessment of structural response within the structure, obtainable by localization analysis, was not considered. An AE homogenization analysis utilizing Kirchhoff-Love plate theory was also done by Lapeyronnie et al. [39]. In this analysis, macroscopic structural responses of 3-D layer-to-layer angle-interlocked composite was represented by using homogeneous isotropic cell, and compared to those of 3-D heterogeneous cell. Cai et al. [40] considered the existence of only in-plane periodicity in AE homogenization analysis of periodic plate structures. The analysis investigated the effective properties of honeycomb plate and excluded the detailed stress responses of the unit-cell. Analytical solutions of an orthotropic multilayered rectangular plate were proposed by He et al. [41], whereby the plate was considered to possess small periodicity in one of in-plane directions. The study employed plane-strain assumption for the constitutive relation, while the thickness effects are investigated by calculating the so-called state vectors on the top and bottom surfaces of the plate.

1.2 Problem Statements and Objectives

As described earlier in the previous section, AE homogenization and localization analysis in some cases of advanced composite structures necessitates the use of finite-thickness unit-cell model. Correspondingly, the periodicity in both in-plane directions is of considered, while that of the thickness direction is relieved. However,

the available literatures show that the consideration of only in-plane periodicity is limited in the plate theory. The implementation of such periodicity in complex composites, with highly heterogeneity and non-uniformity within their microstructure, needs deeper analysis. This fact becomes the main motivation of this thesis.
This thesis generally aims to develop a novel asymptotic expansion homogenization and localization analysis by considering the existence of only in-plane periodicity in composite structure. In this regard, a modified periodic function is introduced in the numerical formulation. The developed formulation in this thesis is numerically implemented by an in-house code written in Fortran 90, and applicable for general composites structures.
The objectives of this thesis are listed below:

1. to mathematically formulate the AE homogenization and localization analysis by relieving periodicity in the thickness direction
2. to implement the formulation into finite element framework for the thermo-mechanical analysis of composites
3. to provide numerical examples by analyzing 2-D composites, brick composites, 3-D composites and sandwich structures
4. to investigate the effects of relieving periodicity in the thickness direction as well as the utilization of finite-thickness unit-cell to the effective properties of composites and the stress responses within the unit-cell

1.3 Overview of the Thesis

This thesis is divided into five chapters as follows:
Chapter 1 presents the background and overview of this thesis. Literature study on multi-scale modeling approach in the analysis of composites is given. Some published

works reviewed in the literature study show that homogenization and localization are powerful methods to deal with unit-cell in hierarchical multi-scale analysis. Literature reviews on the development of homogenization and localization method are also presented. With regard to the consideration of only in-plane periodicity, several related works are found. However, the available works in the literature are only limited to the extension of plate theory.

Chapter 2 discusses the concept and formulation of asymptotic expansion (AE) homogenization and localization method. An overview of the standard technique with 3-D periodicity (i.e. in in-plane and out-of-plane directions) is also presented. With respect to the enhanced approach implemented in this thesis, a modified periodic function is introduced in order to relieve the periodicity in the thickness direction. This is to facilitate the analysis of finite-thickness unit-cell model in which the unit-cell is considered to be infinitely repeated only in the in-plane direction of the macroscopic structure. For such kind of analysis, the periodic function is modified so that: (i) in microscopic representation, microstructural variables within the unit-cell vary in three-directions (i.e. in-plane and out-of-plane directions) and are periodic only in in-plane directions; (ii) in macroscopic representation, the variables vary only in the in-plane directions. The formulation used in this thesis uses the principle of virtual works as a governing equation, and is derived based on linear thermomechanical constitutive relation in both fiber and matrix phases. The utilization of asymptotic expansion series on the displacement field into the governing equation results in three hierarchical equations.

Chapter 3 presents the finite element implementation of AE homogenization and localization method with relieved periodicity in the thickness direction. The hierarchical equations are implemented in finite element framework, and then used to perform homogenization analysis (calculation of characteristic displacement vectors (also known as correctors) for both elastic and thermal problems, and homogenized thermomechanical properties) as well as localization analysis (calculation of stress responses within the unit-cell).

Chapter 4 discusses the case studies and results of homogenization and localization

analyses. In order to understand the effects of relieving periodicity in the thickness direction as well as the utilization of finite-thickness unit-cell model, the analyses are performed to investigate several types of composites namely 2-D laminated composites, brick composites, 3-D orthogonal interlock composites and honeycomb sandwich composites. Homogenized thermomechanical properties and stress responses within the unit-cell due to application of thermal and mechanical loads are of the main interests. Some certain results are then compared to those of standard analysis with 3-D periodicity as well as analytical and finite element analysis.

Chapter 5 summarizes and concludes the findings acquired in this thesis. It is found that relieving periodicity in the thickness direction shows insignificant influence in the analysis of 2-D laminated composites, in both homogenization and localization analyses. It is recommended to implement the relieving periodicity when the composites have geometrical and/or material non-uniformity in the in-plane direction. Excellent agreements between homogenization and analytical results are noted in the results of 2-D laminated composites. With regard to the results of localization analysis, it is found that the application of free-traction boundary condition only on the top and bottom surfaces of the macroscopic model cannot accurately simulate the real condition. This is shown by the different stress responses between the results of standard and present analyses, particularly in the region nearby the top and bottom surfaces of the unit-cell.

Chapter 2

Asymptotic Expansion (AE) Homogenization and Localization

2.1 Overview of the Standard Technique

2.1.1 General Concept

Multi-scale analysis generally considers a structure from at least two spatial scales, which commonly named microscopic and macroscopic scales. The macroscopic scale is a scale when a structure is viewed 'with the naked-eye', or in other word, without looking at the detail of the structure. Contrarily, microscopic scale is the scale whereby the detail structure is seen 'by looking through a microscope'. Macrostructure, or global structure, is usually regarded to possess equivalent properties and behavior of its microstructure. In multi-scale analysis, asymptotic expansion homogenization and localization method can be effectively and efficiently employed to analyze macrostructure which consists of periodic and heterogeneous microstructure by considering both spatial scales. Viewed from macroscopic scale, the microstructure (i.e. unit-cell) is assumed very small and periodic, viz. infinitely repeated within

the macrostructure. The two aforementioned spatial scales are shown in Fig. 2.1, whereby Fig. 2.1(a) is a unit-cell in microscopic scale, whilst Figs. 2.1(b) and (c) are heterogeneous (Ω^ε) and homogeneous (Ω) macrostructure in macroscopic scale. The unit-cell consists of "solid part" ¥ and "hollow part" θ. It is noted that the unit-cell is heterogeneous and periodic. The coordinate system of microscopic scale is $\mathbf{y} = (y_1, y_2, y_3)$, while that of macroscopic scale is $\mathbf{x} = (x_1, x_2, x_3)$. A very small positive number $\varepsilon = \mathbf{x}/\mathbf{y}$ is used to correlate both scales. When ε approaches zero, the heterogeneous macrostructure (Fig. 2.1(b)) can be regarded as a homogeneous system (Fig. 2.1(c)).

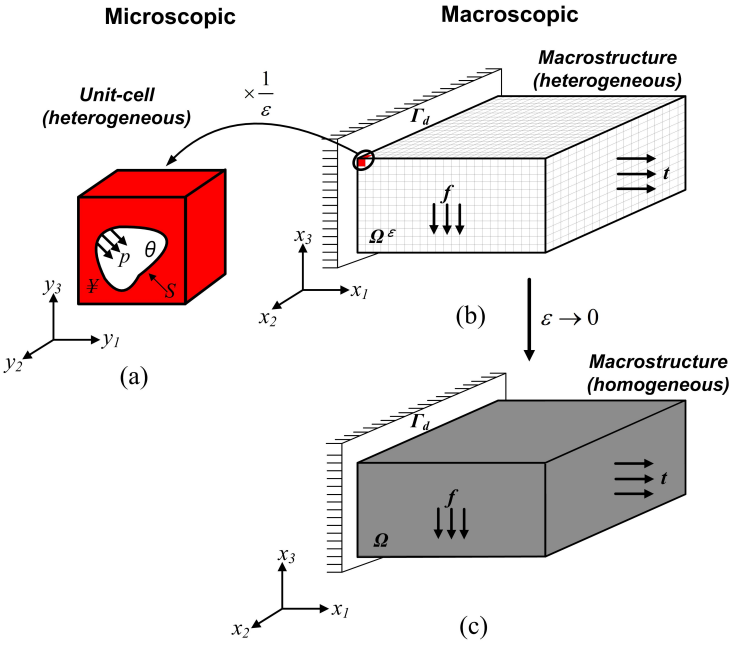

FIGURE 2.1: (a) Heterogeneous and periodic unit-cell, (b) heterogeneous macrostructure, (c) homogeneous macrostructure

The aforementioned scheme is called homogenization, in which is beneficial to obtain equivalent properties and behavior of heterogeneous and periodic microstructure in macroscopic representation. The reverse scheme, called localization, is able to find out the structural responses within the unit-cell in microscopic representation due to certain loading applied on the homogeneous macrostructure. Dealing with such kind of multi-scale problem, asymptotic expansion analysis has a good capability

in transferring the properties and behavior of microstructure into macroscopic representation, and vice versa [23]. In Fig. 2.2(a), a homogeneous macrostructure is subjected to uniaxial traction loading whereby four unit-cells (UC), namely UC1, UC2, UC3 and UC4, are identified as its subset. For simplicity reason, the unit-cells are represented by two-dimensional figure whereby each of them has two black bricks and two white bricks. Line A-A' represents the distance between UC1 and UC4. The structural responses due to external loading, in terms of stress (σ_{11}) and displacement (u_1), are shown in Fig. 2.2(b) and (c), respectively. In Fig. 2.2(b), σ^0 and σ^H denote actual stress and homogenized stress whereby the actual stress is periodic and the homogenized stress is constant. In Fig. 2.2(c), u^ε and u^0 denote actual displacement and macroscopic displacement. The actual displacement is periodic and the macroscopic displacement is changing within line A-A' in linear manner.

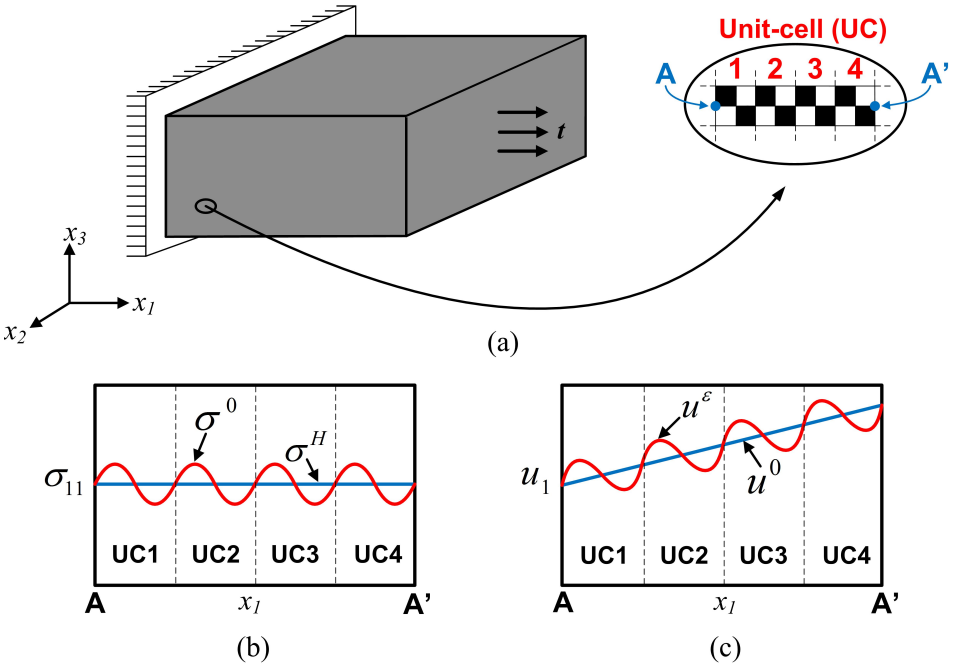

FIGURE 2.2: (a) Homogeneous macrostructure subjected to uniaxial tension loading, (b) stress response of the unit-cell, (c) displacement response of the unit-cell

2.1.2 Periodic Function

Microstructural variables within the unit-cell vary when are viewed from the viewpoint of microscopic and macroscopic scales. Accordingly, a vector function g is introduced as a function of macroscopic coordinate $\mathbf{x}$ and microscopic coordinate $\mathbf{y}$ as follows

$$g^{\varepsilon}(\mathbf{x}) = g(\mathbf{x}, \mathbf{y}) \tag{2.1}$$

where $\mathbf{y} = \mathbf{x}/\varepsilon$. The vector function considers that the periodicity exists on the microscopic coordinate $\mathbf{y}$, which is called Y-periodic. Standard technique is implemented by assuming that the unit-cell is periodic in three directions (x_1, x_2 and x_3). Due to Y-periodicity, Eq. (2.1) can be expressed as follows

$$g(\mathbf{x}, \mathbf{y}) = g(\mathbf{x}, \mathbf{y}+\mathbf{Y}) = g(x_1, x_2, x_3, y_1 + Y_1, y_2 + Y_2, y_3 + Y_3) \tag{2.2}$$

where $\mathbf{Y}$ denotes the dimension of the unit-cell. According to the chain rule, derivatives of g with respect to macroscopic coordinate $\mathbf{x}$ can be obtained by the following equation

$$\frac{\partial}{\partial x_i}[g(\mathbf{x}, \mathbf{y})] = \frac{\partial g}{\partial x_i} + \frac{1}{\varepsilon}\frac{\partial g}{\partial y_i} \tag{2.3}$$

When the heterogeneous macrostructure is considered as a homogeneous system, the following expressions are employed to take the limit of integration of Y-periodic function as ε approaches zero from the positive side

$$\lim_{\varepsilon \to 0^+} \int_{\Omega^{\varepsilon}} \Phi^{\varepsilon}(\mathbf{x}) d\Omega \to \frac{1}{|Y|} \int_{\Omega} \int_{¥} \Phi(\mathbf{x},\mathbf{y}) dY d\Omega \tag{2.4}$$

$$\lim_{\varepsilon \to 0^+} \varepsilon \int_{S^\varepsilon} \Phi^\varepsilon(\mathbf{x}) dS \to \frac{1}{|Y|} \int_\Omega \int_S \Phi(\mathbf{x},\mathbf{y}) dS d\Omega \tag{2.5}$$

where $|Y|$ is the unit-cell volume; $\mathbf{x} = x_1, x_2, x_3$; $\mathbf{y} = y_1, y_2, y_3$; $d\Omega = dx_1 dx_2 dx_3$ and $dY = dy_1 dy_2 dy_3$.

2.2 Enhanced Approach: Relieving Periodicity in the Thickness Direction

2.2.1 General Concept

This thesis considers an enhanced approach of homogenization and localization analysis by relieving periodicity in the thickness direction (i.e. out-of-plane direction) [42]. In this regard, the heterogeneous macrostructure, depicted in Fig. 2.3(a) is composed of heterogeneous and periodic microstructure (i.e. unit-cell) shown in Fig. 2.3(b) whereby the whole thickness of macrostructure is represented by a single unit-cell. Such kind of unit-cell is called finite-thickness unit-cell model. It is noteworthy that the enhanced approach is proposed to facilitate two types of finite-thickness unit-cell: (i). with repeating pattern in thickness direction, (ii). with non-repeating pattern in thickness direction. The modeling of finite-thickness unit-cell model aims to consider the finite thickness effects. Consequently, this enhanced approach necessitates the relieving periodic boundary condition in the out-of-plane direction. In this case, the unit-cell is considered to be periodic only in the in-plane direction of the macroscopic structure, whilst top and bottom surfaces of the unit-cell are free-boundaries. In other words, the top and bottom surfaces are independent between each other and their deformation may not be the same.

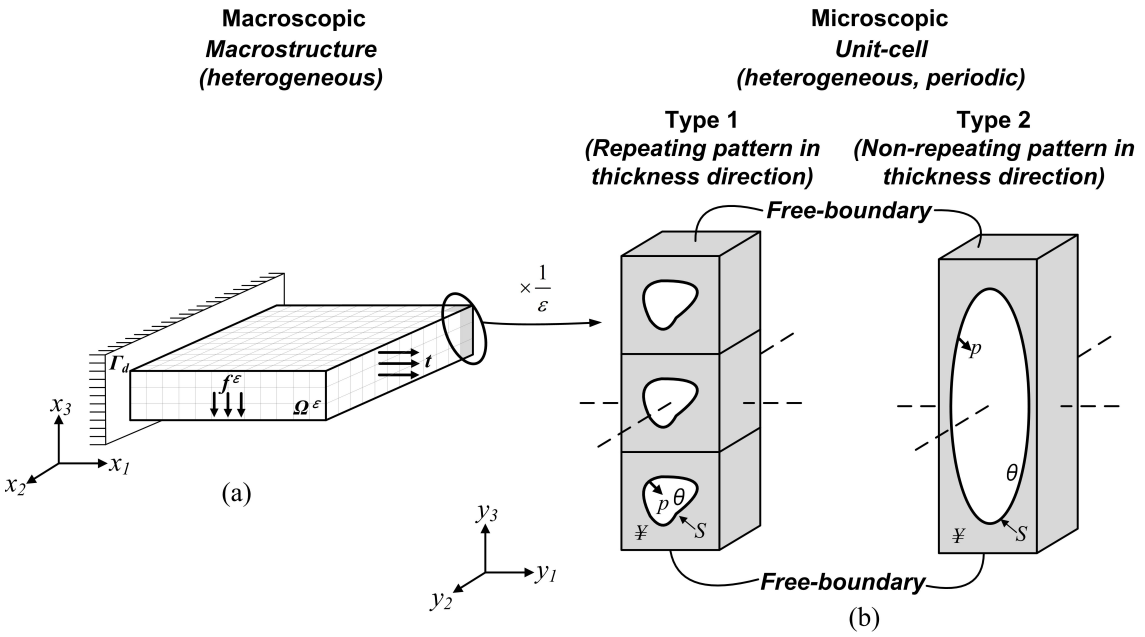

FIGURE 2.3: (a) Heterogeneous macrostructure, (b) heterogeneous, periodic unit-cell with free-boundaries at the top and bottom surfaces

2.2.2 Modified Periodic Function

In present approach, due to the nonexistence of periodicity in the thickness direction, periodic vector function is modified into the following equation

$$g^{\varepsilon}(\mathbf{x}) = g(\mathbf{x}, \mathbf{y}) = g(x_1, x_2, x_3, y_1 + Y_1, y_2 + Y_2) \tag{2.6}$$

where Y_1 and Y_2 are the dimensions of unit-cell in direction -1 and -2.
Due to non-periodic condition in the thickness direction, x_3 is regarded as a finite scale and very small as compared to x_1 and x_2. Thus, x_3 is assumed that can be approximated by the following expression

$$x_3 \approx \varepsilon y_3 \tag{2.7}$$

In consequence, the modified periodic vector function is now expressed as follows

$$g^{\varepsilon}(\mathbf{x}) = g(\mathbf{x},\mathbf{y}) = g(x_1, x_2, y_1 + Y_1, y_2 + Y_2, y_3) \tag{2.8}$$

Expression (2.8) means that: (i) in microscopic representation ($\mathbf{y}$ coordinate system), microstructural variables within the unit-cell vary in three-directions (i.e. in-plane and out-of-plane directions) and are periodic only in in-plane directions; (ii) in macroscopic representation ($\mathbf{x}$ coordinate system), the variables vary only in the in-plane directions.

In accordance with the utilized assumption, derivatives of the modified periodic vector function with respect to macroscopic coordinate $\mathbf{x}$ are as follows

$$\frac{\partial g^{\varepsilon}}{\partial x_1} = \frac{\partial g}{\partial x_1} + \frac{1}{\varepsilon}\frac{\partial g}{\partial y_1} \tag{2.9}$$

$$\frac{\partial g^{\varepsilon}}{\partial x_2} = \frac{\partial g}{\partial x_2} + \frac{1}{\varepsilon}\frac{\partial g}{\partial y_2} \tag{2.10}$$

$$\frac{\partial g^{\varepsilon}}{\partial x_3} = \frac{1}{\varepsilon}\frac{\partial g}{\partial y_3} \tag{2.11}$$

Limit of integration of Y-periodic function, employed when the heterogeneous macrostructure is considered as a homogeneous system, can be expressed as follows

$$\lim_{\varepsilon\to 0^+}\int_{\Omega^{\varepsilon}} \Phi^{\varepsilon}(\mathbf{x})d\Omega \to \frac{1}{|Y|}\int_{\Omega}\int_{¥} \Phi(\mathbf{x},\mathbf{y})dYd\Omega \tag{2.12}$$

$$\lim_{\varepsilon\to 0^+}\varepsilon\int_{S^{\varepsilon}} \Phi^{\varepsilon}(\mathbf{x})dS \to \frac{1}{|Y|}\int_{\Omega}\int_{S} \Phi(\mathbf{x},\mathbf{y})dSd\Omega \tag{2.13}$$

where $|Y|$ is the unit-cell volume; $\mathbf{x} = x_1, x_2$; $\mathbf{y} = y_1, y_2, y_3$; $d\Omega = dx_1dx_2$ and $dY = dy_1dy_2dy_3$.

2.2.3 Formulation of AE Homogenization and Localization Method

In this thesis, formulation of AE homogenization and localization method employs principle of virtual work as a governing equation. The principle of virtual work which has a powerful capability in solving structural problems in equilibrium condition is mathematically expressed by the following equation:

$$\int_{\Omega^\varepsilon} \sigma_{ij}^\varepsilon \frac{\partial v_i}{\partial x_j} d\Omega = \int_{\Omega^\varepsilon} f_i^\varepsilon v_i d\Omega + \int_{\Gamma_t} t_i v_i d\Gamma + \int_{S^\varepsilon} p_i^\varepsilon v_i dS \tag{2.14}$$

where σ_{ij} denotes the stresses acting on the domain Ω, x_j is macroscopic coordinate system, f_i is body force, t_i is traction force acting on boundary Γ_t, p is traction on surface S (see Fig. 2.3(b)), and v_i is virtual displacement. It is noted that superscript ε denotes the variable of total region (i.e. including microstructure).
In linear thermomechanical problem, stress-strain relationship can be expressed as follows

$$\sigma_{ij}^\varepsilon = C_{ijkl}^\varepsilon (e_{kl}^{tot} - e_{kl}^t) \tag{2.15}$$

where C_{ijkl} denotes elastic constants tensor, e_{kl}^{tot} is total strain and e_{kl}^t is thermal strain. Eqs. (2.16) and (2.17) respectively represent total strain-displacement relationship and thermal strain.

$$e_{kl}^{tot} = \frac{1}{2}\left(\frac{\partial u_k^\varepsilon}{\partial x_l} + \frac{\partial u_l^\varepsilon}{\partial x_k}\right) \tag{2.16}$$

$$e_{kl}^t = \alpha_{kl}^\varepsilon \Delta T \tag{2.17}$$

where u_k denotes actual displacement, α_{kl} is coefficient of thermal expansion and ΔT is temperature difference. The substitution of Eqs. (2.16) and (2.17) into Eq. (2.15), and consideration of the symmetry of elastic tensor, yields that the stress can be re-expressed as the following form

$$\sigma_{ij}^{\varepsilon} = C_{ijkl}^{\varepsilon}\left(\frac{\partial u_k^{\varepsilon}}{\partial x_l} - \alpha_{kl}^{\varepsilon}\Delta T\right) \tag{2.18}$$

Substitution of Eq. (2.18) into Eq. (2.14) yields a governing equation as follows

$$\int_{\Omega^{\varepsilon}} C_{ijkl}^{\varepsilon}\left(\frac{\partial u_k^{\varepsilon}}{\partial x_l} - \alpha_{kl}^{\varepsilon}\Delta T\right)\frac{\partial v_i}{\partial x_j}d\Omega = \int_{\Omega^{\varepsilon}} f_i^{\varepsilon} v_i d\Omega + \int_{\Gamma_t} t_i v_i d\Gamma + \int_{S^{\varepsilon}} p_i^{\varepsilon} v_i dS \tag{2.19}$$

Numerical formulation is derived by employing a governing equation given in Eq. (2.19) whereby the actual displacement u_k^{ε} is represented by asymptotic expansion series

$$u_k^{\varepsilon}(\mathbf{x}) = u_k^0(\mathbf{x},\mathbf{y}) + \varepsilon u_k^1(\mathbf{x},\mathbf{y}) + \varepsilon^2 u_k^2(\mathbf{x},\mathbf{y}) + ... \tag{2.20}$$

By substituting Eq. (2.20) into Eq. (2.19), the governing equation can be expanded as follows

$$\begin{aligned}\int_{\Omega^{\varepsilon}} C_{ijkl}^{\varepsilon}\left(\frac{\partial(u_k^0 + \varepsilon u_k^1 + \varepsilon^2 u_k^2 + ...)}{\partial x_l} - \alpha_{kl}^{\varepsilon}\Delta T\right)\frac{\partial v_i}{\partial x_j}d\Omega = \int_{\Omega^{\varepsilon}} f_i^{\varepsilon} v_i d\Omega + \\ \int_{\Gamma_t} t_i v_i d\Gamma + \int_{S^{\varepsilon}} p_i^{\varepsilon} v_i dS\end{aligned} \tag{2.21}$$

It is noted that the formulation considers the thermal effects through the incorporation of thermal strain in Eq. (2.21). By employing Eqs. (2.9)-(2.11) to take the

derivatives of actual and virtual displacements, three hierarchical equations based on the order of ε are obtained as follows

$$\text{Order of } \varepsilon^{-2}: \frac{1}{\varepsilon^2}\int_{\Omega^\varepsilon} C^\varepsilon_{ijkl}\frac{\partial u^0_k}{\partial y_l}\frac{\partial v_i}{\partial y_j}d\Omega = 0 \tag{2.22}$$

$$\begin{aligned}\text{Order of } \varepsilon^{-1}: \frac{1}{\varepsilon}\int_{\Omega^\varepsilon} C^\varepsilon_{ijkl}\left[\frac{\partial u^0_k}{\partial y_l}\frac{\partial v_i}{\partial x_j} + \left(\frac{\partial u^0_k}{\partial x_l} + \frac{\partial u^1_k}{\partial y_l} - \alpha^\varepsilon_{kl}\Delta T\right)\frac{\partial v_i}{\partial y_j}\right]d\Omega \\ = \int_{S^\varepsilon} p^\varepsilon_i v_i dS\end{aligned} \tag{2.23}$$

$$\begin{aligned}\text{Order of } \varepsilon^{0}: \int_{\Omega^\varepsilon} C^\varepsilon_{ijkl}\left[\left(\frac{\partial u^0_k}{\partial x_l} + \frac{\partial u^1_k}{\partial y_l} - \alpha^\varepsilon_{kl}\Delta T\right)\frac{\partial v_i}{\partial x_j} + \left(\frac{\partial u^1_k}{\partial x_l} + \frac{\partial u^2_k}{\partial y_l}\right)\frac{\partial v_i}{\partial y_j}\right]d\Omega = \\ \int_{\Omega^\varepsilon} f^\varepsilon_i v_i d\Omega + \int_{\Gamma_t} t_i v_i d\Gamma\end{aligned} \tag{2.24}$$

Subsequently, the hierarchical equations are solved by assuming that their limits exist when $\varepsilon \to 0^+$. The next subchapters explain the derivation of the hierarchical equations in a more detail manner.

2.2.3.1 Order of ε^{-2}

By multiplying Eq. (2.22) by ε^2, and employing expression (2.12) to take the limit as $\varepsilon \to 0^+$, following equation is obtained

$$\frac{1}{|Y|}\int_\Omega \int_{\text{¥}} C_{ijkl}\frac{\partial u^0_k}{\partial y_l}\frac{\partial v_i}{\partial y_j}dY d\Omega = 0 \tag{2.25}$$

Virtual displacement $\mathbf{v}$ is arbitrary and can be a function of either macroscopic coordinate $\mathbf{x}$ ($\mathbf{v} = \mathbf{v}(\mathbf{x})$) or microscopic coordinate $\mathbf{y}$ ($\mathbf{v} = \mathbf{v}(\mathbf{y})$). Eq. (2.25) will

automatically be satisfied if $\mathbf{v} = \mathbf{v}(\mathbf{x})$. However, choosing $\mathbf{v} = \mathbf{v}(\mathbf{y})$ will result in an expanded form of Eq. (2.25) after applying integration by parts and Gauss' divergence theorem as follows

$$\frac{1}{|Y|}\int_{\Omega}\left[\begin{array}{c} -\int_{Y}\frac{\partial}{\partial y_j}\left(C_{ijkl}\frac{\partial u_k^0}{\partial y_l}\right)v_i(\mathbf{y})dY + \int_{S}C_{ijkl}\frac{\partial u_k^0}{\partial y_l}n_j v_i(\mathbf{y})dS \\ +\int_{Y_1}C_{ijkl}\frac{\partial u_k^0}{\partial y_l}n_j v_i(\mathbf{y})dY_1 + \int_{Y_2}C_{ijkl}\frac{\partial u_k^0}{\partial y_l}n_j v_i(\mathbf{y})dY_2 \\ +\int_{Y_t}C_{ijkl}\frac{\partial u_k^0}{\partial y_l}n_j v_i(\mathbf{y})dY_t + \int_{Y_b}C_{ijkl}\frac{\partial u_k^0}{\partial y_l}n_j v_i(\mathbf{y})dY_b \end{array}\right]d\Omega = 0 \quad (2.26)$$

The square bracket of Eq. (2.26) consists of six integral terms. In this regard, the third and fourth terms cancel each other due to the existence of the in-plane periodicity (i.e. in each pair of surfaces Y_1 and Y_2), while the fifth and sixth terms are zero due to the free-traction condition on the top and bottom surfaces (i.e. surfaces Y_t and Y_b). In accordance with the mathematical treatment described in Ref. [24], the remaining equation is satisfied by the following expression

$$u_k^0 = u_k^0(\mathbf{x}) = u_k^0(x_1, x_2) \quad (2.27)$$

where u_k^0 represents macroscopic displacement. Expression (2.27) asserts that the macroscopic problem is regarded as a two-dimensional (2-D) problem.

2.2.3.2 Order of ε^{-1}

By multiplying Eq. (2.23) by ε, and employing expressions (2.12) and (2.13) to take the limit as $\varepsilon \to 0^+$, following equation is obtained

$$\frac{1}{|Y|}\int_{\Omega}\int_{¥} C_{ijkl}\left[\frac{\partial u_k^0}{\partial y_l}\frac{\partial v_i}{\partial x_j}+\left(\frac{\partial u_k^0}{\partial x_l}+\frac{\partial u_k^1}{\partial y_l}-\alpha_{kl}\Delta T\right)\frac{\partial v_i}{\partial y_j}\right]dYd\Omega = \frac{1}{|Y|}\int_{\Omega}\int_{S} p_i v_i dSd\Omega \tag{2.28}$$

By choosing $\mathbf{v}=\mathbf{v}(\mathbf{x})$, and considering the expression (2.27), following statement is obtained

$$\int_{S} p_i v_i(\mathbf{x})dS = 0 \tag{2.29}$$

By choosing $\mathbf{v}=\mathbf{v}(\mathbf{y})$, and considering Eq. (2.29), following equation is obtained

$$\frac{1}{|Y|}\int_{\Omega}\int_{¥} C_{ijkl}\left[\left(\frac{\partial u_k^0(\mathbf{x})}{\partial x_l}+\frac{\partial u_k^1}{\partial y_l}-\alpha_{kl}\Delta T\right)\frac{\partial v_i(\mathbf{y})}{\partial y_j}\right]dYd\Omega = 0 \tag{2.30}$$

where u_k^1 denotes microscopic displacement which is obtained by involving the solution of variational problem [24] as follows

$$u_k^1(\mathbf{x},\mathbf{y}) = -\chi_k^{pq}(\mathbf{y})\frac{\partial u_p^0(\mathbf{x})}{\partial x_q}-\psi_k(\mathbf{y}) \tag{2.31}$$

where χ and ψ are the characteristic displacement vectors, or correctors, for elastic and thermal problem, respectively.
By substituting Eq. (2.31) into Eq. (2.30), following equation is obtained

$$\frac{1}{|Y|}\int_{\Omega}\int_{¥} C_{ijkl}\frac{\partial u_k^0(\mathbf{x})}{\partial x_l}\frac{\partial v_i(\mathbf{y})}{\partial y_j}dYd\Omega-\frac{1}{|Y|}\int_{\Omega}\int_{¥} C_{ijkl}\frac{\partial \chi_k^{pq}}{\partial y_l}\frac{\partial u_p^0(\mathbf{x})}{\partial x_q}\frac{\partial v_i(\mathbf{y})}{\partial y_j}dYd\Omega - \frac{1}{|Y|}\int_{\Omega}\int_{¥} C_{ijkl}\left(\frac{\partial \psi_k}{\partial y_l}+\alpha_{kl}\Delta T\right)\frac{\partial v_i(\mathbf{y})}{\partial y_j}dYd\Omega = 0 \tag{2.32}$$

Eq. (2.32) is microscopic equilibrium equation (1^{st} order) which can be expressed in a compact form as follows

$$\frac{1}{|Y|}\int_{\Omega}\int_{¥}\left[\begin{array}{c}\left(C_{ijkl}-C_{ijpq}\dfrac{\partial\chi_p^{kl}}{\partial y_q}\right)\dfrac{\partial u_k^0(\mathbf{x})}{\partial x_l}\\ -C_{ijpq}\left(\dfrac{\partial\psi_p}{\partial y_q}+\alpha_{pq}\Delta T\right)\end{array}\right]\frac{\partial v_i(\mathbf{y})}{\partial y_j}dYd\Omega=0 \qquad i,j,k,p,q=1,2,3;l=1,2 \tag{2.33}$$

Eq. (2.33) can be decoupled into two equations for separately calculating the elastic and thermal correctors (i.e. χ and ψ, respectively). Thus, the correctors are obtained by the following equations

$$\text{Elastic problem: }\int_{¥}\left(C_{ijkl}-C_{ijpq}\frac{\partial\chi_p^{kl}}{\partial y_q}\right)\frac{\partial v_i(\mathbf{y})}{\partial y_j}dY=0 \qquad i,j,k,p,q=1,2,3;l=1,2 \tag{2.34}$$

$$\frac{1}{|Y|}\int_{¥}\chi_p^{kl}dY=0 \tag{2.35}$$

$$\text{Thermal problem: }\int_{¥}C_{ijpq}\left(\frac{\partial\psi_p}{\partial y_q}+\alpha_{pq}\Delta T\right)\frac{\partial v_i(\mathbf{y})}{\partial y_j}dY=0 \qquad i,j,p,q=1,2,3 \tag{2.36}$$

$$\frac{1}{|Y|}\int_{¥}\psi_p dY=0 \tag{2.37}$$

2.2.3.3 Order of ε^0

By employing expression (2.12) to take the limit of Eq. (2.24) as $\varepsilon\to 0^+$, following equation is obtained

$$\frac{1}{|Y|}\int_{\Omega}\int_{¥} C_{ijkl}\left[\left(\frac{\partial u_k^0}{\partial x_l}+\frac{\partial u_k^1}{\partial y_l}-\alpha_{kl}\Delta T\right)\frac{\partial v_i}{\partial x_j}+\left(\frac{\partial u_k^1}{\partial x_l}+\frac{\partial u_k^2}{\partial y_l}\right)\frac{\partial v_i}{\partial y_j}\right]dYd\Omega = \frac{1}{|Y|}\int_{\Omega}\int_{¥} f_i v_i dYd\Omega+\int_{\Gamma_t} t_i v_i d\Gamma \tag{2.38}$$

By choosing $\mathbf{v}=\mathbf{v}(\mathbf{x})$, macroscopic equilibrium equation can be obtained as follows

$$\int_{\Omega}\left[\frac{1}{|Y|}\int_{¥} C_{ijkl}\left(\frac{\partial u_k^0(\mathbf{x})}{\partial x_l}+\frac{\partial u_k^1}{\partial y_l}-\alpha_{kl}\Delta T\right)dY\right]\frac{\partial v_i(\mathbf{x})}{\partial x_j}d\Omega = \int_{\Omega}\left(\frac{1}{|Y|}\int_{¥} f_i dY\right)v_i(\mathbf{x})d\Omega+\int_{\Gamma_t} t_i v_i(\mathbf{x})d\Gamma \tag{2.39}$$

Substitution of Eq. (2.31) into Eq. (2.39) yields the compact form of macroscopic equilibrium equations as follows

$$\int_{\Omega} C_{ijkl}^0(\mathbf{x})\frac{\partial u_k^0(\mathbf{x})}{\partial x_l}\frac{\partial v_i(\mathbf{x})}{\partial x_j}d\Omega = \int_{\Omega}\tau_{ij}(\mathbf{x})\frac{\partial v_i(\mathbf{x})}{\partial x_j}d\Omega+\int_{\Omega}\sigma_{ij}^t(\mathbf{x})\frac{\partial v_i(\mathbf{x})}{\partial x_j}d\Omega+ \int_{\Omega} b_i(\mathbf{x})v_i(\mathbf{x})d\Omega+\int_{\Gamma_t} t_i(\mathbf{x})v_i(\mathbf{x})d\Gamma \quad i,k,p,q=1,2,3;\ j,l=1,2 \tag{2.40}$$

where

$$C_{ijkl}^0(\mathbf{x})=\frac{1}{|Y|}\int_{¥}\left(C_{ijkl}-C_{ijpq}\frac{\partial \chi_p^{kl}}{\partial y_q}\right)dY \tag{2.41}$$

$$\tau_{ij}(\mathbf{x})=\frac{1}{|Y|}\int_{¥} C_{ijpq}\frac{\partial \psi_p}{\partial y_q}dY \tag{2.42}$$

$$\sigma_{ij}^t(\mathbf{x})=\frac{1}{|Y|}\int_{¥} C_{ijpq}\alpha_{pq}\Delta T dY \tag{2.43}$$

$$b_i(\mathbf{x}) = \frac{1}{|Y|}\int_{¥} f_i dY \tag{2.44}$$

By choosing $\mathbf{v} = \mathbf{v}(\mathbf{y})$, microscopic equilibrium equation (2^{nd} order) can be obtained as follows

$$\int_{¥} C_{ijkl}\left(\frac{\partial u_k^1}{\partial x_l} + \frac{\partial u_k^2}{\partial y_l}\right)\frac{\partial v_i(\mathbf{y})}{\partial y_j} dY = \int_{¥} f_i v_i(\mathbf{y}) dY \tag{2.45}$$

Chapter 3

Finite Element Formulation

3.1 Finite Element Formulation in Homogenization Scheme

3.1.1 Characteristic Displacement Vector

Characteristic displacement vectors, or correctors, for elastic and thermal problem (i.e. χ and ψ, respectively) are calculated by employing microscopic equilibrium equations (1^{st} order). In finite element viewpoint, the equations can be re-expressed in the vectors form as follows

$$\text{Elastic problem: } \int_{¥_n} \{\epsilon\}^T \{C\}_{kl} dY_n - \int_{¥_n} \{\epsilon\}^T [C] \{\dot{\chi}\}^{kl} dY_n = 0 \tag{3.1}$$

$$\text{Thermal problem: } \int_{¥_n} \{\epsilon\}^T [C] \{\dot{\psi}\} dY_n + \int_{¥_n} \{\epsilon\}^T [C] \{\alpha\} \Delta T dY_n = 0 \tag{3.2}$$

where

$$\{\dot{\chi}\}^{kl} = [B]\{\chi\}^{kl} \tag{3.3}$$

$$\{\dot{\psi}\} = [B]\{\psi\} \tag{3.4}$$

$$\{\epsilon\} = [B]\{v\} \tag{3.5}$$

where $[C]$ denotes the elastic constants matrix, $\{C\}_{kl}$ is the column 'kl' of matrix $[C]$, $[B]$ is the strain shape function matrix which is obtained by taking the derivatives of shape function matrix $[N]$, $\{v\}$ is the virtual displacement vector, $\{\chi\}^{kl}$ is the elastic corrector vector of mode 'kl', and $\{\psi\}$ is the thermal corrector vector. The symbol $¥_n$ indicates the n–th element of domain ¥.

By removing the virtual displacement vector $\{v\}$, Eqs. (3.1) and (3.2) can be expressed as follows

$$\text{Elastic problem: } \int_{¥_n} [B]^T[C][B]dY_n\{\chi\}^{kl} = \int_{¥_n} [B]^T\{C\}_{kl}dY_n \tag{3.6}$$

$$\text{Thermal problem: } \int_{¥_n} [B]^T[C][B]dY_n\{\psi\} = -\int_{¥_n} [B]^T[C]\{\alpha\}\Delta T dY_n \tag{3.7}$$

It is important to note that in Eq. (2.34), $l = 1, 2$, and according to the symmetric property of χ, calculation of elastic correctors results in three independent modes of χ, namely χ^{11}, χ^{22} and χ^{12}.

3.1.2 Periodic Boundary Condition

Calculation of correctors employs periodic boundary conditions which are applied on the surfaces of unit-cell normal to the in-plane directions. Top and bottom surfaces of the unit-cell are free boundaries which means both surfaces are independent from each other and may possess different deformation in terms of magnitude and direction. The aforementioned conditions can be mathematically expressed by the following statements

$$\{\chi\}^{kl}(0, y_2, y_3) = \{\chi\}^{kl}(Y_1, y_2, y_3) \tag{3.8}$$

$$\{\chi\}^{kl}(y_1, 0, y_3) = \{\chi\}^{kl}(y_1, Y_2, y_3) \tag{3.9}$$

$$\{\chi\}^{kl}(y_1, y_2, 0) \neq \{\chi\}^{kl}(y_1, y_2, Y_3) \tag{3.10}$$

where Y_1, Y_2 and Y_3 are the unit-cell dimension in direction-1, -2 and -3, respectively. The inequality represented in expression (3.10) indicates that the top and bottom surfaces of the unit-cell are independent from each other. It is important to note that expressions (3.8)-(3.10) are also valid for the thermal correctors by means of replacing $\{\chi\}^{kl}$ with $\{\psi\}$.

3.1.3 Homogenized Thermomechanical Properties

Homogenized elastic constants are calculated by using Eq. (2.41). In finite element viewpoint, Eq. (2.41) can be expressed in the 'kl' column of the matrix of $[C]$ as follows

$$\{C^0\}_{kl} = \sum_n \frac{1}{|Y|} \int_{¥_n} \{C\}_{kl} - [C][B]\{\chi\}^{kl} dY \tag{3.11}$$

Homogenized coefficient of thermal expansion is calculated by employing the following equation

$$\alpha^0_{kl} = \frac{S^0_{ijkl}}{\Delta T} \left[\frac{1}{|Y|} \int_{¥} C_{ijpq} \left(\frac{\partial \psi_p}{\partial y_q} + \alpha_{pq} \Delta T \right) dY \right] \tag{3.12}$$

or in the matrix and vector forms as follows

$$\{\alpha^0\} = \frac{[S^0]}{\Delta T} \sum_n \frac{1}{|Y|} \int_{¥_n} [C]([B]\{\psi\} + \{\alpha\}\Delta T) dY \tag{3.13}$$

where $[S^0]$ is homogenized compliance matrix, i.e. inverse of homogenized elastic constants matrix $[C^0]$. It is important to note that in Eq. (2.40), subscripts 'j, l' = $1, 2$ and in accordance with the symmetry of stresses and strain energy densities [43], the formulation consequently results in the in-plane homogenized thermomechanical properties.

3.2 Finite Element Formulation in Localization Scheme

3.2.1 Calculation of Stresses

Stresses acting on each point of domain can be calculated by following equation

$$\sigma^{\varepsilon}_{ij} = C_{ijkl} \left(\frac{\partial u^{\varepsilon}_k}{\partial x_l} - \alpha_{kl} \Delta T \right) \tag{3.14}$$

By incorporating the actual displacement u_k^{ε} stated in Eq. (2.20) and its derivatives into Eq. (3.14), following equation is obtained

$$\sigma_{ij}^{\varepsilon} = C_{ijkl}\left[\left(\frac{\partial u_k^0}{\partial x_l} + \frac{\partial u_k^1}{\partial y_l} - \alpha_{kl}\Delta T\right) + \varepsilon\left(\frac{\partial u_k^1}{\partial x_l} + \frac{\partial u_k^2}{\partial y_l}\right) + \varepsilon^2(...)\right] \tag{3.15}$$

Eq. (3.15) can be re-expressed in an asymptotic form as follows

$$\sigma_{ij}^{\varepsilon} = \sigma_{ij}^0 + \varepsilon\sigma_{ij}^1 + \varepsilon^2(...) \tag{3.16}$$

where σ_{ij}^0 denotes the first approximation of stresses. By substituting Eq. (2.31) into the first approximation of stresses, following equation is obtained

$$\sigma_{ij}^{\varepsilon} \approx \sigma_{ij}^0(\mathbf{x},\mathbf{y}) = \left(C_{ijkl} - C_{ijpq}\frac{\partial \chi_p^{kl}}{\partial y_q}\right)\frac{\partial u_k^0}{\partial x_l} - C_{ijpq}\frac{\partial \psi_p}{\partial y_q} - C_{ijpq}\alpha_{pq}\Delta T \tag{3.17}$$

In finite element viewpoint, the first approximation of stress can be expressed as follows

$$\{\sigma^0\} = \left[[C]_{kl} - [C][B][\chi]^{kl}\right][B]\{u^0\} - [C][B]\{\psi\} - [C]\{\alpha\}\Delta T \tag{3.18}$$

or

$$\{\sigma^0\} = \left[[C]_{kl} - [C][B][\chi]^{kl}\right]\{e^0\} - [C][B]\{\psi\} - [C]\{\alpha\}\Delta T \tag{3.19}$$

where $\{e^0\} = [B]\{u^0\}$. It is noted that in present method, $\{\chi\}^{33} = \{\chi\}^{23} = \{\chi\}^{31} = 0$ and $e_{33}^0 = e_{23}^0 = e_{31}^0 = 0$ since macroscopic model analysis is a two-dimensional problem. In Eq. (3.19), subscript and superscript 'kl' indicate that the matrix arrangements are based on column 'kl'.

Homogenized stresses of the unit-cell σ_{ij}^H is calculated by using the following equation

$$\sigma_{ij}^{H} = C_{ijkl}^{0}\left(\frac{\partial u_k^0}{\partial x_l} - \alpha_{kl}^{0}\Delta T\right) \tag{3.20}$$

Relationship between σ_{ij}^{H} and σ_{ij}^{0} can be established by employing averaging operators to Eq. (3.17) as follows

$$\begin{aligned}\frac{1}{|Y|}\int_{¥}\sigma_{ij}^{0}dY = \frac{1}{|Y|}\int_{¥}\left(C_{ijkl} - C_{ijpq}\frac{\partial\chi_p^{kl}}{\partial y_q}\right)dY\frac{\partial u_k^0}{\partial x_l} - \\ \frac{1}{|Y|}\int_{¥}C_{ijpq}\frac{\partial\psi_p}{\partial y_q}dY - \frac{1}{|Y|}\int_{¥}C_{ijpq}\alpha_{pq}\Delta T dY\end{aligned} \tag{3.21}$$

By substituting Eqs. (2.41) and (3.12) into Eq. (3.20), the same results as those of the right hand side of Eq. (3.21) are obtained. The relationship between σ^H and σ^0 is thus expressed in finite element viewpoint as follows

$$\{\sigma^H\} = \sum_n \frac{1}{|Y|}\int_{¥_n}\{\sigma^0\}dY \tag{3.22}$$

Chapter 4

Case Studies and Results

4.1 2-D Laminated Composites

4.1.1 Numerical Model

Unit-cell of 2-D laminated composites is schematically depicted in Fig. 4.1. In this figure, the composite is composed of several plies with certain orientation based on the longitudinal direction of fiber phase. Stacking sequence of the plies is defined by ordering every ply from the top to the bottom. There are two models of 2-D laminated composites utilized in the analysis. Model 1 has 20 plies with the stacking sequence of $[+45/90/\text{-}45/0_2/+45/90_2/\text{-}45/0]_S$; and Model 2 is 8-ply laminated composite with the stacking sequence of $[\pm 45/0/90]_S$.

Model 1 is composed of plies utilizing carbon fiber T-800 as the fiber phase and epoxy XNR/H6813 as the resin phase. The model uses V_{ft} (i.e. fiber volume fraction of tow/ply) of 45% for every ply [44]. Model 2 utilizes carbon fiber T-300 as the fiber phase, while the resin phase is epoxy EP828. The V_{ft} of all plies of this model is 55%. It is noted that the equivalent properties of each ply are calculated by standard homogenization method with 3-D periodicity utilizing a micro-scale unit-cell

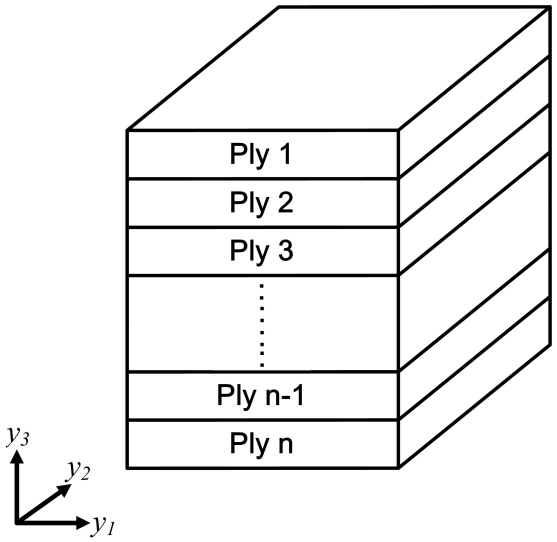

FIGURE 4.1: Schematic unit-cell model of 2-D laminated composites and ply numbering sequence

model consisting fiber and matrix phases arranged in hexagonal array. Thermomechanical properties of carbon fiber T-800 [44, 45], carbon fiber T-300 [44, 46], epoxy XNR/H6813 [44] and epoxy EP828 [47, 48] are given in Table 4.1. Subscripts 'L' and 'T' denote longitudinal and transverse directions of fiber phase, respectively. It is noted that the properties of fiber phases are assumed transversely isotropic.

TABLE 4.1: Thermomechanical properties of carbon fibers and epoxy resins

Properties	Carbon fiber T-800	Carbon fiber T-300	Epoxy XNR/H6813	Epoxy EP828
E_L (GPa)	294	220	8.96	3.4
E_T (GPa)	6.5	13.8	8.96	3.4
G_{LT} (GPa)	18.2	11.35	3.45	1.26
G_{TT} (GPa)	6.5	5.5	3.45	1.26
ν_{LT}	0.32	0.2	0.35	0.35
ν_{TT}	0.41	0.25	0.35	0.35
α_L (/°C)	-5.6×10^{-7}	-4.1×10^{-7}	6.5×10^{-5}	6.45×10^{-5}
α_T (/°C)	5.6×10^{-6}	5.6×10^{-6}	6.5×10^{-5}	6.45×10^{-5}

4.1.2 Homogenization Analysis

4.1.2.1 Homogenized Thermomechanical Properties

As described in Section 3.1.3, the present homogenization analysis results in in-plane homogenized thermomechanical properties, viz. Young's moduli of E_1 and E_2, shear modulus of G_{12}, Poisson's ratio of ν_{12} and coefficients of thermal expansion of α_1 and α_2. The homogenized in-plane thermomechanical properties of both models of 2-D laminated composites are listed in Table 4.2. It is important to note that subscript '1' denotes longitudinal direction of composite structure, while subscripts '2'and '3' denote transverse orientation of composite structure in in-plane and out-of-plane directions, respectively. In order to investigate the influence of relieving periodicity in the thickness direction of the unit-cell to the homogenized thermomechanical properties, the results of both standard (3-D periodicity) and present (2-D periodicity) analyses are given. The results show that the influence of relieving periodic boundary condition on the top and bottom surfaces of the unit-cell is insignificant in the case of 2-D laminated composites. This is revealed by the same outcomes from both models obtained by standard and present analyses.

TABLE 4.2: Homogenized thermomechanical properties of 2-D laminated composites

Properties	Model 1		Model 2	
	Standard Analysis	Present Analysis	Standard Analysis	Present Analysis
E_1 (GPa)	58.45	58.45	45.85	45.85
E_2 (GPa)	58.45	58.45	45.85	45.85
G_{12} (GPa)	16.69	16.69	16.62	16.62
ν_{12}	0.231	0.231	0.315	0.315
α_1 (/°C)	5.67×10^{-6}	5.67×10^{-6}	3.12×10^{-6}	3.12×10^{-6}
α_2 (/°C)	5.67×10^{-6}	5.67×10^{-6}	3.12×10^{-6}	3.12×10^{-6}

The homogenized thermomechanical properties obtained from homogenization analysis are validated with those obtained by analytical calculation in Refs. [49, 50].

TABLE 4.3: Homogenization and analytical results

Properties	Homogenization	Analytic
E_1 (GPa)	58.45	58.45
G_{12} (GPa)	16.69	16.69
ν_{12}	0.231	0.231
α_L (/°C)	5.67×10^{-6}	5.67×10^{-6}

The comparison between homogenization and analytical results is presented in Table 4.3. In this table, homogenized thermomechanical properties (i.e. E_1, G_{12}, ν_{12}, α_1) of Model 1 are utilized to perform numerical validation. It is noted that the homogenization analysis yields the same results between the standard and present methods (see Table 4.2). The results presented in Table 4.3 exhibit excellent agreements between homogenization and analytical results, whereby the same outcomes are obtained in the results of elastic moduli, Poisson's ratio as well as coefficient of thermal expansion. This fact emphasizes that homogenization can be deemed an excellent method in obtaining equivalent properties of 2-D laminated composites.

4.1.3 Localization Analysis

Localization analysis employs an infinite macroscopic model as shown in Fig. 4.2(a). In this figure, the dash-dotted lines indicate that the macroscopic model is infinite in both in-plane directions (x_1 and x_2). The macroscopic model utilizes the homogeneous properties obtained by homogenization analysis of the unit-cell model of 2-D laminated composite. Localization analysis necessitates macroscopic strain (e^0) in the calculation of stress responses within the unit-cell. The strain has a role in transferring the structural response due to external loading applied on macroscopic model into unit-cell representation. In the analysis, Model 2 is employed, and the stress responses are investigated by extracting the stresses along a representative line intersecting the thickness of unit-cell (i.e. Line A) as shown in Fig. 4.2(d).
In essence, localization analysis obtains six components of stresses. However, stress distributions of σ_{11} and σ_{22} are chosen as the representatives of the dominant stress

in thermal loading case, while the results of biaxial loading case are represented by σ_{11} and τ_{12}. Stress distributions along Line A due to application of thermal and biaxial loading are respectively presented in Figs. 4.3 and 4.4. In the figures, the vertical axis indicates normalized thickness coordinate (y_3/h), where h is the thickness of macroscopic model ($h = 2$ mm). The corresponding ply orientations along the thickness direction of the unit-cell are described in the right side of the figures.

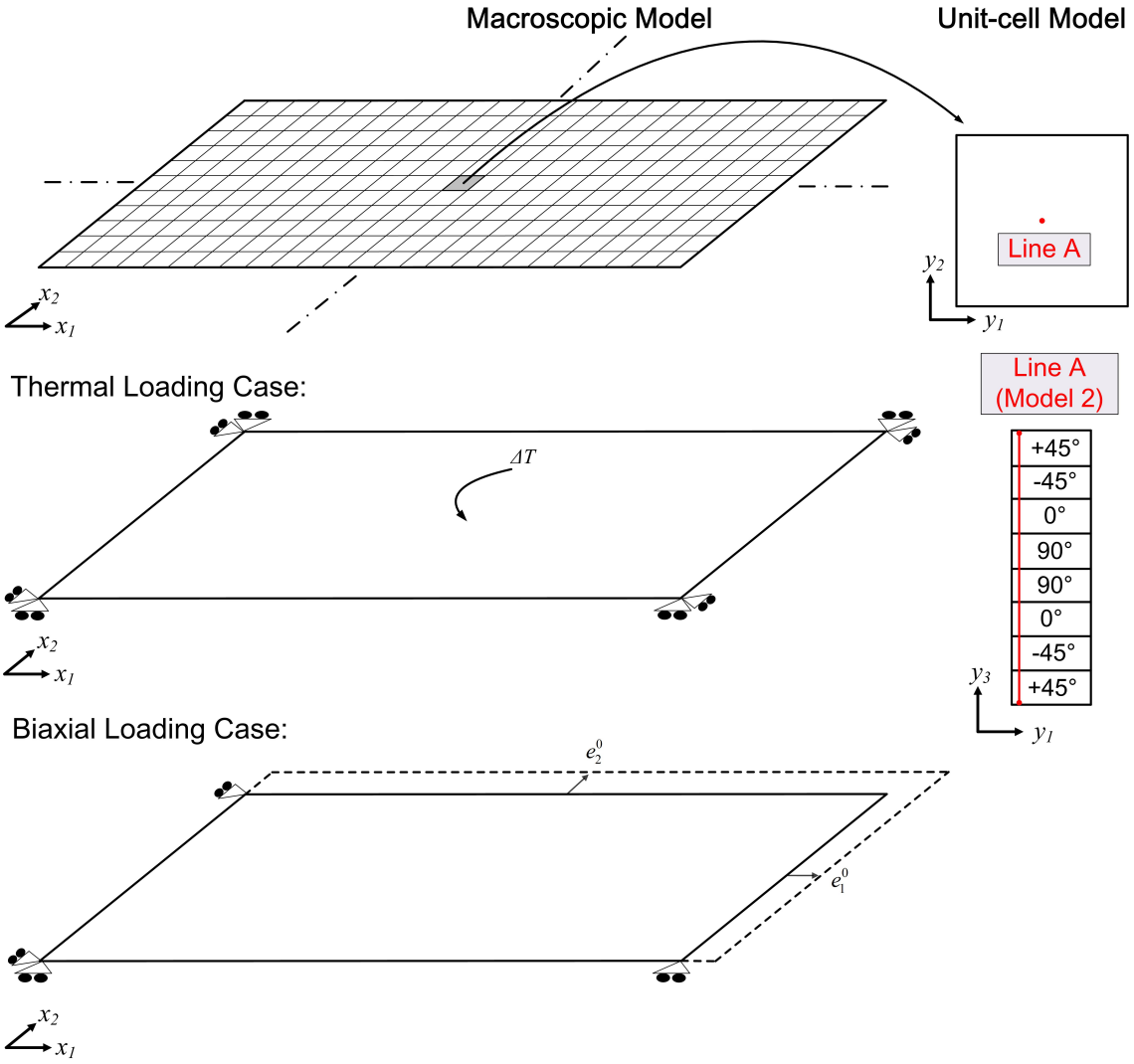

FIGURE 4.2: Localization analysis: (a) homogeneous macroscopic model, (b) thermal loading case, (c) biaxial tension loading case, (d) representative line of Model 2

4.1.3.1 Stresses due to Thermal Loading

In thermal loading case, the homogeneous macroscopic model is subjected to temperature difference ΔT of -130 °C and constrained in order not to move in the in-plane direction as shown in Fig. 4.2(b). It is noted that the top and bottom of its surfaces are free-traction boundaries. In present analysis, this condition is represented by $e^0_{11} = e^0_{22} = e^0_{12} = 0$. Meanwhile, standard analysis regards the macroscopic model analysis as three-dimensional problem. Therefore, in order to calculate all macroscopic strain components of the homogeneous infinite macroscopic model, the following equation is utilized

$$\sigma^M_{ij} = C^0_{ijkl}(e^0_{kl} - \alpha^0_{kl}\Delta T) \tag{4.1}$$

where σ^M denotes the stresses acting on the macroscopic model, C^0_{ijkl} is homogenized elastic constants, e^0_{kl} is macroscopic strain and α^0_{kl} is homogenized coefficients of thermal expansion. In thermal loading case described in Fig. 4.2(b), $e^0_{11} = e^0_{22} = e^0_{23} = e^0_{31} = e^0_{12} = 0$ and $\sigma^M_{33} = 0$ (due to free-traction boundaries on the top and bottom surfaces). Thus, e^0_{33} is obtained as -7.29×10^{-3}.

The stress responses within the unit-cell of Model 2, obtained from both present and standard analyses, are validated by those of analytical analysis based on classical laminate theory (CLT). The stress responses are displayed in Fig. 4.3. The figure shows that the present analysis results of σ_{11} and σ_{22} coincide with those of standard analysis. This indicates that relieving periodicity in the thickness direction of the unit-cell yields negligible effects in the stress calculation of 2-D laminated composite due to application of temperature difference. Regarding to the comparison with analytical results, excellent agreements are noticed between the stress results obtained by localization analysis and CLT. This fact indicates that localization analysis obtains reasonable results.

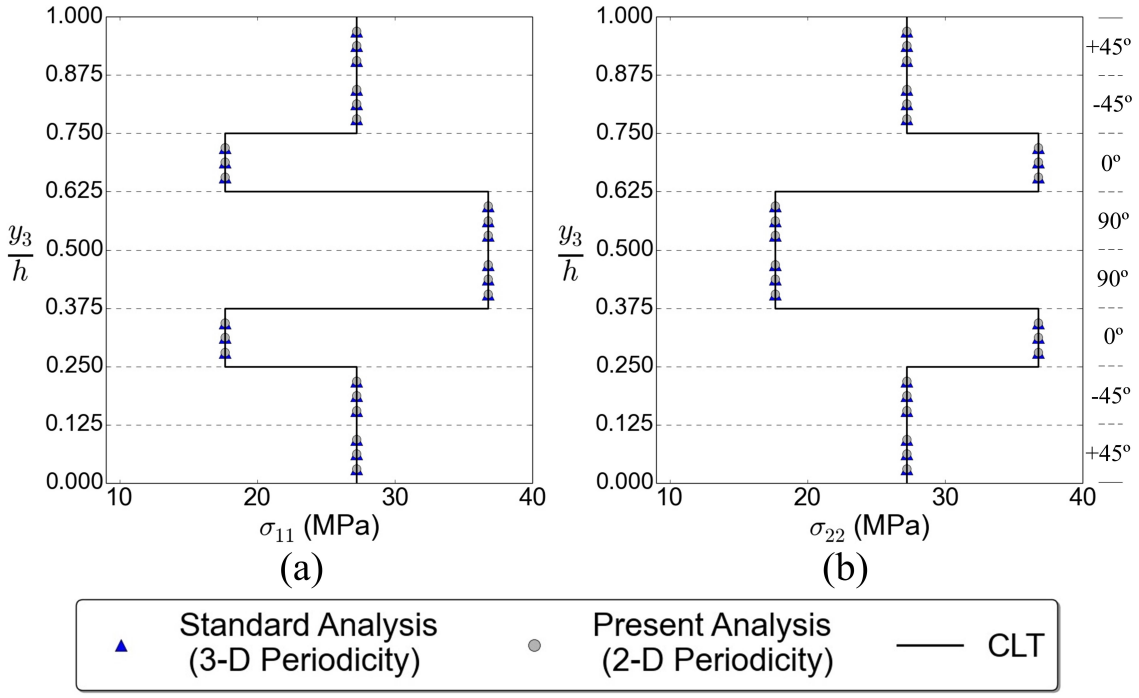

FIGURE 4.3: Stresses along the thickness of Model 2 due to thermal loading

4.1.3.2 Stresses due to Mechanical Loading

In mechanical loading case, the macroscopic model is subjected to biaxial tensile loading which is schematically depicted in Fig. 4.2(c). This loading case is represented by macroscopic strain of $e^0_{11} = 1{\times}10^{-3}$ and $e^0_{22} = 5{\times}10^{-4}$. In present analysis $e^0_{33} = 0$ is given when calculating the stress responses, while in standard analysis e^0_{33} = -5.94×10^{-4} is obtained by Eq. (4.1) whereby $\sigma^M_{33} = 0$ as the representative of the free-traction boundaries on the top and bottom surfaces. It is noted that in mechanical loading case, ΔT is zero due to nonexistence of temperature difference. The obtained stress responses are shown in Fig. 4.4. The figure elucidates that, similar with the results of thermal loading case, standard and present analyses yield the same stresses outcomes. This fact asserts that, in the case of 2-D laminated composites, standard localization analysis is deemed as a sufficient analysis for the calculation of stresses within the unit-cell. In Fig. 4.4, it is also shown that the results of localization analysis and CLT are in excellent agreements.

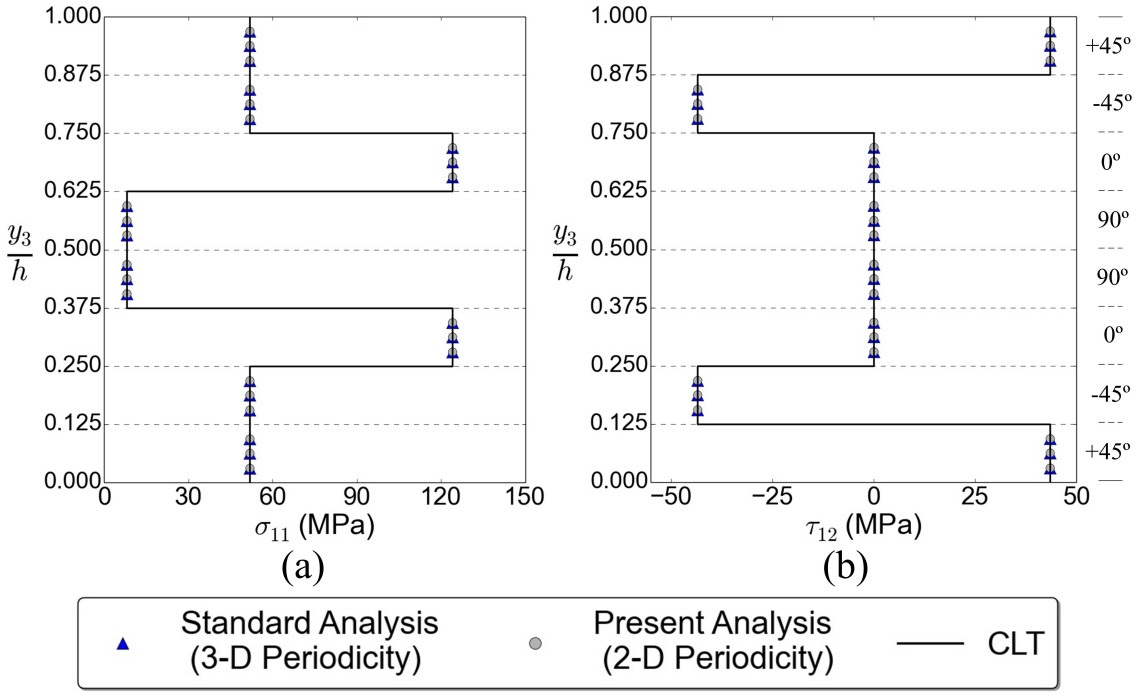

FIGURE 4.4: Stresses along the thickness of Model 2 due to biaxial loading

4.2 Brick Composites

4.2.1 Numerical Model

Fig. 4.5 shows the schematic model of unit-cell of brick composites. The unit-cell consists of 8 bricks arranged in an alternating pattern. Two kinds of materials are employed whereby blue and white bricks represent Material 1 and Material 2, respectively. In the analysis, two models are utilized. Model 1 utilizes Al 7075-T6 as Material 1 and AISI 302 Stainless Steel as Material 2; Model 2 utilizes Al 7075-T6 as Material 1 and Al 2024-T3 as Material 2. Thermomechanical properties of Al 7075-T6 [51], Al 2024-T3 [52] and AISI 302 Stainless Steel [53] are given in Table 4.4.

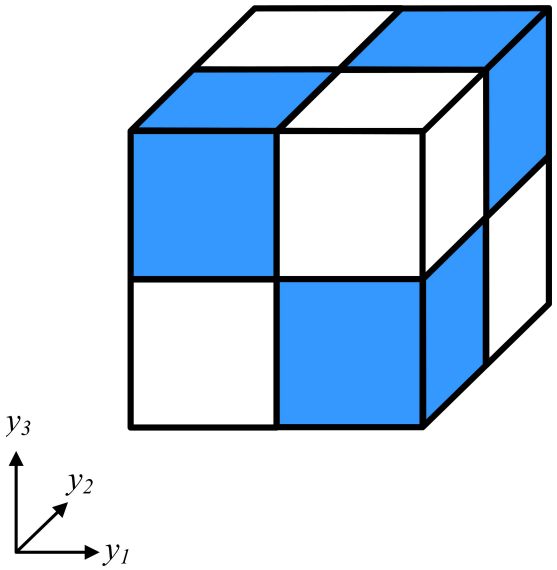

FIGURE 4.5: Schematic unit-cell model of brick composites

TABLE 4.4: Thermomechanical properties of aluminum and steel phases

Properties	Al 7075-T6	Al 2024-T3	AISI 302
E (GPa)	71.7	73.1	193
G (GPa)	26.9	28	77.2
ν	0.33	0.33	0.25
α (/°C)	2.36×10^{-5}	2.32×10^{-5}	1.78×10^{-5}

4.2.2 Homogenization Analysis

4.2.2.1 Characteristic Displacement Vector

As described in Section 3.1.1, three modes of elastic correctors (χ^{11}, χ^{22} and χ^{12}) and thermal corrector (ψ) are obtained by the present homogenization analysis. The elastic and thermal correctors of brick composites are presented in Fig. 4.6. In this figure, the correctors are based on the results of Model 1. The contour elucidates the distribution of normalized characteristic displacement magnitude with respect to the maximum value of each mode.

Fig. 4.6 may not be able to clearly show the different deformation on the top and bottom surfaces of the unit-cell resulted from present analysis. In order to better understand the present deformation of correctors, the result of χ^{11} is again shown

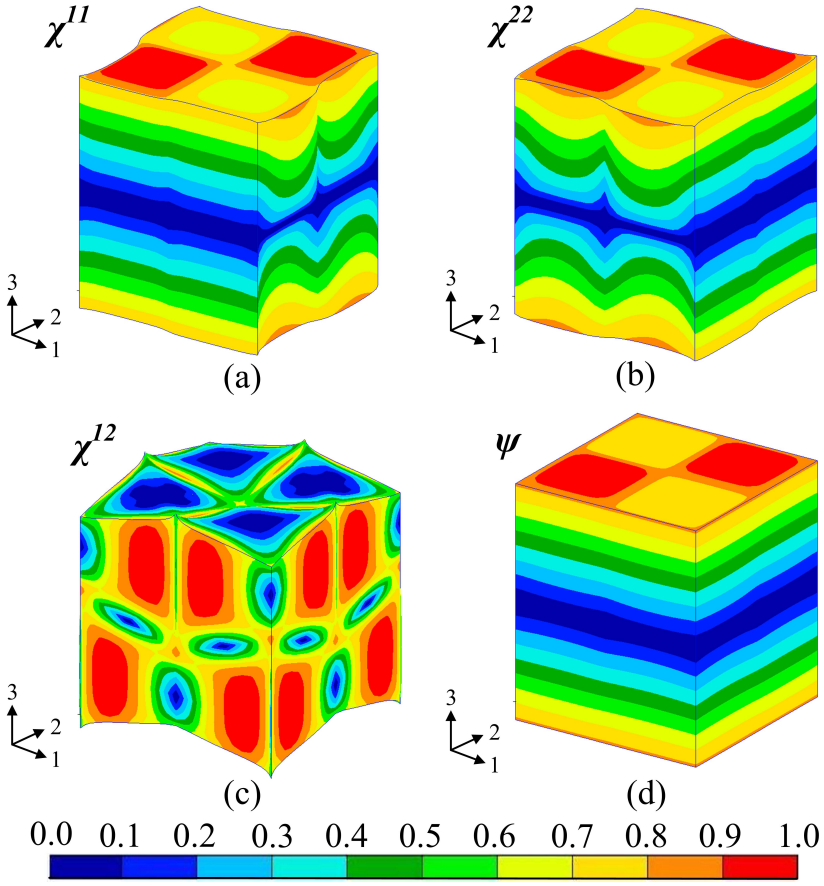

FIGURE 4.6: Correctors of brick composites: (a) χ^{11}, (b) χ^{22}, (c) χ^{12}, (d) ψ

in Fig. 4.7. In this figure, the corrector is given in its undeformed shape for the sake of simplicity in showing the magnitude. In Fig. 4.7(c), it can be seen that the magnitude of corrector on the top and bottom surfaces are different between each other. This fact is different with the results of corrector on the surfaces normal to the in-plane directions shown in Figs. 4.7(a) and (b). The different corrector magnitudes between top and bottom surfaces ensure that the periodicity in the thickness direction has been successfully relieved.

4.2.2.2 Homogenized Thermomechanical Properties

Table 4.5 lists the homogenized in-plane thermomechanical properties of brick composites. In this table, the results of Model 1 and Model 2 are given. The same

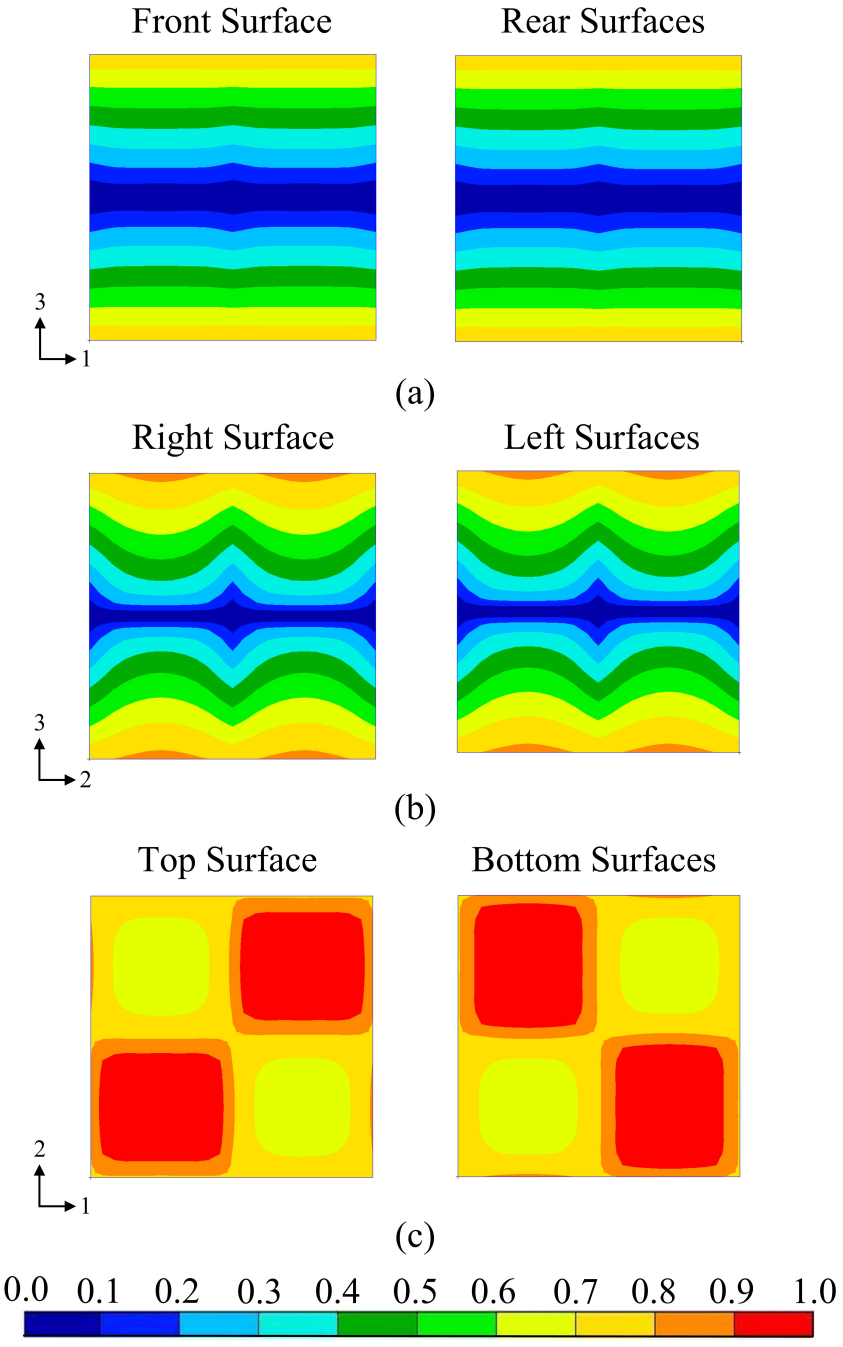

FIGURE 4.7: Corrector of brick composites (χ^{11}): (a) periodic in direction -1, (b) periodic in direction -2, (c) non-periodic in direction -3

homogenized properties in directions -1 and -2 are induced by the isotropic property of both utilized materials. In Table 4.5, the results of both standard and present analyses are given. The results elucidate that relieving periodicity in the thickness direction is significant especially for the results of elastic moduli (E_1 and E_2) as well as ν_{12} of Model 1, whereby the differences of about 2-5% are noted. Nevertheless, Model 2 shows nearly same outcomes for all homogenized thermomechanical properties. This is due to the similar values of thermomechanical properties between Al 7075-T6 and Al 2024-T3, which make Model 2 tends to equalize the behavior of 2-D laminated composites with uniform material configuration in the in-plane direction. These aforementioned facts show the necessity of employing present homogenization analysis with 2-D periodicity when non-uniformity exists in the in-plane direction of composites.

TABLE 4.5: Homogenized thermomechanical properties of brick composites

Properties	Model 1			Model 2		
	Standard Analysis	Present Analysis	Diff. (%)	Standard Analysis	Present Analysis	Diff. (%)
E_1 (GPa)	117.8	114.7	2.67	72.4	72.39	0.01
E_2 (GPa)	117.8	114.7	2.67	72.4	72.39	0.01
G_{12} (GPa)	46.51	46.09	0.91	27.45	27.44	0.04
ν_{12}	0.292	0.308	5.50	0.330	0.330	0.00
α_1 (/°C)	2.03×10^{-5}	2.04×10^{-5}	0.29	2.34×10^{-5}	2.34×10^{-5}	0.00
α_2 (/°C)	2.03×10^{-5}	2.04×10^{-5}	0.29	2.34×10^{-5}	2.34×10^{-5}	0.00

4.2.3 Localization Analysis

Similar with 2-D laminated composites case, two loading cases (i.e. thermal loading and biaxial tension loading) are subjected to the infinite macroscopic model shown in Fig. 4.2(a). The macroscopic model utilizes homogeneous properties of brick composites obtained from homogenization analysis. Schematic representations of the two loading cases are given in Figs. 4.2(b) and (c). In this localization analysis, Model 1 is employed, and stress responses along two representatives lines (i.e. Lines A and B) are extracted to investigate the influence of relieving periodicity in the

thickness direction. Fig. 4.8 shows the location of two representative lines within the unit-cell as well as the corresponding unit-cell constituents.

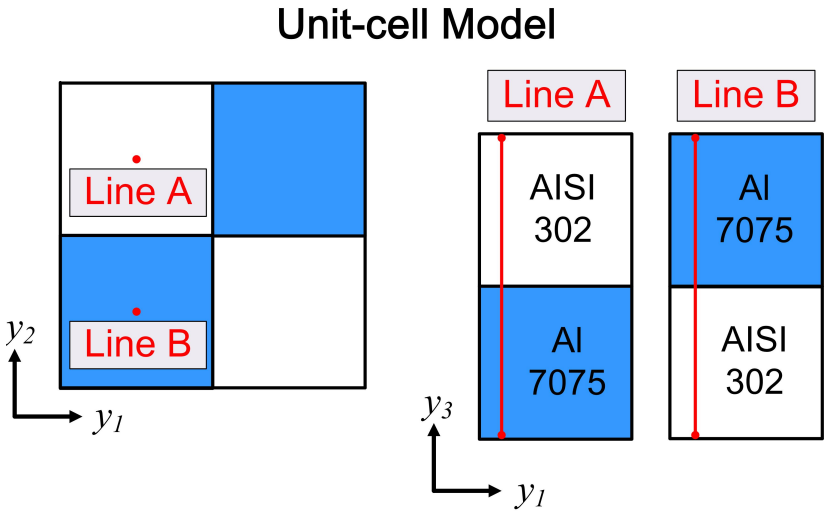

FIGURE 4.8: Localization analysis of brick composites: two representative lines of unit-cell model (Model 1)

4.2.3.1 Stresses due to Thermal Loading

In thermal loading case, temperature difference ΔT of -130 °C is given to the homogeneous macroscopic model. Present analysis utilizes macroscopic strain of $e^0_{11} = e^0_{22} = e^0_{12} = 0$ to represent the responses of macroscopic model, while in standard analysis e^0_{33} of -4.83×10^{-3} is also given to represent the free-traction boundary condition on the top and bottom surfaces of 3-D homogeneous macroscopic model. The macroscopic strain values are calculated based on Eq. (4.1).

In this analysis, stress responses within the unit-cell of Model 1, obtained from both present and standard analyses, are validated by a comparable finite element analysis. A finite element model is built by combining 49 unit-cells to establish a 7×7-cell brick composite model. The boundary condition represented in Fig. 4.2(b) is then given to the 7×7-cell FE model. Fig. 4.9(a) shows the results of FE analysis in terms of σ_{11} whereby the stress distribution is concisely seen to better approximate the result of present analysis shown in Fig. 4.9(c) than that of standard analysis

in Fig. 4.9(b). It is noteworthy that localization analysis substantively produces a rigorous accuracy for infinite problem.

In Fig. 4.9(a), the stress responses obtained by FE analysis shows periodic behavior (i.e. repeating stress pattern) in both in-plane directions (direction -1 and -2), with the exception on the stresses nearby outer boundary. A deeper investigation is performed by extracting the stresses along Lines A and B. In this regard, the results of localization analysis are compared by those of FE analysis within the cells inside red box (see Fig. 4.9(a)). For σ_{11} and σ_{22}, the results of FE analysis and present analysis are in a better agreement as compared to those of standard analysis, albeit both present and standard localization analyses obtain nearly similar values. Nevertheless, a good agreement between the results of FE analysis and present analysis is clearly noted in the result of σ_{33} as shown in Figs. 4.10(b) and (d). In these figures, standard analysis cannot obtain stress results that approximate those of FE analysis. The aforementioned facts indicate that relieving periodicity in the thickness direction of the unit-cell affects the stress calculation of brick composites due to application of temperature difference.

Some parametric studies are performed in order to understand the effectiveness of FE modeling in the validation of localization analysis results. The first study is done by varying number of elements of each FE model cell. In this study, 7×7-cell brick composite model are employed whereby number of elements of each cell is varied by 64, 512 and 1728 elements. It is noted that the localization analysis utilizes a unit-cell model with 1728 elements. Fig. 4.11 shows the stresses along Line A of the cell. From this figure, number of elements exhibits significant effects to the obtained stresses results. The stresses obtained from model with fewer number of elements (i.e. 64 and 512 elements) are different with the results of present localization analysis, particularly for σ_{33}. From Fig. 4.11, the best agreement is noticed in the results of FE model with the same number of unit-cell elements (i.e. 1728 elements).

A parametric study by varying number of cells is also performed. In this regard, FE models with 3×3-cell, 5×5-cell and 7×7-cell are built whereby each model has

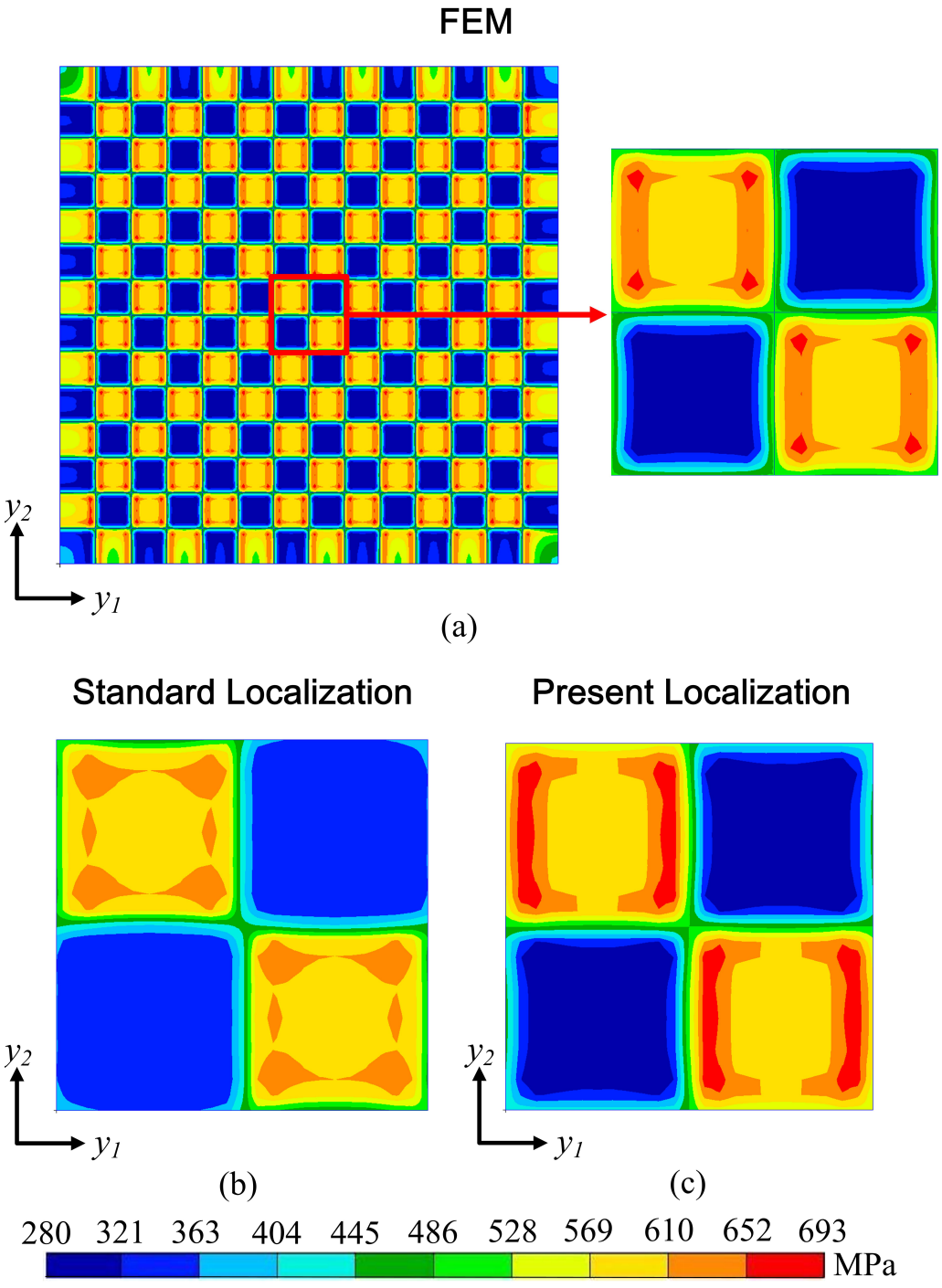

FIGURE 4.9: Stress σ_{11}: (a) FEM, (b) standard localization, (c) present localization

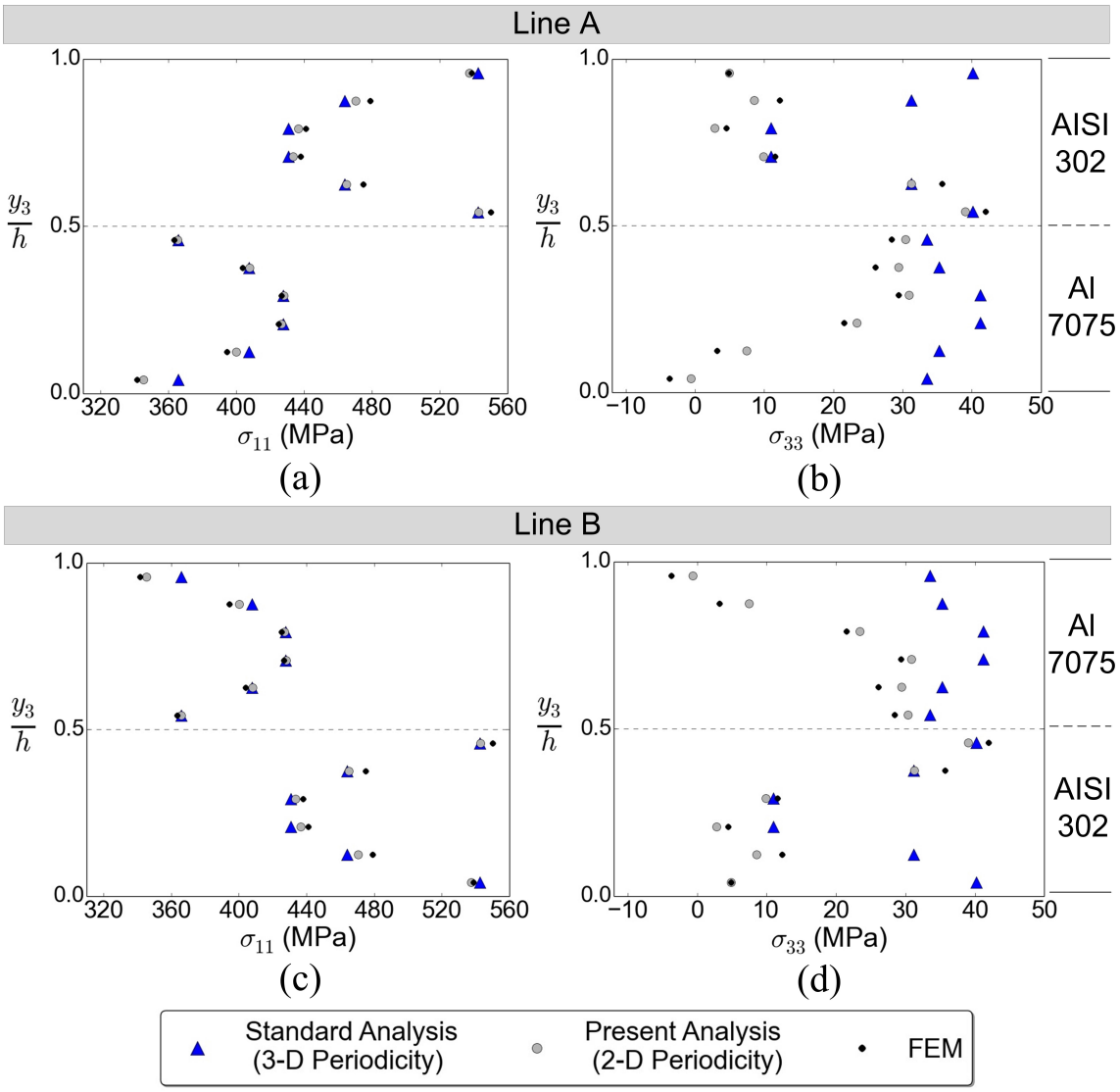

FIGURE 4.10: Stresses along Lines A and B due to thermal loading

1728 elements. Stresses along Line A of the center cell are extracted and listed in Table 4.6. The obtained results show that the increment of number of cells does not significantly affect the stresses within the center cell of FE model. The aforementioned parametric studies assert that number of elements of FE model plays a more important role than number of cells in the numerical validation of localization analysis using FE analysis.

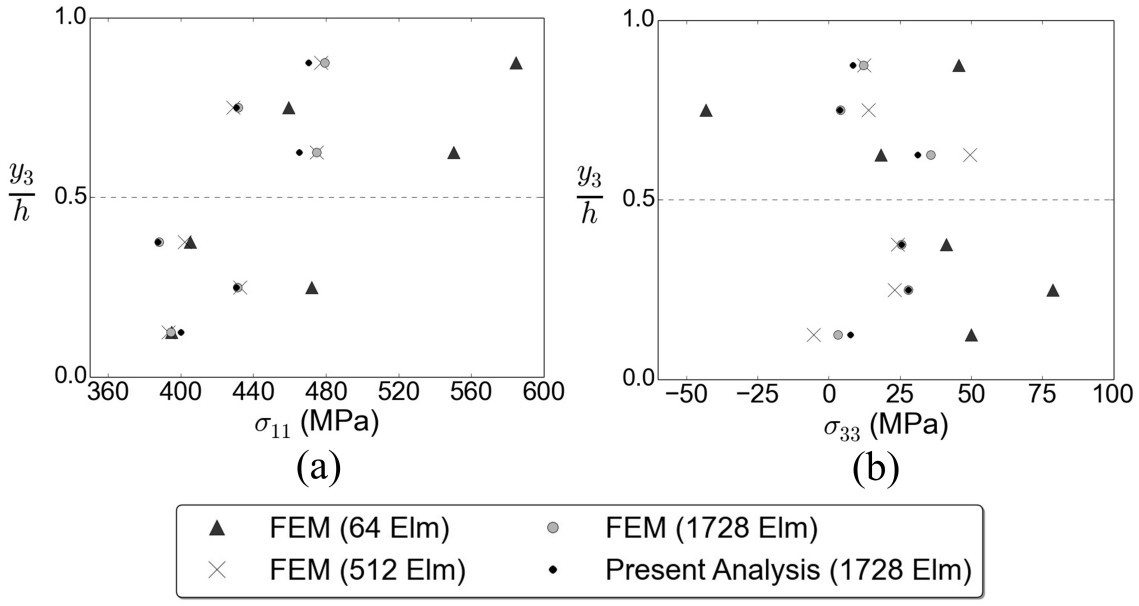

FIGURE 4.11: Influence of FEM number of elements on the stresses results

TABLE 4.6: Influence of FEM number of cells on the stresses results

y_3/h	FEM 3×3 cell	FEM 5×5 cell	FEM 7×7 cell
	σ_{11} (MPa)	σ_{11} (MPa)	σ_{11} (MPa)
0.125	395.78	394.88	394.52
0.250	432.76	431.83	431.45
0.375	405.07	404.23	403.88
0.625	476.72	475.42	474.89
0.750	433.51	432.27	431.79
0.875	481.07	479.69	479.18

4.2.3.2 Stresses due to Mechanical Loading

In mechanical loading case, the analysis utilizes macroscopic strain of $e^0_{11} = 1\times10^{-3}$ and $e^0_{22} = 5\times10^{-4}$ to represent biaxial tension loading subjected to the macroscopic model. In present analysis $e^0_{33} = 0$ is given when calculating the stress responses, while in standard analysis e^0_{33} = -6.19×10^{-4} is given to represent the free-traction boundaries on the top and bottom surfaces.

In this analysis, the stress responses obtained from both present and standard analyses are also validated by a comparable finite element analysis employing 7×7-cell brick composite model. The model is subjected to in-plane macroscopic strain (i.e.

$e^0_{11} = 1\times10^{-3}$ and $e^0_{22} = 5\times10^{-4}$) with boundary condition represented in Fig. 4.2(c). Similar with the results of thermal loading case, Fig. 4.12 shows that the stress distribution obtained from FE analysis has a better agreement with that of present analysis. In order to understand the stress responses throughout the thickness direction, Fig. 4.13 presents the stresses obtained by localization and FE analyses. The numerical validation shown in Fig. 4.13 elucidates that present analysis can obtain stress results with good approximation with those of FE analysis. Meanwhile, standard analysis cannot obtain stress results which represent the real condition whereby free-traction boundaries are given on the top and bottom surfaces of macroscopic model.

A mechanical loading case implementing pure shear load is also performed. In this case, the analysis utilizes macroscopic strain of $e^0_{12} = 4\times10^{-4}$. A numerical validation is conducted by means of a finite element analysis employing 7×7-cell brick composite model with boundary condition represented in Fig. 4.14.

Similar with the results of previous loading cases, Fig. 4.15 shows that the stress distributions τ_{12} obtained through present localization and FE analyses are in a good agreement. It is noted here that localization analysis should obtain more accurate results due to its effectiveness in modeling pure shear loading without any rotation. In order to better understand the stress responses throughout the thickness direction, Table 4.7 lists the stresses obtained by localization and FE analyses. From this table, present analysis results clearly show better approximations with those obtained by FE analysis whereby the differences between both analyses are less than 1%. Meanwhile, standard analysis cannot obtain accurate results particularly in the region nearby top and bottom surfaces. These again indicate that relieving periodicity in the thickness direction of the unit-cell is necessary in the stress calculation of brick composites.

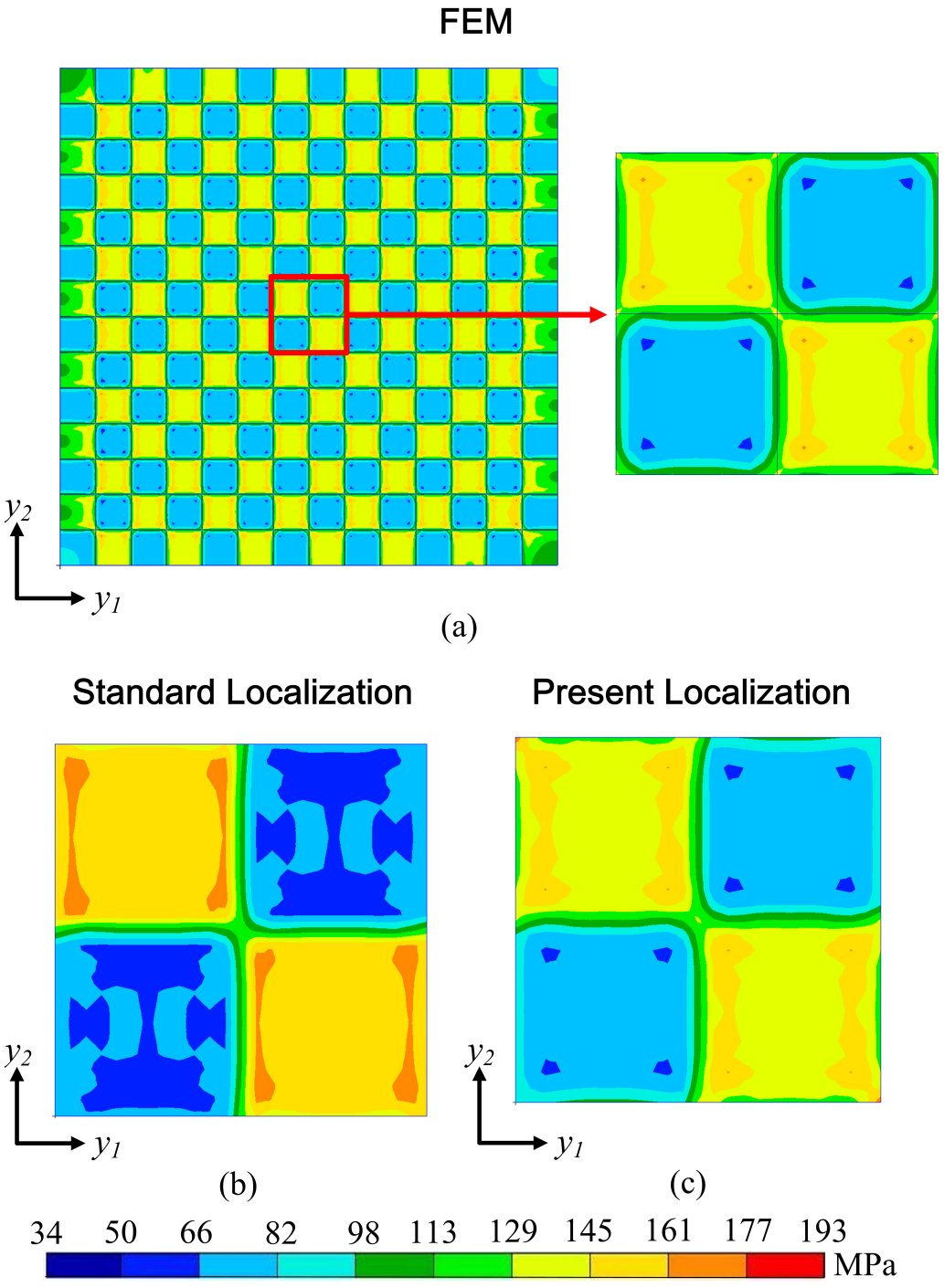

FIGURE 4.12: Stress σ_{22}: (a) FEM, (b) standard localization, (c) present localization

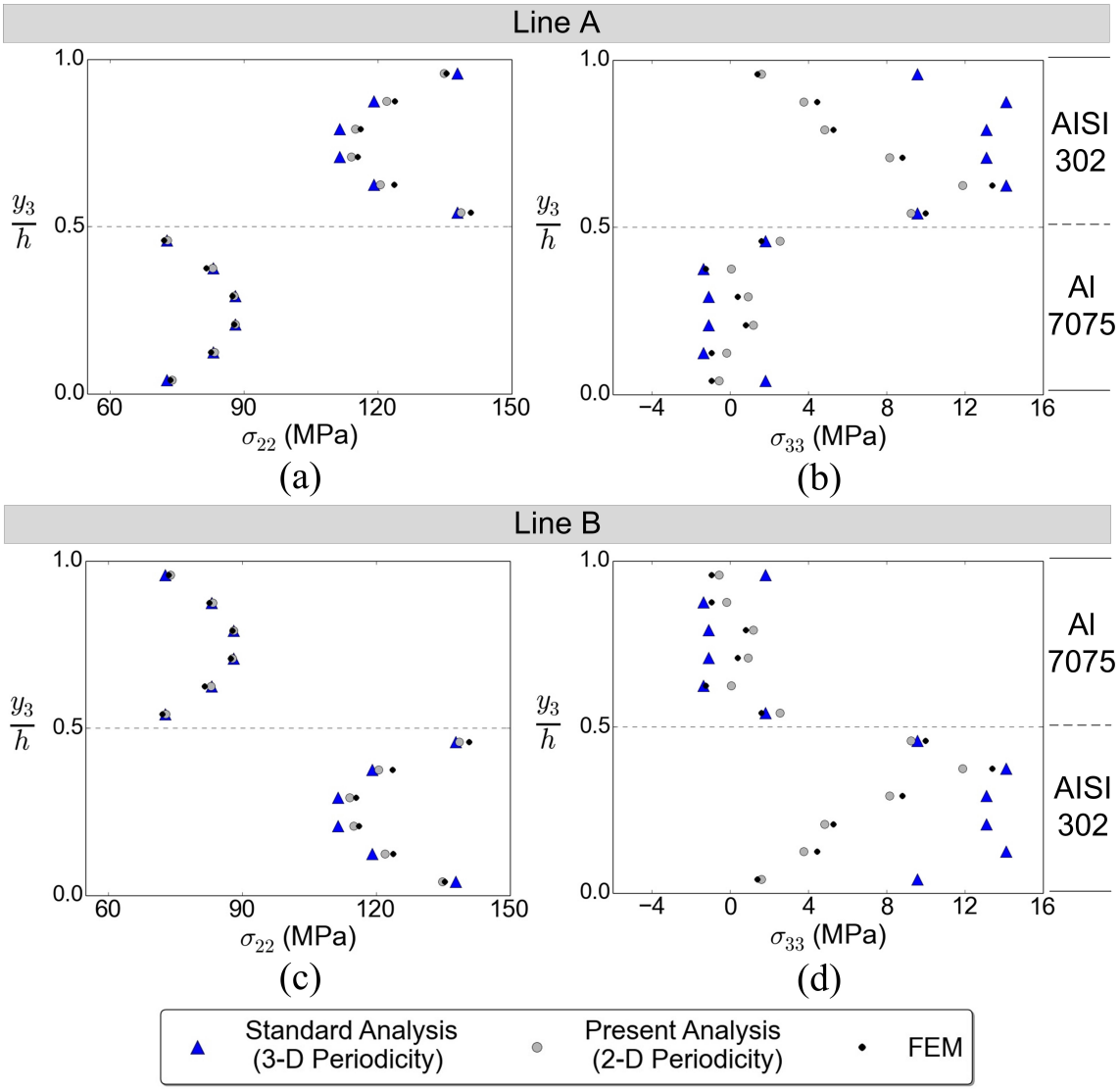

FIGURE 4.13: Stresses along Lines A and B due to biaxial loading

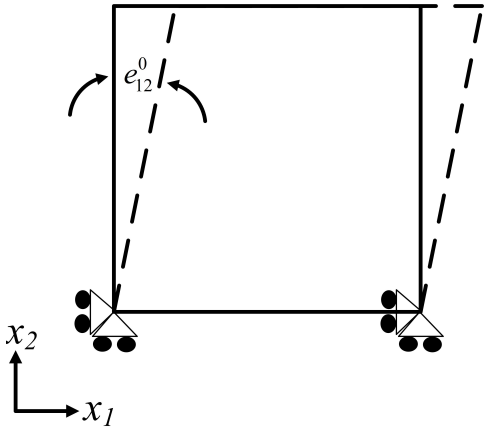

FIGURE 4.14: Schematic of FE analysis under shear loading

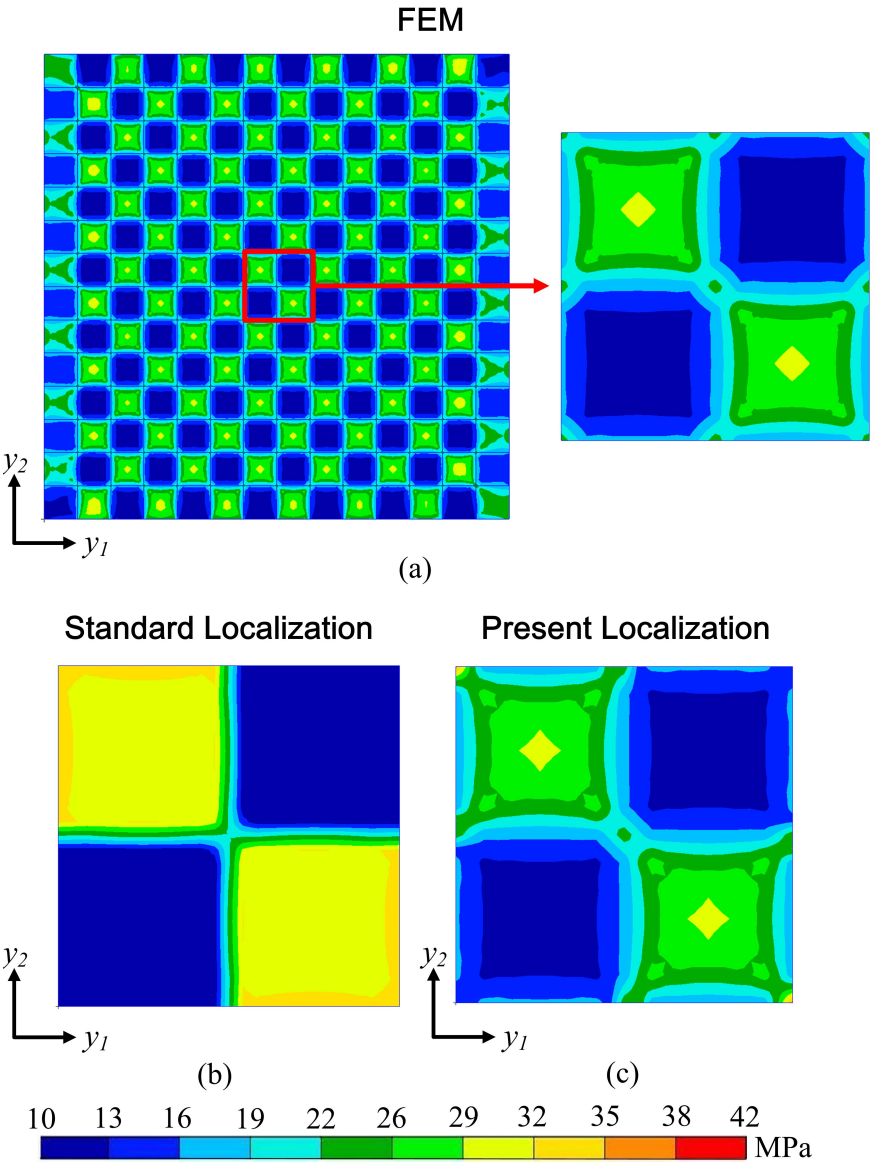

FIGURE 4.15: Stress τ_{12}: (a) FEM, (b) standard localization, (c) present localization

TABLE 4.7: Stress τ_{12} along Line A

y_3/h	τ_{12}			%Diff. (w.r.t. FEM)	
	Standard Analysis	Present Analysis	FEM	Standard Analysis	Present Analysis
0.042	10.58	10.13	10.16	4.09	0.32
0.208	10.79	10.59	10.68	1.08	0.82
0.375	10.74	10.66	10.72	0.15	0.58
0.625	27.70	27.97	28.02	1.17	0.21
0.792	26.99	27.23	27.23	0.88	0.00
0.958	29.14	28.73	28.77	1.28	0.14

4.3 3-D Orthogonal Interlock Composites

4.3.1 Numerical Model

Two kinds of unit-cell model in meso-scale, viz. infinite-thickness (IT) and finite-thickness (FT) models are built based on the optical microscopy and the schematic architecture of 3-D orthogonal interlock composites shown in Figs. 4.16(a) and (b). The analysis utilizes a single stack unit-cell model for the IT model (one-stack IT model) and a model consisting of six unit-cell stacks for the FT model (six-stack FT model), respectively shown in Figs 4.16(c) and (d). The IT model consists of three fiber tows (x-, y-, z- tows) and resin-rich region. It is noted that, in addition to IT model constituents, the FT model also considers the existence of horizontal portion of z-tow in the upper part of the unit-cell as well as the selvage yarn in its lower part. In the unit-cell, the x- and y-tows tows utilize T-300 as the fiber phase, while that of z-tow and selvage yarn is T-900. The resin phase of all fiber tows and resin-rich region is epoxy EP828. Tows' fiber volume fraction (V_{ft}) of x- and y- tows is 55%, whilst V_{ft} of z-tow is 50%. The selvage yarn is idealized so that possesses the same V_{ft} as z-tow. The homogenized thermo-mechanical properties of fiber tows, selvage yarn and resin-rich region are shown in Table 4.8 [42]. It is reminded that the properties are calculated by standard homogenization method with 3-D periodicity utilizing a micro-scale unit-cell model consisting fiber and matrix phases arranged in hexagonal array. In Table 4.8, subscripts 'L' and 'T' of tows and selvage yarn respectively denote longitudinal and transverse directions of the fiber phase.

4.3.2 Homogenization Analysis

4.3.2.1 Characteristic Displacement Vector

The elastic correctors (χ^{11}, χ^{22} and χ^{12}) and thermal corrector (ψ) of 3-D orthogonal interlock composites are shown in Fig. 4.17. The correctors are shown based on

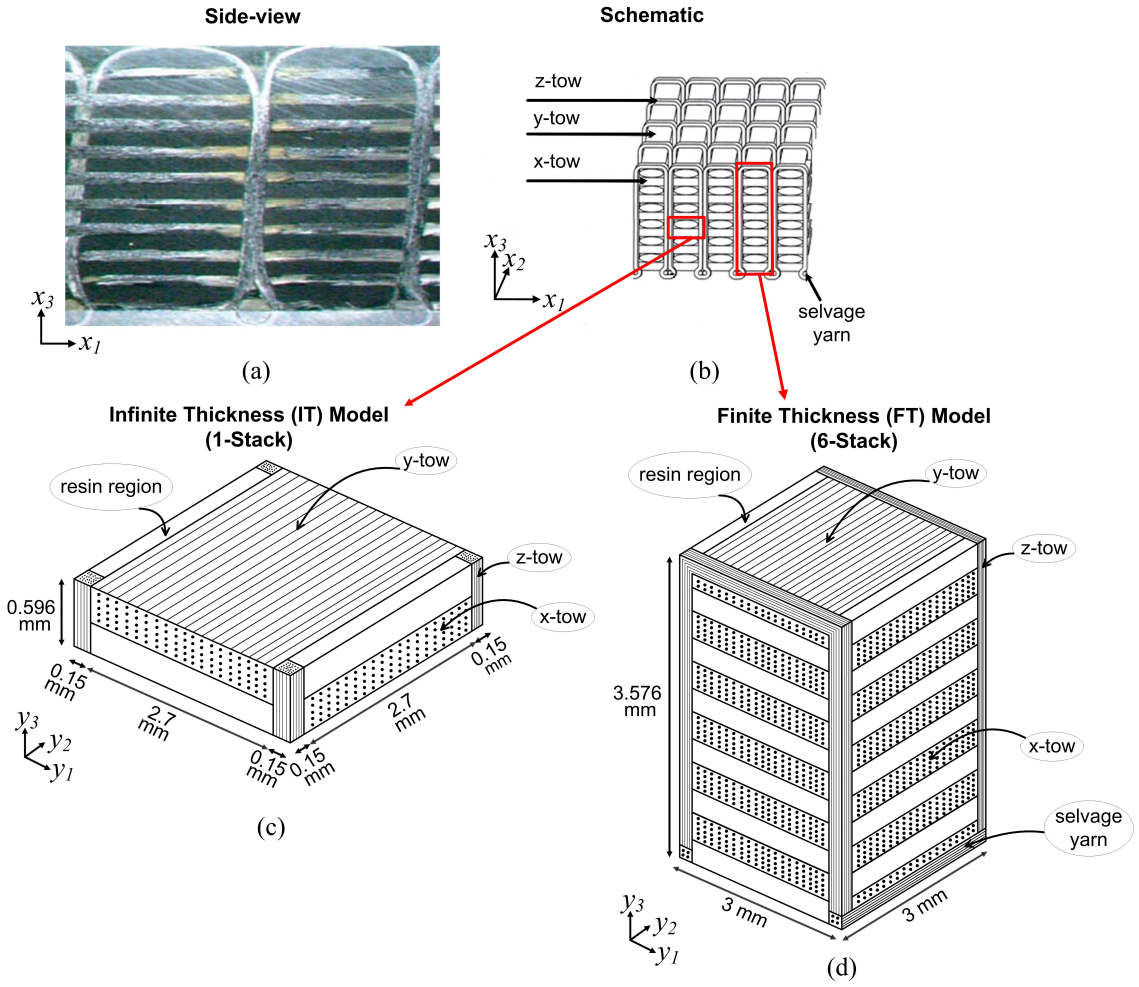

FIGURE 4.16: 3-D orthogonal interlocked composite: (a) side-view observed from optical microscopy, (b) schematic architecture, (c) infinite-thickness (IT) unit-cell model, (d) finite-thickness (FT) unit-cell model

TABLE 4.8: Homogenized thermomechanical properties of fiber tows, selvage yarn and resin-rich region of 3-D orthogonal interlock composites

Properties	x-tow & y-tow	z-tow & selvage yarn	resin-rich region
	T-300 (V_{ft} = 55%)	T-900 (V_{ft} = 50%)	EP828
E_L (GPa)	122.55	148.7	3.4
E_T (GPa)	7.13	4.96	3.4
G_{LT} (GPa)	3.25	3.21	1.26
G_{TT} (GPa)	2.53	2.45	1.26
ν_{LT}	0.263	0.335	0.35
ν_{TT}	0.414	0.476	0.35
α_L (/°C)	5.03×10^{-7}	2×10^{-7}	6.45×10^{-5}
α_T (/°C)	3.94×10^{-5}	4.5×10^{-5}	6.45×10^{-5}

the results of six-stack FT model. Fig. 4.17 shows that the obtained correctors are the same between the opposing faces in the in-plane direction, while those of the top and bottom surfaces of the unit-cell are different. This concludes that the periodicity in the thickness direction has been successfully relieved. For the better understanding, Fig 4.18 shows the comparison of corrector χ^{12} obtained from standard and present analyses. In this figure, unlike the result of present analysis, the corrector obtained from standard analysis has the same deformation between the top and bottom surfaces of the unit-cell.

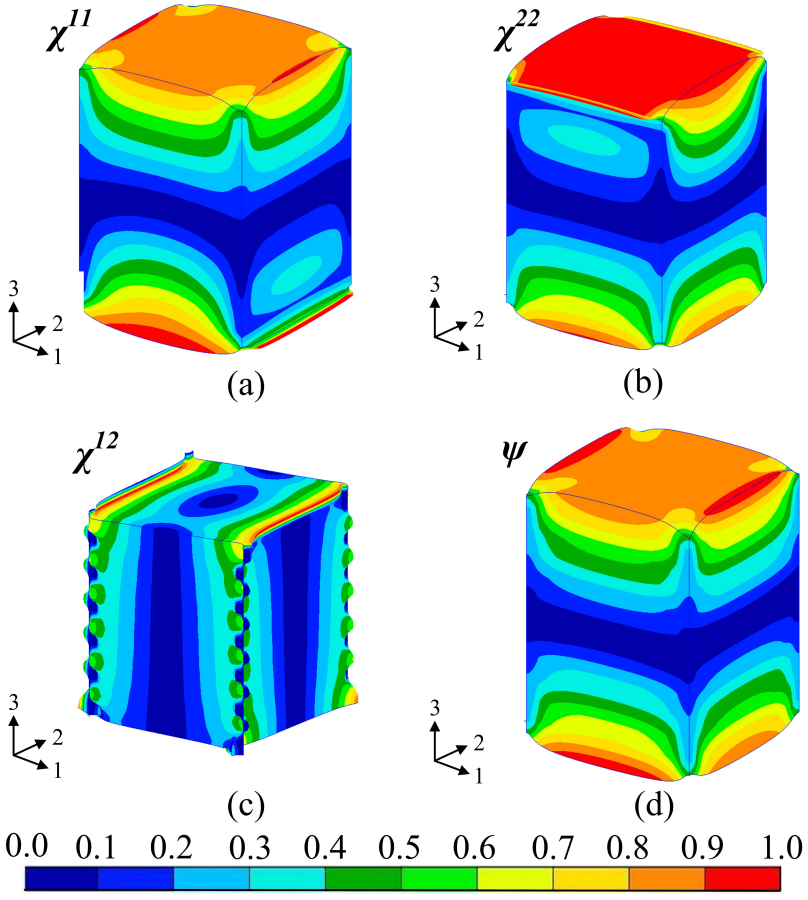

FIGURE 4.17: Elastic and thermal correctors of 3-D orthogonal interlock composites: (a) χ^{11}, (b) χ^{22}, (c) χ^{12}, (d) ψ

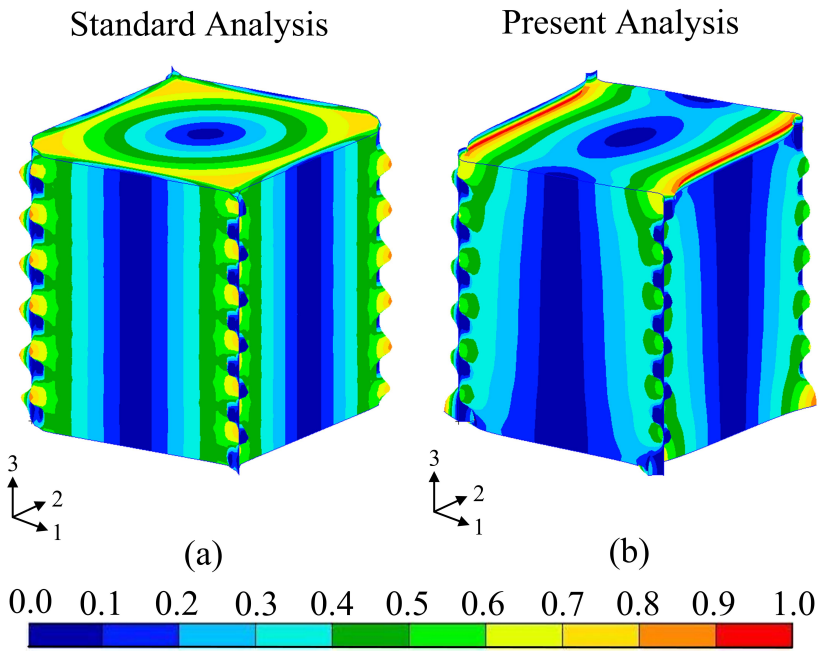

FIGURE 4.18: Elastic corrector (χ^{12}): (a) standard analysis, (b) present analysis

4.3.2.2 Homogenized Thermomechanical Properties

The present analysis is developed to analyze the FT unit-cell model representing the whole thickness of structure. However, with aim of understanding the influence of relieving periodicity in the thickness direction with respect to the in-plane properties of 3-D orthogonal interlock composites, the IT model is also built and analyzed by employing the standard method with 3-D periodicity. In this regard, the IT model has an in-plane stack (one-stack model), while FT models are represented by six, seven, eight, nine and ten-stack models. The employment of FT unit-cell models with increasing number of in-plane stacks consequently leads to the different results between FT and IT models. The differences are caused by not only different periodic boundary conditions, but also the different unit-cell composition due to the existence of horizontal portion of z-tow and selvage yarn. Hence, in order to evaluate the influence of only relieving periodicity in the thickness direction, the FT models are also analyzed by using the standard method with 3-D periodicity. Fig. 4.19 exhibits the effects of relieving periodicity in the thickness direction as

well as the increment of in-plane stack of the unit-cell to the homogenized in-plane properties of 3-D orthogonal interlock composites. The effects are investigated by means of the normalized value of the in-plane properties obtained by FT model calculated by present method with respect to those obtained by both IT and FT models calculated by standard method. Due to the idealization in the modeling of the unit-cell, several homogenized properties have the same value (i.e. $E_1 = E_2$, $\alpha_1 = \alpha_2$). In general, Fig. 4.19 shows that the normalized results have a tendency to approach 1.0 with the increment of in-plane stack. This fact is reasonable in the sense that adding the number of in-plane stack will increase the constraint within the unit-cell so that the average strain will approximate the value of those calculated by standard method. Moreover, the addition of in-plane stack in the FT model will reduce the contribution of horizontal portion of z-tow and selvage yarn to the total V_f of the unit-cell. This will increase the possibility of average strain to approximate the value of that obtained by the IT model. Figs. 4.19(a) and (b) show that the normalized values of Young's moduli (E_1 and E_2) and shear modulus (G_{12}) with respect to those of FT model are insensitive to the increment of in-plane stack, whereby the differences are less than 1%. However, the utilization of IT model shows more profound effects to the Young's moduli. Meanwhile, Figs. 4.19(c) and (d) show that the employment of present analysis has a larger influence in Poisson's ratio of ν_{12}, and coefficients of thermal expansion (CTE) of α_1 and α_2, whereby differences of up to about 4% are noticeable. The results also show that the differences will increase as the number of in-plane stack decreases. The aforementioned facts show that when the aim of analysis is to obtain in-plane homogenized properties of 3-D composites, present analysis with FT model should be employed especially when the composite consists of a few numbers of in-plane stack.

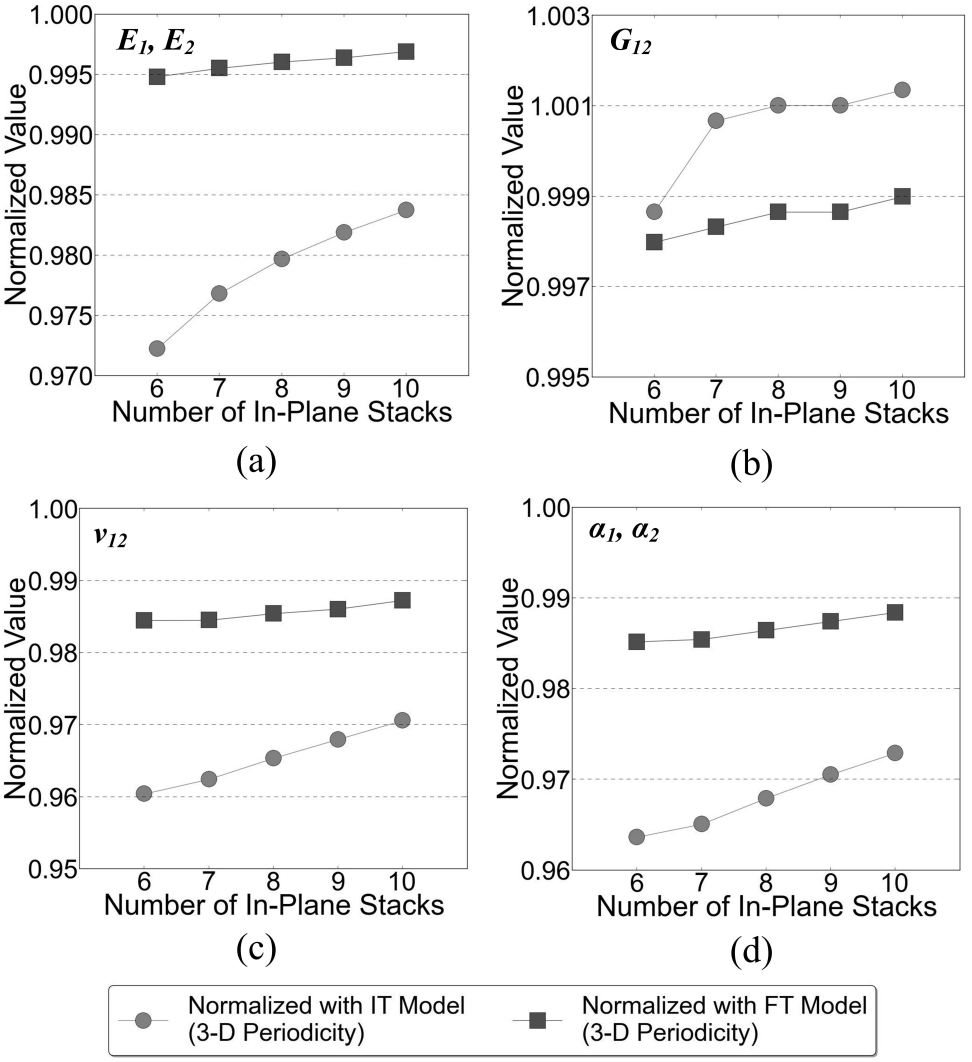

FIGURE 4.19: Normalized value of homogenized thermomechanical properties: (a) E_1, E_2, (b) G_{12}, (c) ν_{12}, (d) α_1, α_2

4.3.3 Localization Analysis

In this analysis, the infinite macroscopic model shown in Fig. 4.2(a) is also subjected to two loading cases (i.e. thermal loading and biaxial tension loading) which are schematically represented in Figs. 4.2(b) and (c). In this localization analysis, six-stack FT unit-cell model is employed, and the stress responses are investigated by extracting the stresses from four representative lines intersecting the thickness of the unit-cell. The four lines, shown in Fig. 4.20, are Line A, Line B, Line C and Line D.

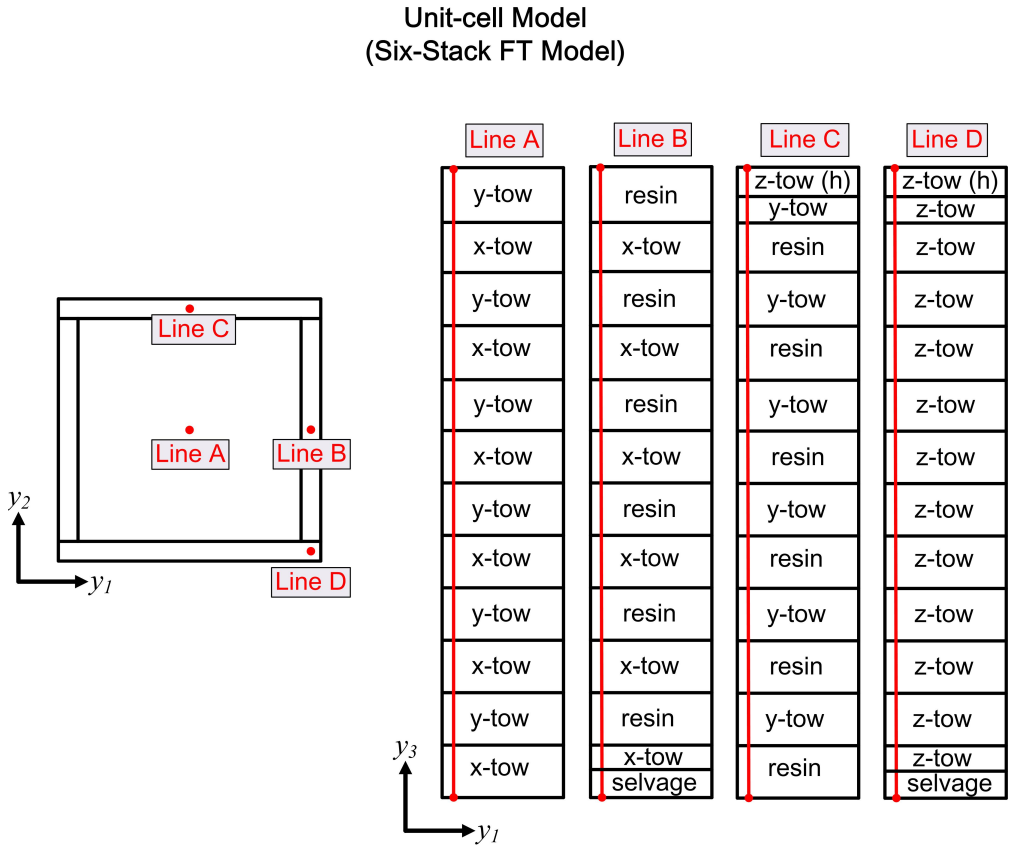

FIGURE 4.20: Localization analysis of 3-D orthogonal interlock composites: four representative lines of unit-cell model

4.3.3.1 Stresses due to Thermal Loading

In thermal loading case, temperature difference ΔT of -150 °C is given to the homogeneous macroscopic model. Present analysis utilizes macroscopic strain of $e^0_{11} = e^0_{22} = e^0_{12} = 0$ to represent the responses of macroscopic model. In standard analysis, e^0_{33} of -8.45×10^{-3} is also given to represent the free-traction boundary condition on the top and bottom surfaces of macroscopic model. In this analysis, a 3×3-cell 3-D orthogonal interlock composite model is built for the sake of numerical validation using FE analysis. The model is constrained in order not to move in the in-plane direction as represented in Fig. 4.2(b). Similar with the result of brick composites, Fig. 4.21(a) shows periodic stress pattern in both in-plane directions (direction -1 and -2). However, in the case of 3-D orthogonal interlock composite,

the different stress pattern nearby outer surfaces induced by the boundary effects is not significant. In Fig. 4.21, the stress results of FE analysis again show a better approximation with the results of present analysis as compared to those of standard analysis.

Stress distributions along Lines A, B, C and D due to application of thermal loading are shown in Fig. 4.22 (for those of Lines A and B) and Fig. 4.23 (for those of Lines C and D). In the figures, the vertical axis indicates normalized thickness coordinate (y_3/h), where $h = 3.576$ mm. The corresponding unit-cell constituents along each line are described in the right side of the figures. In this regard, X denotes x-tow; Y denotes y-tow; Z denotes z-tow; Z-h denotes horizontal portion of z-tow; R denotes resin rich region; S denotes selvage yarn.

The stress results shown in Figs. 4.22 and 4.23 elucidate that standard and present analyses obtain different stress results in terms of stress values and patterns. For the results of σ_{11} and σ_{22}, the results of standard and present analyses are not significantly different, except in the region nearby the top and bottom surfaces. Nevertheless, the considerably different stress values and patterns between the outcomes of both analyses are noticed in the result of σ_{33}. In Figs. 4.22(d) and 4.23(b), the stress responses are different throughout the thickness of the unit-cell whereby the differences are getting larger in the region nearby the top and bottom surfaces of the unit-cell. In addition, Figs. 4.22(b) and 4.23(d) show that the significant differences are not only found in the region nearby the top and bottom surfaces, but also in the whole thickness of the unit-cell. Particularly in Fig. 4.23(d), the difference of about 25% between standard and present analyses is very important to be noticed because the through-thickness reinforcement (i.e. z-tow) experiences very high stress (σ_{33}). With regard to the numerical validation, Figs. 4.22 and 4.23 show that good agreements are compared between the stress results obtained by the present analysis and the comparable FE analysis. These facts emphasize that application of free-traction boundary condition only on the top and bottom surfaces of macroscopic model is not able to obtain accurate stress within the unit-cell of 3-D orthogonal

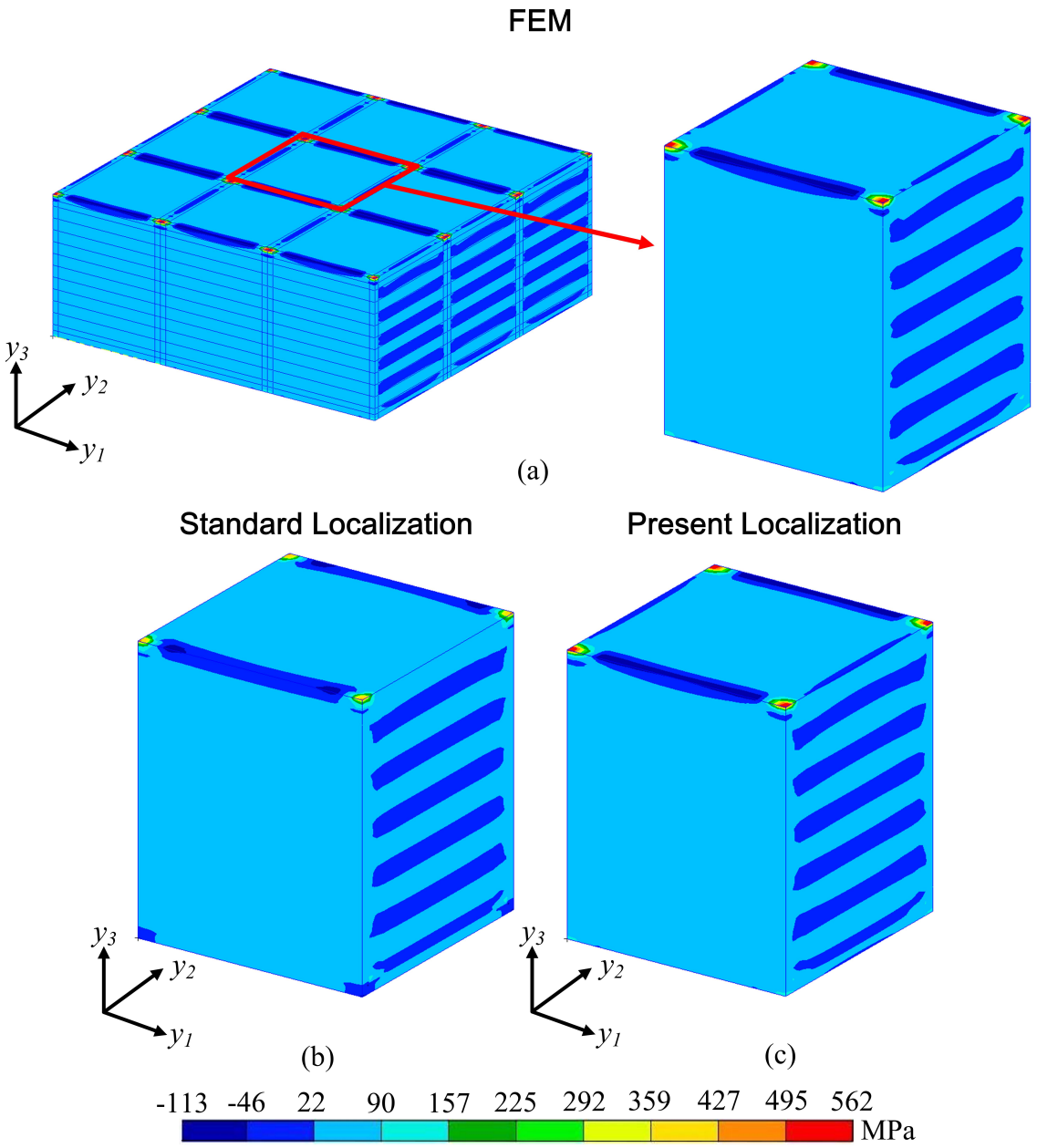

FIGURE 4.21: Stress σ_{11}: (a) FEM, (b) standard localization, (c) present localization

interlock composites. When the unit-cell possesses through-thickness reinforcement, the real free-traction condition necessitates the relieving periodic boundary condition throughout its thickness.

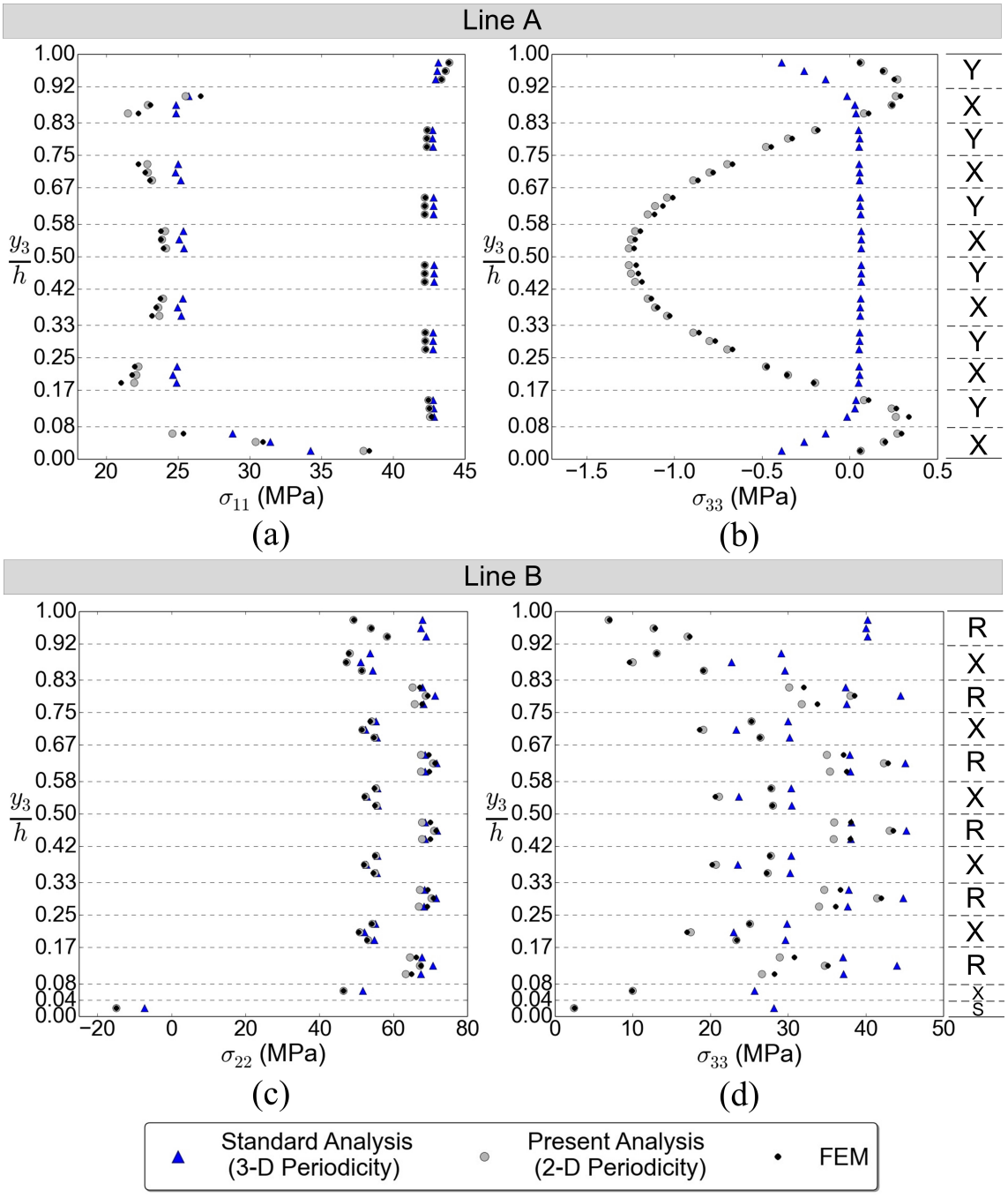

FIGURE 4.22: Stresses along Lines A and B due to thermal loading

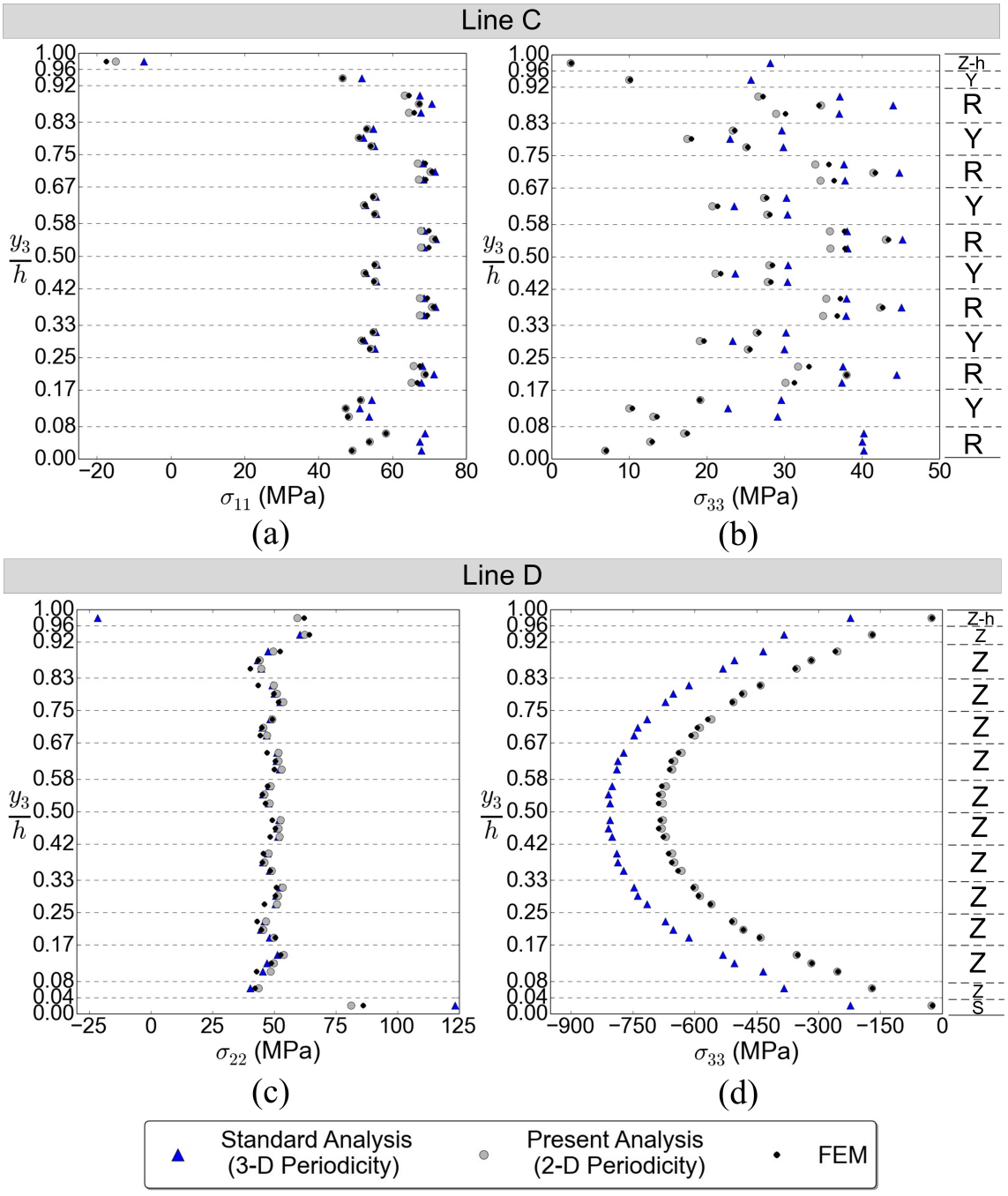

FIGURE 4.23: Stresses along Lines C and D due to thermal loading

4.3.3.2 Stresses due to Mechanical Loading

In mechanical loading case, macroscopic strains of $e^0_{11} = 1\times10^{-3}$ and $e^0_{22} = 5\times10^{-4}$ are utilized to represent biaxial tension loading. Present analysis utilizes $e^0_{33} = 0$ in the calculation stress responses, while in standard analysis e^0_{33} = -5.63$\times10^{-4}$ is given to represent the free-traction boundaries on the top and bottom surfaces of macroscopic model.

Stress responses obtained from localization analysis are also validated by those obtained from a comparable FE analysis employing 3×3-cell 3-D orthogonal interlock composite model. Similar with the previous cases, Fig. 4.24 shows that the stress distribution of FE analysis has a better agreement with that of present analysis. The slight different stress distributions on the surfaces normal to the in-plane directions between the results of localization and FE analysis are found. This fact is reasonable in the sense that the stresses calculated by localization analysis are based on periodic boundary condition whilst those of FE analysis are influenced by the prescribed boundary condition on the FE model. In order to understand the stress responses throughout the thickness direction, the obtained stresses are shown in Fig. 4.25 (for those of Lines A and B) and Fig. 4.26 (for those of Lines C and D). With the exception for the region nearby the top and bottom surfaces, the results show that σ_{11} and σ_{22} obtained by both standard and present analyses nearly coincide. Similar with the stresses due to thermal loading, significant differences between the results of standard and present analyses are found in the result of σ_{33} in terms of stress values and patterns, as shown in Figs. 4.25(b), 4.25(d), 4.26(b) and 4.26(d). It is noteworthy that the differences are not only found in the region nearby the top and bottom surfaces, but also in the whole thickness of the unit-cell. The aforementioned facts assert that the relieving periodic boundary condition in the thickness direction of unit-cell model having through-thickness reinforcement would result in the different and more accurate stress values and patterns [42].

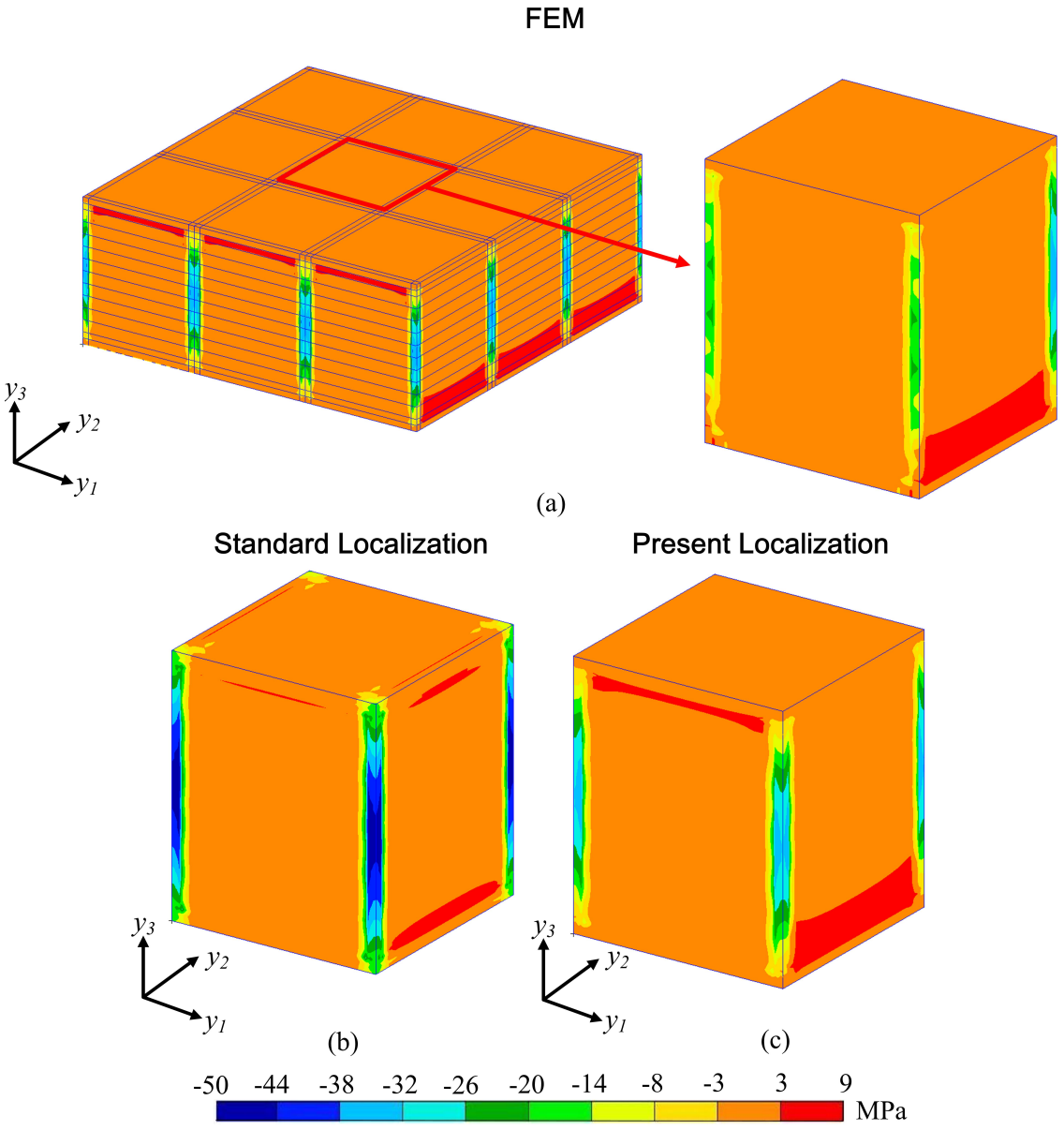

FIGURE 4.24: Stress σ_{33}: (a) FEM, (b) standard localization, (c) present localization

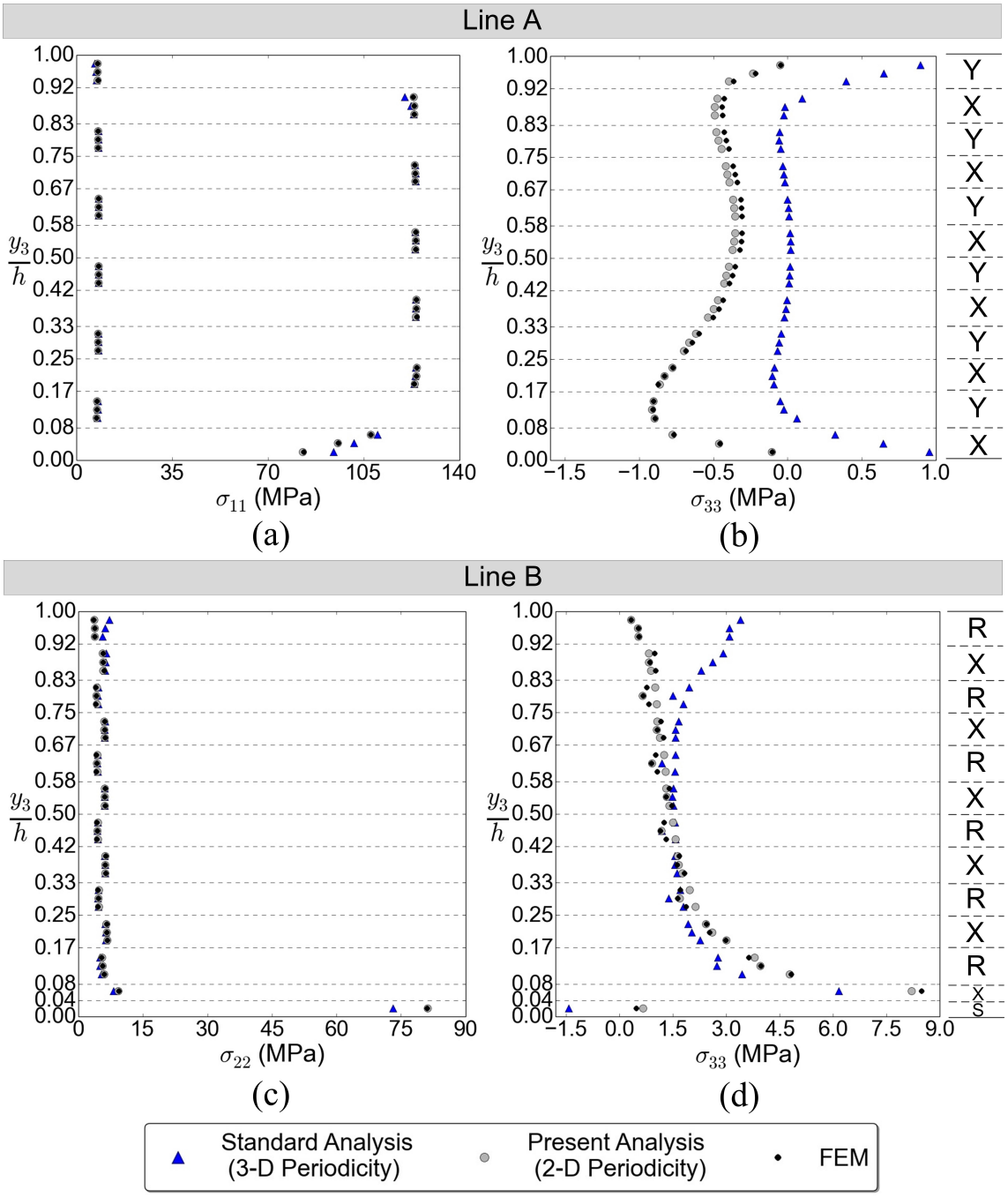

FIGURE 4.25: Stresses along Lines A and B due to biaxial loading

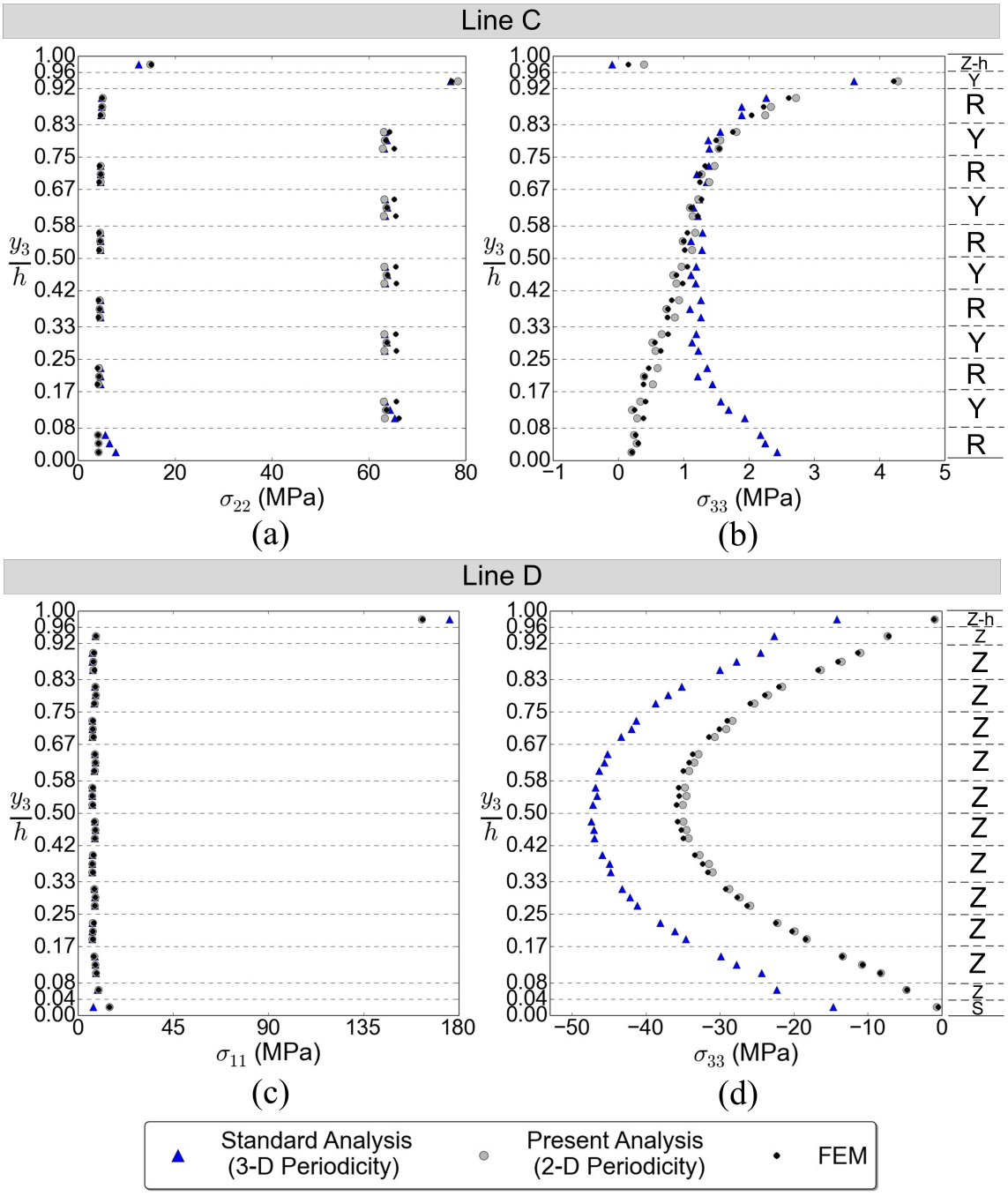

FIGURE 4.26: Stresses along Lines C and D due to biaxial loading

4.4 Sandwich Composites

4.4.1 Numerical Model

This analysis investigates unit-cell model of honeycomb sandwich composites as shown in Fig. 4.27. In this figure, t_c denotes core thickness, b denotes core width, a denotes core length, h_c denotes core height and t_f denotes face thickness.

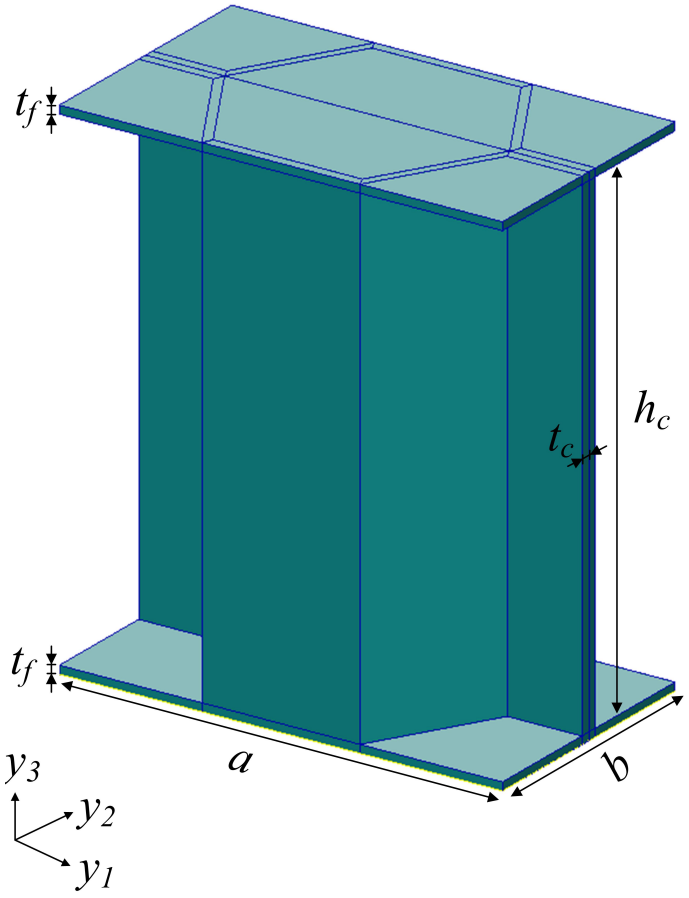

FIGURE 4.27: Unit-cell model of CFRP-Al honeycomb sandwich composites

Four unit-cell models of honeycomb sandwich composites are built, i.e. Models H1-H4. Geometrical configurations of the unit-cell models of CFRP-Al sandwich composites as well as stacking sequence of the face laminates are given in Table 4.9, while the thermomechanical properties of CFRP face prepreg sheet and aluminum core are listed in Table 4.10 [54, 55]. It should be noted that, for the sake of

simplicity, the analysis utilizes the homogenized properties of face laminate lay-up obtained by standard homogenization method with 3-D periodicity. Due to the consideration of numerical accuracy in the analysis, a modeling idealization is performed by thickening the thickness of Al core to ten times of its actual size. As the consequence of such idealization, in the analysis, the elastic moduli (Young's and shear moduli) of core, included in Table 4.10, are altered into its 1/10 value [55, 56].

TABLE 4.9: Geometrical configuration of sandwich composite unit-cell models

Model	Face		Core			
	t_f (mm)	Stacking Sequence	t_c (mm)	b (mm)	a (mm)	h_c (mm)
H1	0.2	$[0/\pm 60]_S$	0.01778	9.525	16.5	18.5
H2	0.2	[0]	0.01778	9.525	16.5	18.5
H3	0.2	[90]	0.01778	9.525	16.5	18.5
H4	0.2	$[0/90]_S$	0.01778	9.525	16.5	18.5

TABLE 4.10: Material properties of CFRP face prepreg sheet and Al honeycomb core (L and T directions correspond to those of 0° face lamina)

Properties	Face (T-300/Q-122)	Core (Al 5056)
E_L (GPa)	140	68.6
E_T (GPa)	11	68.6
G_{LT} (GPa)	5.84	26.4
G_{TT} (GPa)	4.44	26.4
ν_{LT}	0.3	0.3
ν_{TT}	0.28	0.3
α_L (/°C)	-7×10^{-7}	2.35×10^{-5}
α_T (/°C)	3×10^{-5}	2.35×10^{-5}

4.4.2 Homogenization Analysis

4.4.2.1 Characteristic Displacement Vector

Fig. 4.28 shows the typical modes of elastic and thermal correctors of honeycomb sandwich composites. In this figure, the correctors are based on those of Model H2. The obtained correctors show that the out-of-plane periodicity has been successfully

relieved. This is described by the same characteristic deformations between the opposing faces in the in-plane direction, while the deformations on the top and bottom surfaces of the unit-cell are different as shown by the opposing direction of correctors between each other.

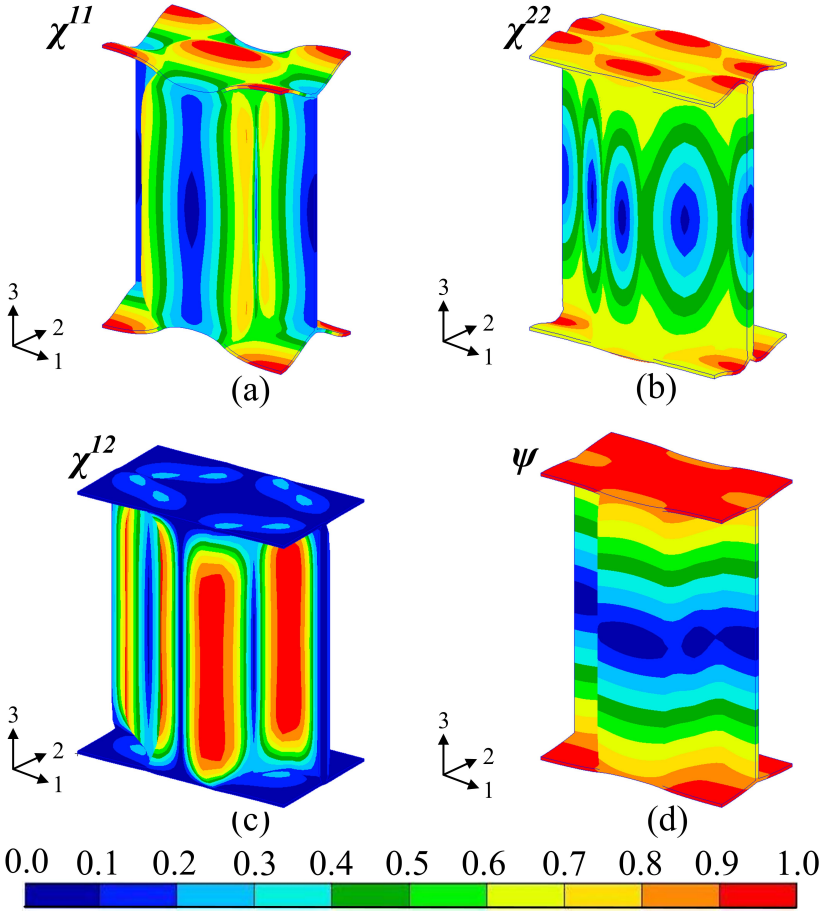

FIGURE 4.28: Elastic and thermal correctors of honeycomb sandwich composites: (a) χ^{11}, (b) χ^{22}, (c) χ^{12}, (d) ψ

4.4.2.2 Homogenized Thermomechanical Properties

Table 4.11 lists the in-plane homogenized properties of unit-cell models H1-H4. The properties obtained from both standard and present analyses of each model are presented. Based on the obtained homogenized properties, the influence of relieving periodicity in the thickness direction shows insignificant effects for the homogenized

elastic moduli and Poisson's ratio whereby differences of less than 1% with the results of standard analysis are compared. However, the present analysis is found to be more influential in the calculation of CTE. The results given in Table 4.11 show that Models H2 and H3 result in larger differences of homogenized CTE between both homogenization analyses as compared to those of Models H1 and H4. It is noted that Models H2 and H3 utilize unidirectional ply laminate (i.e. 0° laminate and 90° laminate, respectively) with highly different values between E_1 and E_2 as well as α_1 and α_2. These facts assert that the present analysis with relieved periodicity in the thickness direction should be employed in the analysis of sandwich composites, particularly if the faces have large different values between the thermomechanical properties in both in-plane directions.

TABLE 4.11: Homogenized thermomechanical properties of Models H1-H4

Model	Analysis	Properties					
		E_1 (GPa)	E_2 (GPa)	G_{12} (GPa)	ν_{12}	α_1 (/°C)	α_2 (/°C)
H1	Standard	1.213	1.206	0.421	0.338	3.863×10^{-6}	3.696×10^{-6}
	Present	1.210	1.206	0.420	0.338	3.816×10^{-6}	3.707×10^{-6}
	Diff. (%)	0.25	0.00	0.12	0.03	1.22	0.30
H2	Standard	3.006	0.302	0.128	0.443	-3.449×10^{-7}	3.348×10^{-5}
	Present	3.003	0.301	0.128	0.443	-3.713×10^{-7}	3.350×10^{-5}
	Diff. (%)	0.10	0.20	0.39	0.14	7.37	0.06
H3	Standard	0.308	2.999	0.128	0.045	3.333×10^{-5}	-4.009×10^{-7}
	Present	0.306	2.998	0.128	0.045	3.342×10^{-5}	-4.070×10^{-7}
	Diff. (%)	0.91	0.03	0.39	0.02	0.27	1.51
H4	Standard	1.680	1.673	0.128	0.081	3.828×10^{-6}	3.732×10^{-6}
	Present	1.677	1.672	0.128	0.081	3.793×10^{-6}	3.731×10^{-6}
	Diff. (%)	0.18	0.06	0.31	0.02	0.92	0.03

4.4.3 Localization Analysis

In this localization analysis, an infinite macroscopic model shown in Fig. 4.29(a) is utilized as the homogeneous macroscopic model. Macroscopic strain (e^0) are given in the calculation of stress responses within the unit-cell to represent the loading

condition in Fig. 4.29(b). It is again noted that the top and bottom of its surfaces are free-traction boundaries.

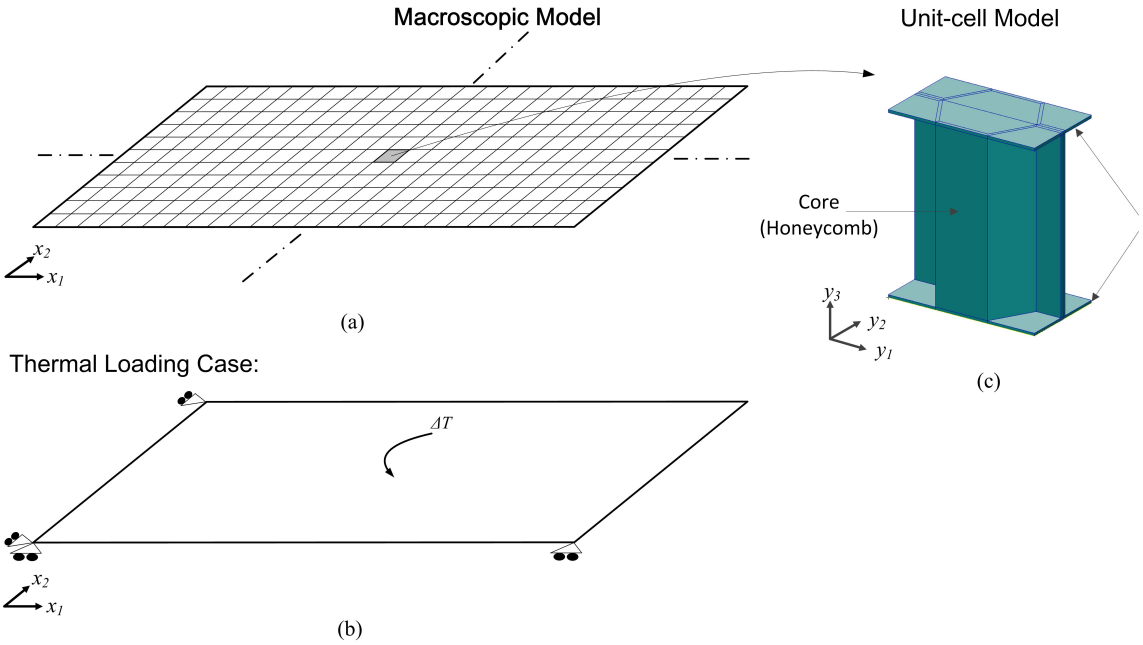

FIGURE 4.29: Localization analysis: (a) homogeneous beam model, (b) thermal loading case, (c) unit-cell model of honeycomb sandwich composites

4.4.3.1 Stresses due to Thermal Loading

In this thermal loading case, due to the loading case described in Fig. 4.29(b), the macroscopic strain can be calculated by the following equation

$$e^0_{kl} = \alpha^0_{kl}\Delta T \tag{4.2}$$

Localization analysis of sandwich composites utilizes ΔT of -120 °C as the thermal load. In the analysis, numerical validation is performed by building a 7×7-cell honeycomb sandwich composite model implementing the boundary condition described in Fig. 4.29(b). In the numerical validation described in Fig. 4.30, the stresses acting on the top and bottom faces of the unit-cell (Model H2) calculated by present

localization analysis show a good agreement with those of FE analysis. Meanwhile, standard analysis result exhibits larger difference with that of FE analysis.

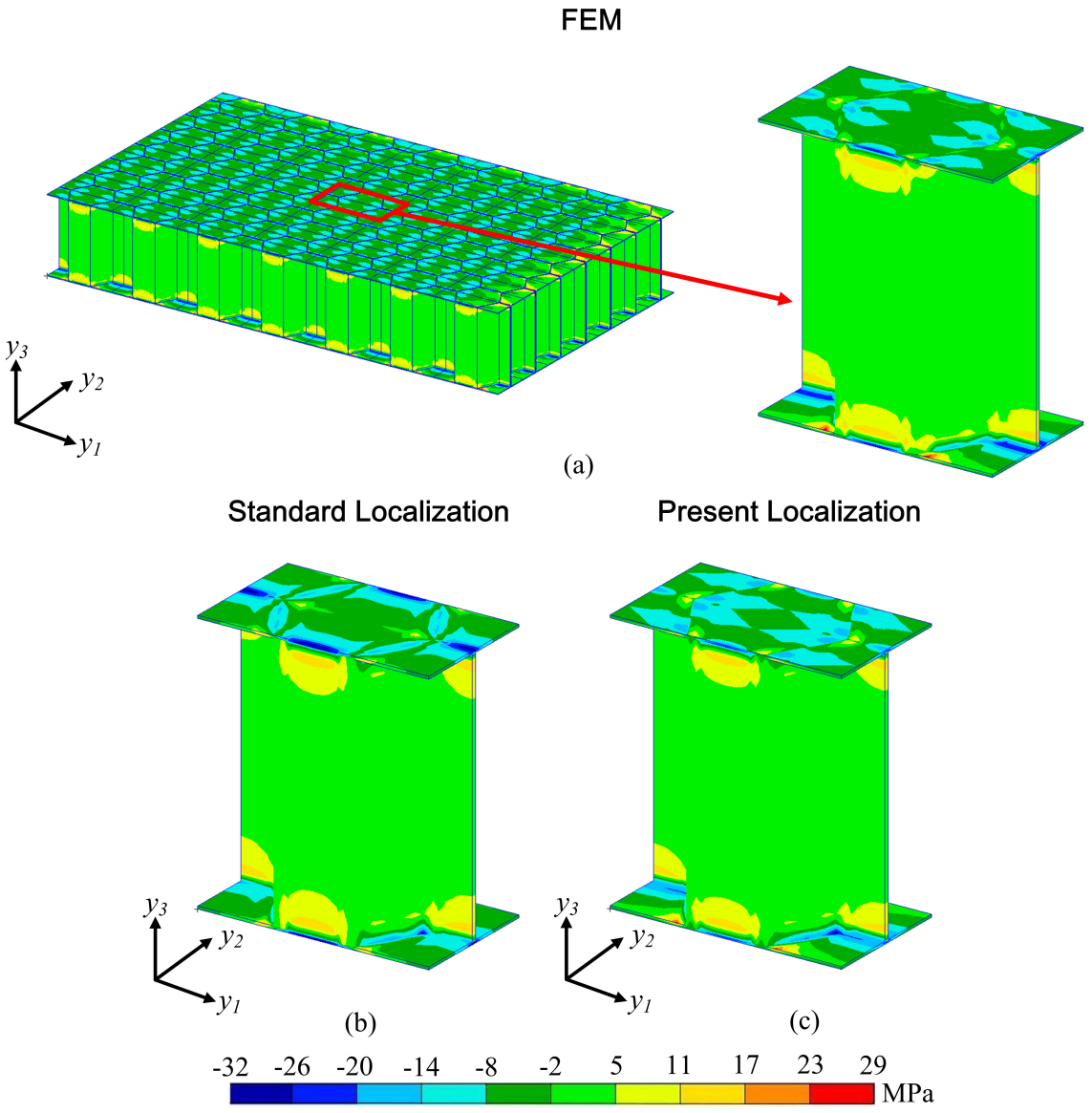

FIGURE 4.30: Stress σ_{11} of Model H2: (a) FEM, (b) standard localization, (c) present localization

The stress distribution of the one-eighth of Model H2 is shown in Fig. 4.31. In this figure, the stresses acting on the core are not significantly different between the results of standard and present analyses. However, compared to the result of standard analysis, the stress distribution acting on the hexagonal face obtained by

present analysis shows a better agreement with that of FE analysis. The aforementioned facts show the necessity of employing present analysis for the sake of obtaining accurate stress results in sandwich composites.

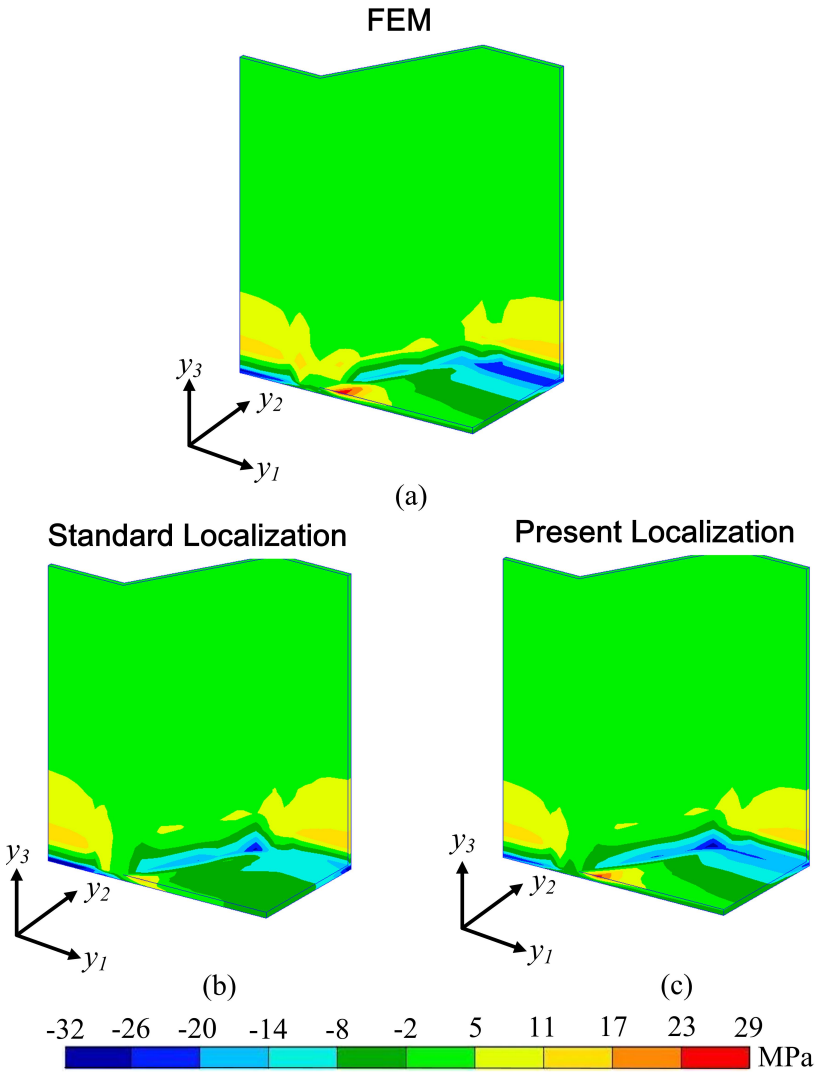

FIGURE 4.31: Stress σ_{11} of the one-eighth of Model H2: (a) FEM, (b) standard localization, (c) present localization

Table 4.12 lists the homogenized thermomechanical properties and average stresses $\bar{\sigma}_{11}$ and $\bar{\sigma}_{22}$ of the face of Models H1-H4. In this table, the relieving periodicity in the thickness direction shows more profound effects in the results of models with unidirectional laminate faces (i.e. Models H2 and H3) whereby the thermomechanical properties in directions -1 and -2 are highly different. In both models, the

TABLE 4.12: Homogenized properties and average stress of face (Models H1-H4)

Model	Elastic Modulus		CTE		Average Stress, $\bar{\sigma}$ (MPa)		
	E_1 (GPa)	E_2 (GPa)	α_1 (/°C)	α_2 (/°C)	Analysis	$\bar{\sigma}_{11}$	$\bar{\sigma}_{22}$
H1	55.1	55.1	2.1×10^{-6}	2.1×10^{-6}	Standard	-16.56	-15.71
					Present	-16.24	-15.69
					Diff. (%)	1.94	0.16
H2	140	11	-7×10^{-7}	3×10^{-5}	Standard	-7.40	-4.77
					Present	-6.96	-4.78
					Diff. (%)	6.11	0.34
H3	11	140	3×10^{-5}	-7×10^{-7}	Standard	-4.55	-6.39
					Present	-4.66	-6.32
					Diff. (%)	2.54	1.06
H4	75.9	75.9	2.1×10^{-6}	2.1×10^{-6}	Standard	-16.55	-15.71
					Present	-16.23	-15.69
					Diff. (%)	1.95	0.15

differences of 6.11% and 2.54% are found in the results of $\bar{\sigma}_{11}$, while the outcomes of average stresses of the face of Models H1 and H4 (i.e. with the same properties in both in-plane directions) are not significantly different. These facts assert that the present analysis should be employed in the analysis of sandwich composites, particularly if the faces have large different thermomechanical properties in both in-plane directions.

Chapter 5

Conclusions and Recommendations

5.1 Conclusions

In this thesis, mathematical framework and finite element implementation of asymptotic expansion (AE) homogenization and localization method have been proposed by including the thermomechanical effects. A novel enhanced homogenization and localization analysis is also proposed by considering the finite thickness effect of unit-cell model. This enhanced analysis deals with the development of unit-cell model of composites structure having relieved periodicity in through-thickness direction (i.e. on the top and bottom surfaces of the unit-cell). In this analysis, the mathematical treatment yields that the macroscopic problem is regarded as a two-dimensional (2-D) problem.

The proposed AE homogenization and localization method is performed to investigate several types of composites namely 2-D laminated composites, brick composites, 3-D orthogonal interlock composites and sandwich composites. For the analysis of 2-D laminated composites (composites with uniform geometrical and material configuration in in-plane direction), the standard analysis (3-D periodicity) and present

analysis (2-D periodicity) yield the same outcomes in terms of homogenized thermomechanical properties (viz. elastic moduli, Poisson's ratio and coefficients of thermal expansion) as well as the stress responses within the unit-cell. These facts assert that, in the case of 2-D laminated composite, standard homogenization and localization analysis is deemed as a sufficient analysis for the calculation of homogenized thermomechanical properties as well as stresses within the unit-cell.

In the analysis of 2-D laminated composites, excellent agreements between homogenization and analytical results are noted whereby the same outcomes are obtained in the results of equivalent thermomechanical properties. The stresses within the unit-cell obtained by localization analysis are also in excellent agreements with those obtained by classical laminate theory.

The relieving periodicity in the thickness direction has more profound effects in the analysis of composites with geometrical and/or material non-uniformity in the in-plane direction. In the analysis of brick composites, 3-D orthogonal interlock composites and sandwich composites, in general, standard and present analyses result in different outcomes of homogenized thermomechanical properties. The differences tend to increase if the composite constituents possess large different material properties. Numerical validation of localization analysis with a comparable finite element analysis emphasizes that relieving periodicity throughout the thickness direction of unit-cell is necessary to accurately simulate the real free-traction condition. Different stress responses between the results of standard and present analyses are particularly found in the region nearby the top and bottom surfaces of the unit-cell. In accordance to this finding, the analysis also reveals profound effects of the relieving periodicity in the results of sandwich composites with unidirectional face laminate.

5.2 Recommendations

Several potential future works and recommendations for other researchers as extensions of this study are listed below:

1. More realistic unit-cell model (especially for 3-D textile composites) can be developed by considering: (i) shape improvement of cross-section of fiber tows and resin region; (ii) fiber tow undulation; (iii) variation of width and thickness of the fiber tows.

2. Extension analysis can be performed by investigating another loading conditions and considering initial damage as well as damage progression.

3. Numerical calculation of thermal and elastic correctors can be decoupled into seven independent calculations (for standard method) and four independent calculations (for present method). Thus, parallel computing technique can be implemented to simultaneously calculate the independent corrector modes.

4. Extension analysis aims to consider the free-edge effects of composites can be performed by relieving the periodicity in in-plane transverse direction (preliminary formulation is given in the appendix).

Appendix A

Preliminary Formulation of AE Homogenization Method with Relieving Periodicity in Both Transverse Directions

A.1 Periodic Function

In this preliminary formulation, periodicity only exists in the longitudinal direction of composites (direction -1). Correspondingly, periodic vector function is altered into the following equation

$$g^{\varepsilon}(\mathbf{x}) = g(\mathbf{x}, \mathbf{y}) = g(x_1, x_2, x_3, y_1 + Y_1) \tag{A.1}$$

where Y_1 is the dimensions of unit-cell in direction -1.

By concerning that x_2 and x_3 are finite and very small as compared to x_1, it is

assumed that x_2 and x_3 can be approximated by expressions (A.2) and (A.3), respectively

$$x_2 \approx \varepsilon y_2 \tag{A.2}$$

$$x_3 \approx \varepsilon y_3 \tag{A.3}$$

The modified periodic vector function can be re-expressed as follows

$$g^{\varepsilon}(\mathbf{x}) = g(\mathbf{x}, \mathbf{y}) = g(x_1, y_1 + Y_1, y_2, y_3) \tag{A.4}$$

Derivatives of the modified periodic vector function with respect to macroscopic coordinate $\mathbf{x}$ are as follows

$$\frac{\partial g^{\varepsilon}}{\partial x_1} = \frac{\partial g}{\partial x_1} + \frac{1}{\varepsilon}\frac{\partial g}{\partial y_1} \tag{A.5}$$

$$\frac{\partial g^{\varepsilon}}{\partial x_2} = \frac{1}{\varepsilon}\frac{\partial g}{\partial y_2} \tag{A.6}$$

$$\frac{\partial g^{\varepsilon}}{\partial x_3} = \frac{1}{\varepsilon}\frac{\partial g}{\partial y_3} \tag{A.7}$$

Limit of integration of Y-periodic function can be expressed by explicitly specifying one-dimensional macroscopic problem as follows

$$\lim_{\varepsilon \to 0^+} \int_{\Omega^{\varepsilon}} \Phi^{\varepsilon}(\mathbf{x}) d\Omega \to \frac{1}{|Y|} \int_0^L \int_{¥} \Phi(\mathbf{x},\mathbf{y}) dY dL \tag{A.8}$$

$$\lim_{\varepsilon\to 0^+} \varepsilon \int_{S^\varepsilon} \Phi^\varepsilon(\mathbf{x}) dS \to \frac{1}{|Y|} \int_0^L \int_S \Phi(\mathbf{x},\mathbf{y}) dS dL \tag{A.9}$$

where $|Y|$ is the unit-cell volume; $\mathbf{x} = x_1$; $\mathbf{y} = y_1, y_2, y_3$; and $dY = dy_1 dy_2 dy_3$.

A.2 Formulation of AE Homogenization Method

The three hierarchical equations, given in Eqs. (2.22)-(2.24), are solved by assuming that their limits exist when $\varepsilon \to 0^+$. The derivation of the hierarchical equations is explained in the following steps

Order of ε^{-2}

By multiplying Eq. (2.22) by ε^2, and employing expression (A.8) to take the limit as $\varepsilon \to 0^+$, following equation is obtained

$$\frac{1}{|Y|} \int_0^L \int_{Y} C_{ijkl} \frac{\partial u_k^0}{\partial y_l} \frac{\partial v_i}{\partial y_j} dY dL = 0 \tag{A.10}$$

Choosing $\mathbf{v} = \mathbf{v}(\mathbf{x})$ will automatically satisfy Eq. (A.10). However, choosing $\mathbf{v} = \mathbf{v}(\mathbf{y})$ yields an expanded form of Eq. (A.10) after applying integration by parts and Gauss' divergence theorem as follows

$$\frac{1}{|Y|} \int_0^L \left[\begin{array}{r} -\int_{Y} \frac{\partial}{\partial y_j} \left(C_{ijkl} \frac{\partial u_k^0}{\partial y_l} \right) v_i(\mathbf{y}) dY + \int_S C_{ijkl} \frac{\partial u_k^0}{\partial y_l} n_j v_i(\mathbf{y}) dS \\ + \int_{Y_1} C_{ijkl} \frac{\partial u_k^0}{\partial y_l} n_j v_i(\mathbf{y}) dY_1 + \int_{Y_2} C_{ijkl} \frac{\partial u_k^0}{\partial y_l} n_j v_i(\mathbf{y}) dY_2 \\ + \int_{Y_3} C_{ijkl} \frac{\partial u_k^0}{\partial y_l} n_j v_i(\mathbf{y}) dY_3 \end{array} \right] dL = 0 \tag{A.11}$$

The square bracket of Eq. (A.11) consists of five integral terms. The third term will result in zero due to the existence of periodicity in direction -1 (i.e. periodic boundary condition on the pair surfaces of Y_1), while the fourth and fifth terms are zero due to the free-traction condition on the surfaces normal to both transverse directions -2 and -3 (i.e. each pair of surfaces Y_2 and Y_3). The remaining equation is satisfied by representing macroscopic displacement u_k^0 as follows

$$u_k^0 = u_k^0(\mathbf{x}) = u_k^0(x_1) \tag{A.12}$$

Expression (A.12) confirms that the macroscopic problem is regarded as a one-dimensional (1-D) problem.

Order of ε^{-1}

By multiplying Eq. (2.23) by ε, and employing expressions (A.8) and (A.9) to take the limit as $\varepsilon \to 0^+$, following equation is obtained

$$\begin{aligned} \frac{1}{|Y|}\int_0^L \int_{¥} C_{ijkl}\left[\frac{\partial u_k^0}{\partial y_l}\frac{\partial v_i}{\partial x_j} + \left(\frac{\partial u_k^0}{\partial x_l} + \frac{\partial u_k^1}{\partial y_l} - \alpha_{kl}\Delta T\right)\frac{\partial v_i}{\partial y_j}\right] dY dL \\ = \frac{1}{|Y|}\int_0^L \int_S p_i v_i dS dL \end{aligned} \tag{A.13}$$

By choosing $\mathbf{v} = \mathbf{v}(\mathbf{x})$, and considering the expression (A.12), following statement is obtained

$$\int_S p_i v_i(\mathbf{x}) dS = 0 \tag{A.14}$$

Choosing $\mathbf{v} = \mathbf{v}(\mathbf{y})$ and considering Eq. (A.14) yield

$$\frac{1}{|Y|}\int_0^L \int_{¥} C_{ijkl}\left[\left(\frac{\partial u_k^0(\mathbf{x})}{\partial x_l} + \frac{\partial u_k^1}{\partial y_l} - \alpha_{kl}\Delta T\right)\frac{\partial v_i(\mathbf{y})}{\partial y_j}\right] dY dL = 0 \tag{A.15}$$

By substituting Eq. (2.31) into Eq. (A.15), the microscopic equilibrium equation (1^{st} order) is obtained as follows

$$\frac{1}{|Y|}\int_0^L \int_{¥} \left[\begin{array}{c} \left(C_{ijkl} - C_{ijpq}\dfrac{\partial \chi_p^{kl}}{\partial y_q} \right) \dfrac{\partial u_k^0(\mathbf{x})}{\partial x_l} \\ -C_{ijpq}\left(\dfrac{\partial \psi_p}{\partial y_q} + \alpha_{pq}\Delta T \right) \end{array} \right] \frac{\partial v_i(\mathbf{y})}{\partial y_j} dY dL = 0 \qquad i,j,k,p,q = 1,2,3; l = 1 \tag{A.16}$$

Elastic and thermal correctors (χ and ψ) are calculated by decoupling Eq. (A.16) as follows

$$\text{Elastic problem: } \int_{¥} \left(C_{ijkl} - C_{ijpq}\frac{\partial \chi_p^{kl}}{\partial y_q} \right) \frac{\partial v_i(\mathbf{y})}{\partial y_j} dY = 0 \qquad i,j,k,p,q = 1,2,3; l = 1 \tag{A.17}$$

$$\frac{1}{|Y|}\int_{¥} \chi_p^{kl} dY = 0 \tag{A.18}$$

$$\text{Thermal problem: } \int_{¥} C_{ijpq}\left(\frac{\partial \psi_p}{\partial y_q} + \alpha_{pq}\Delta T \right) \frac{\partial v_i(\mathbf{y})}{\partial y_j} dY = 0 \qquad i,j,p,q = 1,2,3 \tag{A.19}$$

$$\frac{1}{|Y|}\int_{¥} \psi_p dY = 0 \tag{A.20}$$

It is noteworthy that in Eq. (A.17), $l = 1$, and due to the symmetric property of χ, one independent mode of elastic corrector is calculated, namely χ^{11}.

Order of ε^0

By employing expression (A.8) to take the limit of Eq. (2.24) as $\varepsilon \to 0^+$, following equation is obtained

$$\frac{1}{|Y|}\int_0^L\int_{¥} C_{ijkl}\left[\left(\frac{\partial u_k^0}{\partial x_l}+\frac{\partial u_k^1}{\partial y_l}-\alpha_{kl}\Delta T\right)\frac{\partial v_i}{\partial x_j}+\left(\frac{\partial u_k^1}{\partial x_l}+\frac{\partial u_k^2}{\partial y_l}\right)\frac{\partial v_i}{\partial y_j}\right]dYdL = \frac{1}{|Y|}\int_0^L\int_{¥} f_i v_i dYdL+\int_{\Gamma_t} t_i v_i d\Gamma \tag{A.21}$$

By choosing $\mathbf{v}=\mathbf{v}(\mathbf{x})$ and substituting Eq. (2.31) into Eq. (A.21), the compact form of macroscopic equilibrium equation can be obtained as follows

$$\int_0^L C_{ijkl}^0(\mathbf{x})\frac{\partial u_k^0(\mathbf{x})}{\partial x_l}\frac{\partial v_i(\mathbf{x})}{\partial x_j}dL=\int_0^L \tau_{ij}(\mathbf{x})\frac{\partial v_i(\mathbf{x})}{\partial x_j}dL+\int_0^L \sigma_{ij}^t(\mathbf{x})\frac{\partial v_i(\mathbf{x})}{\partial x_j}dL+ \int_0^L b_i(\mathbf{x})v_i(\mathbf{x})dL+\int_{\Gamma_t} t_i(\mathbf{x})v_i(\mathbf{x})d\Gamma \quad i,k,p,q=1,2,3;\ j,l=1 \tag{A.22}$$

where

$$C_{ijkl}^0(\mathbf{x})=\frac{1}{|Y|}\int_{¥}\left(C_{ijkl}-C_{ijpq}\frac{\partial \chi_p^{kl}}{\partial y_q}\right)dY \tag{A.23}$$

$$\tau_{ij}(\mathbf{x})=\frac{1}{|Y|}\int_{¥} C_{ijpq}\frac{\partial \psi_p}{\partial y_q}dY \tag{A.24}$$

$$\sigma_{ij}^t(\mathbf{x})=\frac{1}{|Y|}\int_{¥} C_{ijpq}\alpha_{pq}\Delta T dY \tag{A.25}$$

$$b_i(\mathbf{x})=\frac{1}{|Y|}\int_{¥} f_i dY \tag{A.26}$$

Bibliography

[1] Anon. *Status of FAA's actions to oversee the safety of composites airplanes. Technical Report GAO-11-849*. U.S. Government Accountability Office, 2011.

[2] W.G. Roeseler, B. Sarh, and M.U. Kismarton. Composites structures: The first 100 years. In *Proc. 16th International Conference on Composite Materials*, Kyoto, Japan, 2007.

[3] C. Zweben. Advanced composites for aerospace applications, A review of current status and future prospects. *Composites*, pages 235–240, 1981.

[4] R. Rolfes, G. Ernst, M. Vogler, and C. Huhne. Material and failure models for textile composites. In *Mechanical response of composites*, pages 27–56. Springer Science + Business Media B.V., 2008.

[5] S.V. Lomov, D.S. Ivanov, I. Verpoest, M. Zako, T. Kurashiki, H. Nakai, and S. Hirosawa. Meso-FE modelling of textile composites: Road map, data flow and algorithms. *Composites Science and Technology*, 67:1870–1891, 2007.

[6] X.F. Wang, X.W. Wang, G.M. Zhou, and C.W. Zhou. Multi-scale analyses of 3D woven composite based on periodicity boundary conditions. *Journal of Composite Materials*, 41(14):1773–1788, 2007.

[7] S.S. Vel and A.J. Goupee. Multiscale thermoelastic analysis of random heterogeneous materials Part I: Microstructure characterization and homogenization of material properties. *Computational Materials Science*, 48:22–38, 2010.

[8] M.R.E. Nasution, N. Watanabe, A. Kondo, and A. Yudhanto. Thermomechanical properties and stress analysis of 3-D textile composites by asymptotic expansion homogenization method. *Composites: Part B*, 60:378–391, 2014.

[9] Y.F. Xing, Y. Yang, and X.M. Wang. A multiscale eigenelement method and its application to periodical composite structures. *Composites Structures*, 92: 2265–2275, 2010.

[10] J. Rannou, N. Limodin, J. Rethore, A. Gravouil, W. Ludwig, M-C. Baietto-Dubourg, J-Y. Buffiere, A. Combescure, F. Hild, and S. Roux. Three dimensional experimental and numerical multiscale analysis of a fatigue crack. *Computer Methods in Applied Mechanics and Engineering*, 199:1307–1325, 2010.

[11] F.V. Souza, D.H. Allen, and Y.R. Kim. Multiscale model for predicting damage evolution in composites due to impact loading. *Composites Science and Technology*, 68:2624–2634, 2008.

[12] G. Nilakantan, M. Keefe, T.A. Bogetti, R. Adkinson, and J.W. Gillespie Jr. On the finite element analysis of woven fabric impact using multiscale modeling techniques. *International Journal of Solids and Structures*, 47:2300–2315, 2010.

[13] L. Wu, L. Noels, L. Adam, and I. Doghri. A multiscale mean-field homogenization method for fiber-reinforced composites with gradient-enhanced damage models. *Computer Methods in Applied Mechanics and Engineering*, 233-236: 164–179, 2012.

[14] A. Visrolia and M. Meo. Multiscale damage modelling of 3D weave composite by asymptotic homogenisation. *Composite Structures*, 95:105–113, 2013.

[15] Z. Hashin. Analysis of composite materials - A survey. *Journal of Applied Mechanics*, 50:481–505, 1983.

[16] Z. Hashin and S. Shtrikman. On some variational principles in anisotropic and nonhomogeneous elasticity. *Journal of the Mechanics and Physics of Solids*, 10: 335–342, 1962.

[17] Z. Hashin and S. Shtrikman. A variational approach to the theory of the elastic behaviour of multiphase materials. *Journal of the Mechanics and Physics of Solids*, 11:127–140, 1963.

[18] T. Mori and K. Tanaka. Average stress in matrix and average elastic energy of materials with misfitting inclusions. *Acta Metallurgica*, 21:571–574, 1973.

[19] P. Kanoute, D.P. Boso, J.L. Chaboche, and B.A. Schrefler. Multiscale methods for composites: A review. *Archives of Computational Methods in Engineering*, 16:31–75, 2009.

[20] T. Ishikawa and T.W. Chou. Stiffness and strength behavious of woven fabric composites. *Journal of Materials Science*, 17:3211–3220, 1982.

[21] C. Yan. *On homogenization and de-homogenization of composite materials. PhD Thesis*. Drexel University, Philadelphia, 2003.

[22] Y. Davit, C.G. Bell, H.M. Byrne, L.A.C. Chapman, L.S. Kimpton, G.E. Lang, K.H.L. Leonard, J.M. Oliver, N.C. Pearson, R.J. Shipley, S.L. Waters, J.P. Whiteley, B.D. Wood, and M. Quintard. Homogenization via formal multiscale asymptotics and volume averaging: How do the two techniques compare? *Advances in Water Resources*, 62:178–206, 2013.

[23] A. Bensoussan, J.L. Lion, and G. Papanicolaou. *Asymptotic analysis for periodic structures*. North-Holland Pub. Co., Amsterdam, 1978.

[24] J.M. Guedes and N. Kikuchi. Preprocessing and postprocessing for materials based on the homogenization method with adaptive finite element methods. *Computer Methods in Applied Mechanics and Engineering*, 83:143–198, 1990.

[25] P.W. Chung, K.K. Tamma, and R.R. Namburu. Asymptotic expansion homogenization for heterogeneous media: computational issues and applications. *Composites: Part A*, 32:1291–1301, 2001.

[26] T. Matsuda, Y. Nimiya, N. Ohno, and M. Tokuda. Elastic–viscoplastic behavior of plain-woven GFRP laminates: Homogenization using a reduced domain of analysis. *Composite Structures*, 79:493–500, 2007.

[27] S.L. Angioni, M. Meo, and A. Foreman. A comparison of homogenization methods for 2-D woven composites. *Composites: Part B*, 42:181–189, 2011.

[28] J.A. Oliveira, J. Pinho-da-Cruz, and F. Teixeira-Dias. Asymptotic homogenisation in linear elasticity. Part II: Finite element procedures and multiscale applications. *Computational Materials Science*, 45:1081–1096, 2009.

[29] G.A. Francfort. Homogenization and linear thermoelasticity. *SIAM Journal on Mathematical Analysis*, 14(4):696–708, 1983.

[30] Y.M. Shabana and N. Noda. Numerical evaluation of the thermomechanical effective properties of a functionally graded material using the homogenization method. *International Journal of Solids and Structures*, 45:3494–3506, 2008.

[31] A. Dasgupta, R.K. Agarwal, and S.M. Bhandarkar. Three-dimensional modeling of woven-fabric composites for effective thermo-mechanical and thermal properties. *Composites Science and Technology*, 56:209–223, 1996.

[32] J. Pinho-da-Cruz, J.A. Oliveira, and F. Teixeira-Dias. Asymptotic homogenisation in linear elasticity. Part I: Mathematical formulation and finite element modelling. *Computational Materials Science*, 45:1073–1080, 2009.

[33] T. Hobbiebrunken, B. Fiedler, M. Hojo, S. Ochiai, and K. Schulte. Microscopic yielding of CF/epoxy composites and the effect on the formation of thermal residual stresses. *Composites Science and Technology*, 65:1626–1635, 2005.

[34] L. Yang, Y. Yan, J. Ma, and B. Liu. Effects of inter-fiber spacing and thermal residual stress on transverse failure of fiber-reinforced polymer–matrix composites. *Computational Materials Science*, 68:255–262, 2013.

[35] G.A. Kassem. *Micromechanical material models for polymer composites through advanced numerical simulation techniques. PhD Thesis.* RWTH Aachen University, Aachen, 2009.

[36] K. Woo and J.D. Whitcomb. Effects of fiber tow misalignment on the engineering properties of plain weave textile composites. *Composite Structures*, 37(3/4): 343–355, 1997.

[37] F. Rostam-Abadi, C.M. Chen, and N. Kikuchi. Design analysis of composite laminate structures for light-weight armored vehicle by homogenization method. *Computers and Structures*, 76:319–335, 2000.

[38] N. Buannic, P. Cartraud, and T. Quesnel. Homogenization of corrugated core sandwich panels. *Composite Structures*, 59:299–312, 2003.

[39] P. Lapeyronnie, P.L. Grognec, C. Binetruy, and F. Boussu. Homogenization of the elastic behavior of a layer-to-layer angle-interlock composite. *Composite Structures*, 93:2795–2807, 2011.

[40] Y. Cai, L. Xu, and G. Cheng. Novel numerical implementation of asymptotic homogenization method for periodic plate structures. *International Journal of Solids and Structures*, 51:284–292, 2014.

[41] W. He, W. Chen, and H. Qiao. Two-scale analytical solutions of multilayered composite rectangular plates with in-plane small periodic structure. *European Journal of Mechanics A/Solids*, 40:123–130, 2013.

[42] M.R.E. Nasution, N. Watanabe, A. Kondo, and A. Yudhanto. A novel asymptotic expansion homogenization analysis for 3-D composite with relieved periodicity in the thickness direction. *Composites Science and Technology*, 97: 63–73, 2014.

[43] R.F. Gibson. *Principle of composite material mechanics., 3rd ed.* CRC Press, Florida, 2012.

[44] A. Yudhanto. *Mechanical characteristics and damage mechanisms of stitched carbon/epoxy composites under static and fatigue loads. PhD Thesis.* Tokyo Metropolitan University, Tokyo, 2013.

[45] M. Trinquecoste, J.L. Carlier, A. Derre, P. Delhaes, and P. Chadeyron. High temperature thermal and mechanical properties of high tensile carbon single filaments. *Carbon*, 34:923–929, 1996.

[46] P. Tan, L. Tong, and G.P. Steven. Behavior of 3D orthogonal woven CFRP composites. Part II. FEA and analytical modeling approaches. *Composites: Part A*, 31:273–281, 2000.

[47] A. Yudhanto, Y. Iwahori, N. Watanabe, and H. Hoshi. Open hole fatigue characteristics and damage growth of stitched plain weave carbon/epoxy laminates. *International Journal of Fatigue*, 43:12–22, 2012.

[48] H. Mibayashi. *Damage development analyses of 3D-CFRP by using node separation method. Master Thesis.* Tokyo Metropolitan University, Tokyo, 2003.

[49] T.A. Bogetti, C.P.R. Hoppel, and W.H. Drysdale. *Three-dimensional effective property and strength prediction of thick laminated composite media.* U.S. Army Research Laboratory, Aberdeen, 1995.

[50] P.C. Chou, J. Carleone, and C.M. Hsu. Elastic constants of layered media. *Journal of Composite Materials*, 6(1):80–93, 1972.

[51] Asm aerospace specification metals inc., . URL `http://asm.matweb.com/search/SpecificMaterial.asp?bassnum=MA7075T6`.

[52] Asm aerospace specification metals inc., . URL `http://asm.matweb.com/search/SpecificMaterial.asp?bassnum=MA2024T3`.

[53] Asm aerospace specification metals inc., . URL `http://asm.matweb.com/search/SpecificMaterial.asp?bassnum=MQ302AP`.

[54] N. Watanabe, H. Sato, and Y. Nishi. Thermal buckling behavior in Al honeycomb sandwich plates with very thin CFRP faces. In *Proc. 38th AIAA/ASME/ASCE/AHS/ASC Structures, Structural Dynamics, and Materials Conference. Paper No. AIAA-97-1249*, Kissimmee, FL, 1997.

[55] N. Watanabe and K. Teranishi. Thermal stress analysis for Al honeycomb sandwich plates with very thin CFRP faces. In *Proc. 36th AIAA/ASME/ASCE/AHS/ASC Structures, Structural Dynamics, and Materials Conference, Paper No. AIAA-95-1394*, New Orleans, LA, 1995.

[56] N. Watanabe and K. Teranishi. Stiffness and buckling analysis for sandwich plates with thermal buckling CFRP face sheets: Qualitative approach. In *Proc. 35th AIAA/ASME/ASCE/AHS/ASC Structures, Structural Dynamics, and Materials Conference, Paper No. AIAA-94-1575*, Hilton Head, SC, 1994.

Acknowledgements

All praise belongs to Allah, the most compassionate, the most merciful, who always has solution for every problem. In the completion of this work, I received invaluable help and support from many individuals and institutions. I would like to express my sincere gratitude to my advisor, Prof. Naoyuki Watanabe for his excellent supervision and academic supports during my PhD study at Tokyo Metropolitan University (TMU). I would also like to thank Tokyo Metropolitan Government for the generous funding and scholarship under the project of Asian Network of Major Cities 21 (ANMC-21) and Asian Human Resources Fund program. My sincere gratitude goes to Dr. Arief Yudhanto (KAUST) and Dr. Atsushi Kondo (e-Xtream Engineering, MSC Software), who selflessly helped and supported me during my research. I am deeply indebted to Prof. Masahito Asai who has been a wonderful host at TMU. I would like to extend my gratefulness to my PhD thesis committee: Prof. Hiroshi Suemasu (Sophia University), Prof. Koichi Kitazono (TMU) and Prof. Satoshi Kobayashi (TMU), for their review, critics and comments. Many thanks to my resident advisor in Hirayama, Prof. Ayumu Inasawa, and staff of TMU International Center (Ms. Yamada, Ms. Sasaki, Ms. Suzuki) and Hino Campus (Mr. Kodaira) for their kind help and support. I would like to gratefully acknowledge the support from former and current members of Watanabe Laboratory, especially Dr. Satoshi Morooka, Mr. Jonny Herwan, Mr. Worawat Parasil, Mr. Prabij Joshi, Mr. Saharat Chantanumataporn, Prof. Shumpei Ozawa (Chiba Tech), my tutor Mr. Suguru Takahashi (Sumitomo Precision), Mr. Yousuke Oishi (Fuji Heavy Industries), Mr. Yasuhito Mikami, Mr. Norimasa Goto, Mr. Takuya Yoshida et al. Living in Japan would not be easier without heartfelt companionship with Indonesian friends (Dr. Mochamad Dady Ma'mun, Ms. Ressa Octavianty, Dr. Triwanto Simanjuntak, the late Dr. Agus Trilaksono, Dr. Sugeng Supriyadi, Dr. Fahamsyah Hamdan Latief, Dr. Bambang Bakri, Mr. Banung Grahita, Mr. Bakhtiar Yusuf, Mr. Azhar Aulia Saputra, Ms. Nurjanah, Mr. Pramudita Satria Palar et al.). My sincere gratitude also goes to Prof. Bambang Kismono Hadi and Dr. Djarot Widagdo, who had introduced composite and structural mechanics during my study at Bandung Institute of Technology. This study would not be possible without generous prayers from my family (Tajuddin Nasution family), in-laws (Miswar Zein family) and my big family in Indonesia. Last but not the least, I would like to sincerely thank my wife Meizanti Listiyani Zein for her love, prayers, patience and encouragement.

Vita

Author was born in Yogyakarta, a special monarchy region in Indonesia, in June 1988. He received his bachelor of engineering degree (*Sarjana Teknik*) from the Department of Aeronautics and Astronautics, Bandung Institute of Technology (ITB), Indonesia, in July 2010. He then enrolled to the same department to continue his master course under ITB Voucher scholarship, while he was also working as a research and teaching assistant at ITB. One year later, he received his master of engineering degree (*Magister Teknik*). In October 2011, he pursued his doctoral degree at the Department of Aerospace Engineering, Tokyo Metropolitan University, Japan, under the Asian Human Resources Fund program.

The research reported in this thesis was carried out at the Department of Aerospace Engineering, Graduate School of System Design, Tokyo Metropolitan University, 6-6 Asahigaoka, Hino-shi, Tokyo 191-0065, Japan.

This research is financially supported by Tokyo Metropolitan Government under the project of Asian Network of Major Cities 21 (ANMC-21).

This thesis is typeset using LaTeX, under Ubuntu Linux operating system.